

UNCLASSIFIED

AD 262 146

*Reproduced  
by the*

ARMED SERVICES TECHNICAL INFORMATION AGENCY  
ARLINGTON HALL STATION  
ARLINGTON 12, VIRGINIA



Best Available Copy

UNCLASSIFIED

NOTICE: When government or other drawings, specifications or other data are used for any purpose other than in connection with a definitely related government procurement operation, the U. S. Government thereby incurs no responsibility, nor any obligation whatsoever; and the fact that the Government may have formulated, furnished, or in any way supplied the said drawings, specifications, or other data is not to be regarded by implication or otherwise as in any manner licensing the holder or any other person or corporation, or conveying any rights or permission to manufacture, use or sell any patented invention that may in any way be related thereto.

62146  
Final Report

Cy 22  
Covering the Period 1 November 1956  
to 31 May 1961

## ANTENNA DESIGN PARAMETERS

Prepared for:

U.S. ARMY SIGNAL RESEARCH AND DEVELOPMENT LABORATORY  
FORT MONMOUTH, NEW JERSEY

CONTRACT DA 36-039 SC-73106  
DA PROJECT 3-99-00-100  
SIGNAL CORPS TASK 3-99-06-106

By: R. C. Honey E. D. Sharp C. M. Ahlow L. A. Robinson  
J. L. Brenner M. G. Andreasen J. Aasted

STANFORD RESEARCH INSTITUTE

MENLO PARK, CALIFORNIA

\*SRI

61-4-3  
XEROX

May 1961

Final Report

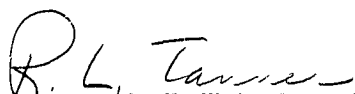
Covering the Period 1 November 1956  
to 31 May 1961**ANTENNA DESIGN PARAMETERS**

Prepared for:

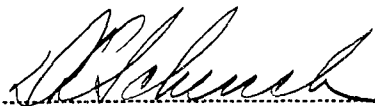
U.S. ARMY SIGNAL RESEARCH AND DEVELOPMENT LABORATORY  
FORT MONMOUTH, NEW JERSEYCONTRACT DA 36-039 SC-73106  
DA PROJECT 3-99-00-100  
SIGNAL CORPS TASK 3-99-06-106By: R. C. Honey E. D. Sharp C. M. Ablow L. A. Robinson  
J. L. Brenner M. G. Andreasen J. Aasted

SRI Project No. 1954

Approved:



R. L. TANNER, MANAGER ELECTROMAGNETICS LABORATORY



D. R. SCHEUCH, DIRECTOR ELECTRONICS AND RADIO SCIENCES DIVISION

Copy No. 22

## ABSTRACT

---

This report describes the results obtained during the last year of a four year study program on antenna design parameters. Thus, the complete results of this program are contained in the three previous annual reports and in this final report. A summary of the project discusses the various investigations carried out during the course of the project.

A modified form of the Purcell linear slotted array is proposed that features great mechanical simplicity and ruggedness. For these reasons, this type of design is particularly well suited for scaling to millimeter wavelengths. To demonstrate this, a five-foot long array was built and tested for the 35-Gc band. The design data for this antenna were obtained experimentally. The first steps in applying a novel analytical technique to the Purcell array geometry have been taken. This technique promises to yield design data that would be sufficiently precise even for very long arrays.

A variety of linear arrays with widely and variably spaced elements have been designed using both analog and digital computer techniques. These arrays all have many fewer elements than Dolph-Tchebyscheff arrays with the same beamwidth and side-lobe level. One of the arrays has 21 elements and is 76 wavelengths long when used as a broadside array. The 3-db beamwidth is 0.74 degree; the side-lobe level -7.4 db. The array has perfect steerability in a 1.8:1 bandwidth with no interelement spacing smaller than a half wavelength in this band. A Dolph-Tchebyscheff array with the same beamwidth and side-lobe level uses 53 elements, and the steerability is not perfect even at a single frequency.

The problem of finding the optimum spacing for the elements in an array of isotropic elements has been set up precisely, and solutions found for the two distinct cases of even and odd numbers of radiators.

The computed *H*-plane beam-broadening effects of several mechanical modifications are reported for six leaky-wave antennas whose radiating

apertures consist of inductive wire grids. It is shown that change in the half-power beamwidth by a factor of 5.2 was obtained with a 20-wavelength-long antenna by simple linear displacement of the solid metal wall with respect to the wire grid. This change was accompanied, however, by a significant reduction in the amount of power radiated. For simple wall displacements that did not result in reduction of the radiated power, the largest beamwidth change reported for 20-wavelength-long antennas is a factor of 3.8. More complex wall displacements are demonstrated to produce beamwidth changes by a factor of 7.4 for a 20-wavelength-long antenna, and by a factor of 20 for a 50-wavelength-long antenna. The results of this study indicate that even larger changes in beamwidth are probably possible.

A double-layered pillbox in which the parabolic reflecting surface is replaced by a gradual waveguide bend is designed and tested for horizontal polarization over the frequency band from 8.5 to 12.5 Gc. The advantages of this design include wide-band operation, no aperture blocking, and hence low side-lobe radiation patterns.

Three types of wide-band omniazimuthal, instantaneous direction-finding antennas that have been built and tested at Stanford Research Institute for the Signal Corps are compared in detail.

# CONTENTS

ABSTRACT . . . . .	iii
LIST OF ILLUSTRATIONS . . . . .	vii
LIST OF TABLES . . . . .	xi
OBJECTIVES . . . . .	xiii
PUBLICATIONS AND CONFERENCES . . . . .	xv
I SUMMARY OF THE PROJECT . . . . .	1
II MODIFIED PURCELL ARRAY . . . . .	5
A. General . . . . .	5
B. A Modified Purcell Array . . . . .	5
1. Design . . . . .	5
2. Construction . . . . .	17
3. Tests . . . . .	17
C. Analysis of Array Junctions . . . . .	25
References . . . . .	30
III INVESTIGATIONS OF LINEAR ARRAYS . . . . .	31
A. Linear Arrays with Variable Interelement Spacings . . . . .	31
1. Introduction . . . . .	31
2. General . . . . .	33
3. Array Computation . . . . .	39
a. General . . . . .	39
b. Computations with Analog Computer . . . . .	40
c. Computations with Digital Computer . . . . .	41
4. Conclusions . . . . .	56
B. Linear Arrays with Constant Interelement Spacings . . . . .	57
1. Introduction . . . . .	57
2. The Far Field . . . . .	58
a. General . . . . .	58
b. The Case for $N$ Odd . . . . .	60
c. The Case for $N$ Even . . . . .	66
References . . . . .	72
IV VARIABLE-BEAMWIDTH LEAKY-WAVE ANTENNAS . . . . .	75
A. General . . . . .	75
B. Designs Beginning with Narrow-Beam Antennas . . . . .	76
1. Antennas A and B . . . . .	76
2. Antenna C . . . . .	82
a. General . . . . .	82
b. Wall Moved Toward Grid at Input End . . . . .	85

## CONTENTS

c. Wall Moved Toward Grid at Load End . . . . .	87
d. Wall Moved Toward Grid at Both Ends . . . . .	89
e. Wall Moved Toward Grid at Center . . . . .	91
f. Comparison of Wall Movements . . . . .	97
3. Antenna D . . . . .	99
C. Designs Beginning with Broad-Beam Antennas . . . . .	104
1. Antenna E . . . . .	104
2. Antenna F . . . . .	112
D. Conclusions . . . . .	117
E. Recommendations . . . . .	118
References . . . . .	119
V BROADBAND ROLLED PILLBOX . . . . .	121
A. General . . . . .	121
B. Estimate of Phase Error . . . . .	127
C. Mechanical Design . . . . .	129
D. Measurements . . . . .	129
References . . . . .	143
VI. INSTANTANEOUS DIRECTION-FINDING ANTENNAS . . . . .	145
A. General . . . . .	145
B. Recommendations . . . . .	149
References . . . . .	150
VII CONCLUSIONS . . . . .	151
VIII RECOMMENDATIONS . . . . .	153
IDENTIFICATION OF KEY TECHNICAL PERSONNEL . . . . .	155
APPENDIX A PROOF OF THEOREMS . . . . .	159



## ILLUSTRATIONS

Fig. II- 1	Cross Section of Modified Purcell Array Scaled to Millimeter Wavelengths . . . . .	6
Fig. II- 2	24-Slot X-Band Test Section . . . . .	8
Fig. II- 3	Tilt Angle vs Slot Length for Various Slot Heights, $b'$ . . . . .	9
Fig. II- 4	Tilt Angle vs Slot Length for Various Main Waveguide Heights, $b$ . . . . .	10
Fig. II- 5	Tilt Angle vs Slot Spacing for Various Slot Heights, $b'$ . . . . .	11
Fig. II- 6	Slot Height vs Slot Spacing for Tilt Angle of -5.25 Degrees . . . . .	12
Fig. II- 7	Slot Height vs Power Coupled Out per Slot . . . . .	14
Fig. II- 8	Slot Height vs Slot Number for Final Array . . . . .	16
Fig. II- 9	Slot Spacing vs Slot Number for Final Array . . . . .	16
Fig. II-10	Modified Purcell Array on Pattern Range . . . . .	18
Fig. II-11	Typical Radiation Patterns—28.75 Gc . . . . .	19
Fig. II-12	Typical Radiation Patterns—29.98 Gc . . . . .	20
Fig. II-13	Measured Beam Positions as a Function of Frequency . . . . .	21
Fig. II-14	Measured Beamwidth vs Frequency . . . . .	22
Fig. II-15	Measured Gain vs Frequency . . . . .	22
Fig. II-16	Junction Between Feed Waveguide and Slot . . . . .	26
Fig. II-17	Equivalent Circuit of Junction . . . . .	27
Fig. II-18	Terminal-Plane Positions of Junction . . . . .	28
Fig. II-19	Equivalent Circuit Parameters of Junction . . . . .	29
Fig. III- 1	Symmetric Linear Array with $2N + 1$ Elements . . . . .	34
Fig. III- 2	Space Factor of 11-Element Array Synthesized from Initial Array 1— $d_{av} = 3\lambda$ . . . . .	43
Fig. III- 3	Space Factor of 11-Element Array Synthesized from Initial Array 2— $d_{av} = 3\lambda$ . . . . .	44
Fig. III- 4	Space Factor of 11-Element Array Synthesized from Initial Array 3— $d_{av} = 3\lambda$ . . . . .	45
Fig. III- 5	Space Factor of 11-Element Array Synthesized from Initial Array 3— $d_{av} = 2\lambda$ . . . . .	46
Fig. III- 6	Space Factor of 11-Element Array Synthesized from Initial Array 4— $d_{av} = 3\lambda$ . . . . .	47
Fig. III- 7	Space Factor of 11-Element Array Synthesized from Initial Array 4— $d_{av} = 2\lambda$ . . . . .	48

# ILLUSTRATIONS

Fig. III- 8	Space Factor of 21-Element Array Synthesized from Initial Array 3— $d_{av} = 3\lambda$ . . . . .	49
Fig. III- 9	Space Factor of 21-Element Array Synthesized from Initial Array 3— $d_{av} = 2\lambda$ . . . . .	50
Fig. III-10	Space Factor of 51-Element Array Synthesized from Initial Array 3— $d_{av} = 3\lambda$ . . . . .	51
Fig. III-11	The Far Field . . . . .	57
Fig. III-12	Desired Far-Field Pattern . . . . .	58
Fig. III-13	Symmetrically Placed, Equally Spaced Radiators . . . . . (a) Odd Number of Radiators, $N = 9$ (b) Even Number of Radiators, $N = 8$	61
Fig. III-14	Graph of the Polynomial Defined by Elliptic Functions (Case iv, $N = 8$ illustrated) . . . . .	71
Fig. IV- 1	Inductive Sheet Antenna . . . . .	75
Fig. IV- 2	Dimensions of Antenna A as Designed for Constant Phase Velocity . . . . .	77
Fig. IV- 3	Dimensions of Antenna B as Designed for Constant Phase Velocity . . . . .	78
Fig. IV- 4	Aperture Distributions of Antenna A . . . . .	80
Fig. IV- 5	Aperture Distributions of Antenna B . . . . .	81
Fig. IV- 6	Dimensions of Antennas C and D as Designed for Constant Phase Velocity . . . . .	83
Fig. IV- 7	Radiation Patterns of Antenna C with the Solid Wall Moved Toward the Grid at the Input End . . . . .	84
Fig. IV- 8	Aperture Distributions of Antenna C with the Solid Wall Moved Toward the Grid at the Input End . . . . .	86
Fig. IV- 9	Radiation Patterns of Antenna C with the Solid Wall Moved Toward the Grid at the Load End . . . . .	88
Fig. IV-10	Aperture Distributions of Antenna C with the Solid Wall Moved Toward the Grid at the Load End . . . . .	90
Fig. IV-11	Radiation Patterns of Antenna C with the Solid Wall Moved Toward the Grid at Both Ends, the Center Point Being Fixed . . . . .	92
Fig. IV-12	Aperture Distributions of Antenna C with the Solid Wall Moved Toward the Grid at Both Ends, the Center Point Being Fixed . . . . .	93
Fig. IV-13	Radiation Patterns of Antenna C with the Solid Wall Moved Toward the Grid at the Center Point, Both Ends Being Fixed . . . . .	94
Fig. IV-14	Aperture Distributions of Antenna C with the Solid Wall Moved Toward the Grid at the Center Point, Both Ends Being Fixed . . . . .	95
Fig. IV-15	Beam Broadening Resulting from Movement of the Solid Wall of Antenna C Toward Its Grid . . . . .	96
Fig. IV-16	Radiation Patterns of Antenna D with the Solid Wall Moved Away from the Grid at the Input End . . . . .	98
Fig. IV-17	Aperture Distributions of Antenna D with the Solid Wall Moved Away from the Grid at the Input End . . . . .	100

# ILLUSTRATIONS

Fig. IV-18	Radiation Patterns of Antenna D with the Solid Wall Moved Away from the Grid at the Load End . . . . .	101
Fig. IV-19	Aperture Distributions of Antenna D with the Solid Wall Moved Away from the Grid at the Load End . . . . .	102
Fig. IV-20	Beam Broadening Resulting from Movement of the Solid Wall of Antenna D Away from Its Grid . . . . .	103
Fig. IV-21	Dimensions of Antenna E . . . . .	106
Fig. IV-22	Radiation Patterns of Antenna E . . . . .	109
Fig. IV-23	Aperture Distributions of Antenna E . . . . .	110
Fig. IV-24	Beam Broadening Resulting from Movement of the Solid Wall of Antenna E . . . . .	112
Fig. IV-25	Dimensions of Antenna F . . . . .	114
Fig. IV-26	Radiation Patterns of Antenna F . . . . .	115
Fig. IV-27	Aperture Distributions of Antenna F . . . . .	116
Fig. V- 1	Sketch of Rolled Pillbox . . . . .	122
Fig. V- 2	Cross Section of Rolled Pillbox . . . . .	122
Fig. V- 3	VSWR for H-Plane Bends vs $\lambda/2a$ for Different Values of $r_0/a$ . . . . .	123
Fig. V- 4	Geometry of Parabola . . . . .	124
Fig. V- 5	Geometry of Rolled Pillbox with Toroidal Approximation . . . . .	124
Fig. V- 6	Sketch of Rolled Pillbox Showing Approximate Ray Path . . . . .	126
Fig. V- 7	Maximum Phase Error in the Aperture vs $\lambda/2a$ for Different Tolerances . . . . .	128
Fig. V- 8	Tools for Cutting Curved Surfaces, Rolled Pillbox . . . . .	130
Fig. V- 9	Male Part, Rolled Pillbox . . . . .	131
Fig. V-10	Female Part, Rolled Pillbox . . . . .	131
Fig. V-11	Partially Assembled Pillbox . . . . .	132
Fig. V-12	Sketch of Primary Feed Horn . . . . .	132
Fig. V-13	Sketch of Cross Section of the Pillbox with Primary Feed Horn . . . . .	133
Fig. V-14	Level of First Side Lobes or Highest Shoulder Below Main Lobe as a Function of Feed Position . . . . .	134
Fig. V-15	E-Plane Radiation Patterns, Pillbox with Feed A, $d = 1-1/4"$ . . . . .	136
Fig. V-16	E-Plane Radiation Patterns, Pillbox with Feed B, $d = 1-1/2"$ . . . . .	137
Fig. V-17	E-Plane Radiation Patterns, Pillbox with Feed C, $d = 1-3/4"$ . . . . .	138
Fig. V-18	Half-Power Beamwidth of Pillbox vs Frequency . . . . .	139
Fig. V-19	Gain of Rolled Pillbox vs Frequency . . . . .	139
Fig. V-20	Side-Lobe Level vs Frequency for Three Different Feed Horns . . . . .	140
Fig. V-21	Rollled Pillbox Feeding Leaky-Wave Antenna . . . . .	141

# ILLUSTRATIONS

Fig. V-22	Radiation Patterns of Leaky-Wave Antenna Fed with Rolled Pillbox . . . . .	142
Fig. V-23	Radiation Patterns of Leaky-Wave Antenna Fed with Hog Horn . . . . .	142
Fig. V-24	Radiation of Rolled Pillbox with Special Feed Horn . . . . .	143
Fig. VI- 1	Comparison of Instantaneous, Omniazimuth, Direction-Finding Antennas . . . . .	147
Fig. A- 1	Relation Between Graphs of $T_n(x)$ and $P(x)$ , Where $n = 5$ . . . . .	162
Fig. A- 2	Special Case of Fig. A- 1 . . . . .	164

## TABLES

---

Table II-1	Equivalent Circuit Parameters of Junction . . . . .	27
Table II-2	Measured and Theoretical Parameters of Junction . . . . .	30
Table III-1	Initial Arrays Used in Computations with Digital Computer . . . . .	43
Table III-2	11-Element Arrays Synthesized with Digital Computer . . . . .	52
Table III-3	Radiation Pattern Data of 11-Element Arrays Synthesized with Digital Computer . . . . .	52
Table III-4	21-Element Arrays Synthesized with Digital Computer . . . . .	53
Table III-5	Radiation Pattern Data of 21-Element Arrays Synthesized with Digital Computer . . . . .	53
Table III-6	51-Element Array Synthesized with Digital Computer . . . . .	54
Table III-7	Radiation Pattern Data of 51-Element Array Synthesized with Digital Computer . . . . .	54
Table IV-1	Dimensions of Antenna E . . . . .	108
Table IV-2	Dimensions of Antenna F . . . . .	113

## OBJECTIVES

---

The objectives of this program are to develop new antenna designs and design techniques for the particular needs of Signal Corps ground-based systems. The various tasks include experimental as well as theoretical study, and every effort has been made to avoid duplication of other work.

## PUBLICATIONS AND CONFERENCES

---

A paper entitled "Line Sources and Linear Arrays for Millimeter Wavelengths" was presented at the Symposium on Millimeter Waves (March 31 to April 2, 1959) in New York by R. C. Honey. This paper described the work carried out under this contract on the leaky-wave array and the Purcell array and was published in the Symposium Proceedings, Vol. IX, entitled "Millimeter Waves" by the Microwave Research Institute of the Polytechnic Institute of Brooklyn.

A paper entitled "A Wide-Band Turnstile Junction and Direction-Finding Antenna," by R. C. Honey and J. K. Shimizu, was presented at the National Symposium of the Professional Group on Microwave Theory and Techniques of the IRE (May 9 to 11, 1960) in Coronado, California.

A paper entitled "Arrays with Variable Interelement Spacings," by M. G. Andreassen was presented at the joint URSI-IRE Meeting, Boulder, Colorado (December 1960).

# ANTENNA DESIGN PARAMETERS

## I SUMMARY OF THE PROJECT

This research program entitled "Design Parameters for Antennas" has covered a variety of tasks during the four-year period of the contract. A number of these tasks were selected at the beginning of the contract; however, new tasks were selected each year by mutual agreement to keep the program oriented so as to best satisfy the needs of the Signal Corps and to keep pace with the state of the art in the antenna field.

The results of each year's efforts are contained in the Annual Reports for that year, so that the three Annual Reports and this Final Report together describe the whole of the unclassified work accomplished under this contract. A preliminary study of various artificial beam-sharpening techniques applicable to the Signal Corps' ground-to-ground IFF systems was issued as a classified supplement to the Third Quarterly Progress Report.

Because some of the tasks have continued for several years during this contract, and to help the reader of this report in locating pertinent material in the previous annual reports, a summary of the entire unclassified program will be given here.

One of the principal tasks that has continued throughout this program concerned the design and construction of long linear-array and line-source antennas that were suitable for use at millimeter wavelengths. In this connection, three linear arrays five feet in length were built and tested over the 35-Gc band.

The first such antenna to be completed was a leaky-wave line-source consisting of a waveguide with one side wall replaced by an inductive grid of parallel wires. This array was designed to have a Taylor aperture distribution radiating 95 percent of the input power in a pattern with



-35-db side lobes, as described in the Second Annual Report. The experimental results obtained with this antenna, described in the Third Annual Report, agreed substantially with the theoretical predictions. The maximum side-lobe level at the design frequency, 35 Gc, was -28 db due to the finite tolerances that could be maintained in its construction. Elsewhere in the band from 26 to 50 Gc the maximum side-lobe levels varied from -24 to -29 db.

The second type of millimeter-wavelength antenna investigated under this program was the Purcell array. Two arrays were designed and tested, the first a conventional Purcell array as originally proposed by Purcell, and the second a modified form of the array that greatly simplified the construction. The design of the first array is described in the Second Annual Report and the results of the experimental tests are described in the Third Annual Report. This array did not turn out to be nearly as satisfactory as the modified Purcell array, the design and testing of which are described in Section II.

End-fed arrays and line sources as many wavelengths long as those described above, are subject to losses due to the energy propagating through an appreciable length of waveguide before being radiated. For this reason, a complete analysis of the effects of this attenuation on the antenna characteristics resulted in the following conclusions as reported in the Third Annual Report. The dissipative attenuation along the aperture of an end-fed linear array has relatively little effect on the radiation pattern of the array, aside from a reduction of the absolute gain. In general, the losses in an end-fed array designed with an asymmetric aperture distribution peaked up toward the feed end are less than the losses in the same array designed with a symmetric aperture distribution. Furthermore, the use of an asymmetric component superimposed on the symmetric component in the aperture distribution can be used to fill in the nulls in a radiation pattern, which for radar applications, results in less ambiguity in target direction than a pattern with discrete side-lobes.

Two tasks involved refinements in conventional paraboloidal reflectors. The first, described in the First Annual Report, optimized the design of horn-fed paraboloidal reflectors in order to obtain constant beamwidths over very wide frequency bands. This task involved both analytical study

and experimental verification, and a large number of primary and secondary radiation patterns were measured. Beamwidth variations of the order of  $\pm 6\frac{1}{2}$  percent were obtained over 1.6 to 1 bandwidths.

The second task involving paraboloidal reflectors attempted to reduce the spill-over and back lobes from such reflectors using novel structures to constrain all of the energy from the feed to be incident on the reflector. The first technique, described in the Second Annual Report, uses two parallel wire grids that are transparent to energy incident normally on the antenna, but are essentially opaque to energy incident at large angles. The grids are placed over the aperture of the reflector in the plane of the feed. The second technique, described in the Third Annual Report, uses metal sheets to constrain the energy. These sheets are perforated with quadruply ridged resonant apertures, making them essentially transparent to energy at a given angle of incidence, yet opaque to energy at grazing incidence. Either technique proved to be only marginally effective in reducing the spill-over and back lobes.

The design of a new type of instantaneous wide-band direction-finding antenna is described in the Second Annual Report, and the complete tests of this antenna are contained in the Third Annual Report. The probable bearing errors remained less than  $\pm 1.7$  degrees for all azimuth directions and for all signals in the frequency range from 5 to 14.29 Gc. The maximum bearing error measured anywhere within this band was less than 4 degrees. The characteristics of this direction-finding antenna are summarized in Section VI and compared with those of two previous instantaneous direction-finding antennas built and tested at SRI for the Signal Corps.

In the First Annual Report several dispersive waveguide prisms are analyzed that can be used as frequency-scanning antennas. They include flat waveguide prisms, compressed waveguide prisms, and compressed waveguide prisms fed by slotted-waveguide line sources. All of these prisms can be designed to have the same performance as the folded-waveguide type of frequency scanning antenna, and the most dispersive prism is compared quantitatively with the folded-waveguide array.

Also in the First Annual Report are the measured radiation patterns of two E-plane sectoral-horns compared with theoretical patterns computed using Chu's analysis and a new theoretical analysis developed on a previous

Signal Corps contract. The new analysis shows appreciably better agreement with the experimental results than Chu's analysis, particularly in the side-lobe regions.

In this final report, several new topics are covered. The first is a study of linear arrays with variable interelement spacings. Computer techniques have been developed which minimize the side-lobe levels for a given length of array and a given number of elements. In addition to requiring many fewer elements for a given beamwidth, such arrays can be scanned over wider angles and over greater frequency bandwidths than normal equispaced arrays.

As a first step in obtaining analytical solutions to the variably spaced array problem, rigorous solutions have been obtained for the optimum directivity of equispaced arrays with either even or odd numbers of elements.

Another new topic is the use of the unique properties of wire-grid leaky-wave antennas to obtain beam shaping and beam broadening by making simple mechanical changes in the shape of the conducting sheet in back of the wire grid.

The last new topic described in this final report is the design, construction, and testing of a double-layer pillbox antenna with a gradually rolled reflecting region replacing the usual parabolic reflector. This type of pillbox is shown to have a much greater bandwidth than the usual pillboxes and to have lower side-lobe levels.

## II MODIFIED PURCELL ARRAY

### A. GENERAL

Linear arrays and line-source antennas are used in many applications that require a radiated beam that is very narrow in one plane, and end-fed antennas of this type are often used where space, weight, and size are at a premium. However, when such antennas are designed to be hundreds of wavelengths long at millimeter wavelengths, the mechanical tolerance problems become particularly acute. The modified Purcell array, first described in the Second and Third Annual Reports on this contract,<sup>1,2\*</sup> is an antenna that is well adapted for these applications because of its relatively simple and rugged mechanical design. In Part B, the empirical design, construction, and tests of a 5-foot modified Purcell array at  $K_u$ -band frequencies will be described. In Part C, a promising theoretical approach to the analysis of the modified Purcell array geometry will be described and some preliminary results presented.

### B. A MODIFIED PURCELL ARRAY

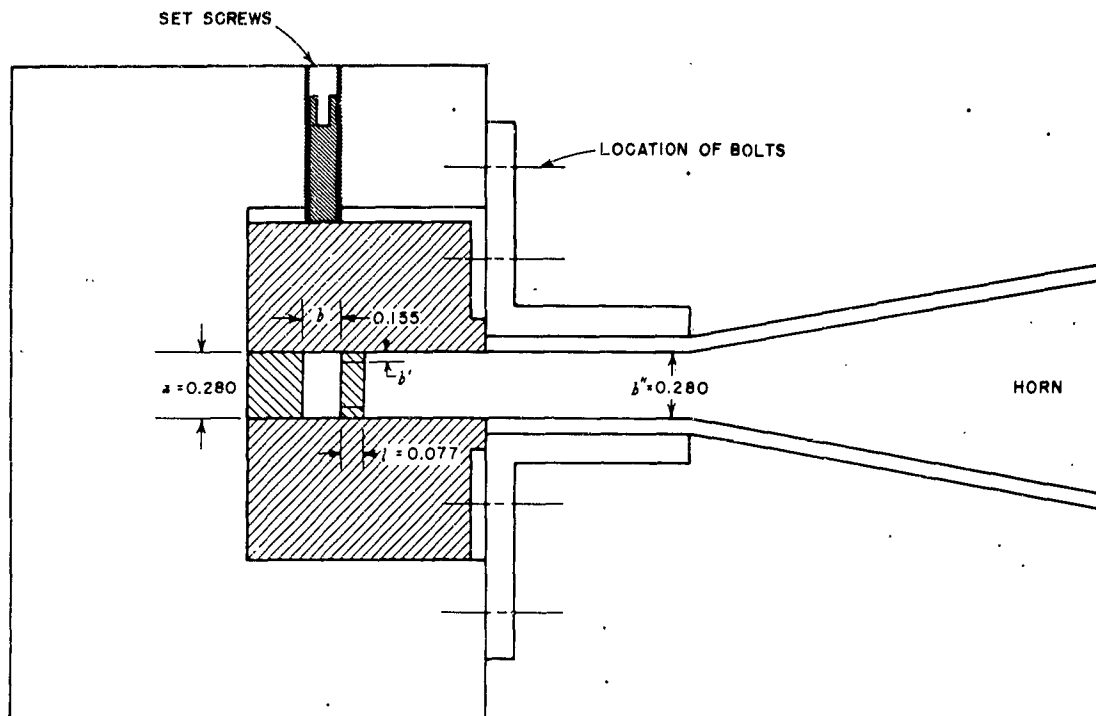
#### 1. DESIGN

The modified Purcell array differs from the more conventional Purcell array<sup>3,4</sup> because the spacing of the parallel plate region into which the slotted array radiates is identical with the width of the feeding waveguide as shown in Fig. II-1. Furthermore, it has been found possible to keep most of the dimensions constant along the full length of the array, changing only the slot heights and slot spacings to maintain uniform phase velocity. The modified form thus greatly simplifies the construction of the array, and permits closer tolerances to be maintained on the most critical dimensions in the array.

Unfortunately, the approximate design theory for the normal Purcell array proved to be inadequate for the modified array. Thus, in order to accumulate sufficiently accurate design data for the final array, as well as to check any modified theory that might be developed, an experimental

---

\* References are listed at the end of the section.



RA-1554-103

FIG. II-1

#### CROSS SECTION OF MODIFIED PURCELL ARRAY SCALED TO MILLIMETER WAVELENGTHS

program was undertaken to measure accurately the phase velocity and the coupling coefficients along uniform sections of the modified Purcell array.

The parallel plate region into which the slotted array radiates is wide enough to propagate TE and TM modes as well as the normal TEM mode. Therefore, it was first necessary to determine the extent to which these modes might interfere in the radiation pattern of the final antenna. An examination of the symmetry of an infinitely long, uniformly illuminated, broadside array of this type shows that two higher modes are coupled by the slots; and that they are exactly at their cut-off frequencies. Additional modes could be excited for a finite antenna, having an amplitude taper along the aperture, and could appear as lobes in the far-field radiation pattern. However, if the frequency is slightly lowered from the frequency required to produce broadside radiation, the strongly excited TE and TM modes are slightly below cut-off; and, in addition, small reflections from each slot do not add in phase at the input to the array.

Tests of several 24-slot X-band test sections with uniform sizes and spacings (producing an exponentially tapered aperture illumination with abrupt discontinuities at each end) indicated that these spurious lobes could be reduced to negligible proportions by lowering the frequency until the main lobe from the antenna was tilted several degrees from the normal to the array toward the input end. A longer array, with more gradual changes in the aperture distribution, should couple to these higher-order modes even less than in these test sections.

The experimental measurements to accumulate design data were performed at X-band frequencies for the sake of convenience. Thus, for all the test sections,  $a = a' = b'' = 0.900$  inch, where  $a'$  is the width of the slot and the other dimensions are shown in Fig. II-1. The experimental frequency chosen, 10.91 Gc, was near the upper edge of the normal waveguide band. Much higher frequencies appeared to accentuate the spurious lobes described above. Much lower frequencies would increase the losses (which are very significant in the 35-Gc array) and decrease the allowable tolerance on the width of the main waveguide in the final array. The 24-slot test sections were constructed with uniform slot sizes and spacings, as shown in Fig. II-2; and the radiation patterns from these test sections were measured with a short circuit on the output of each section. As long as the radiation was not nearly normal to the array, which was the case here, two distinct beams were formed from each section—one from the forward wave, the other from the wave reflected from the short circuit. The angular difference between these two beams provided very precise information on the phase velocity along the array, and the relative amplitudes of the two beams provided accurate information on the power coupled out per slot. For many of the test sections, individual patterns were also measured with a matched termination instead of a short circuit on the load end of the array. This technique turned out to yield considerably more accurate data than the best possible bench measurements, and in considerably less time. Furthermore, since the technique is a more direct method, any difficulties from spurious lobes in any of the many test sections will show up immediately in the radiation patterns.

The first set of experimental data is shown in Fig. II-3, in which the tilt angle,  $\phi$ , measured from the normal to the array with positive angles in the end-fire direction, is plotted as a function of the slot length,  $l$ , for various slot heights,  $b'$ , with the slot spacing,  $s$ , fixed

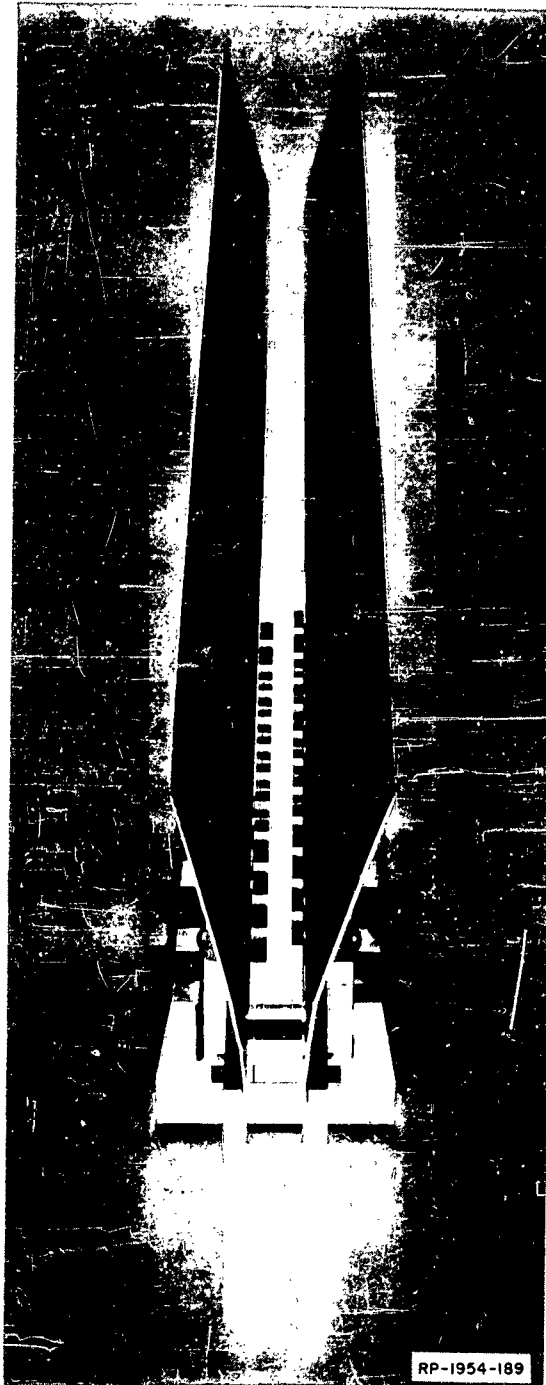


FIG. 11-2  
24-SLOT X-BAND TEST SECTION

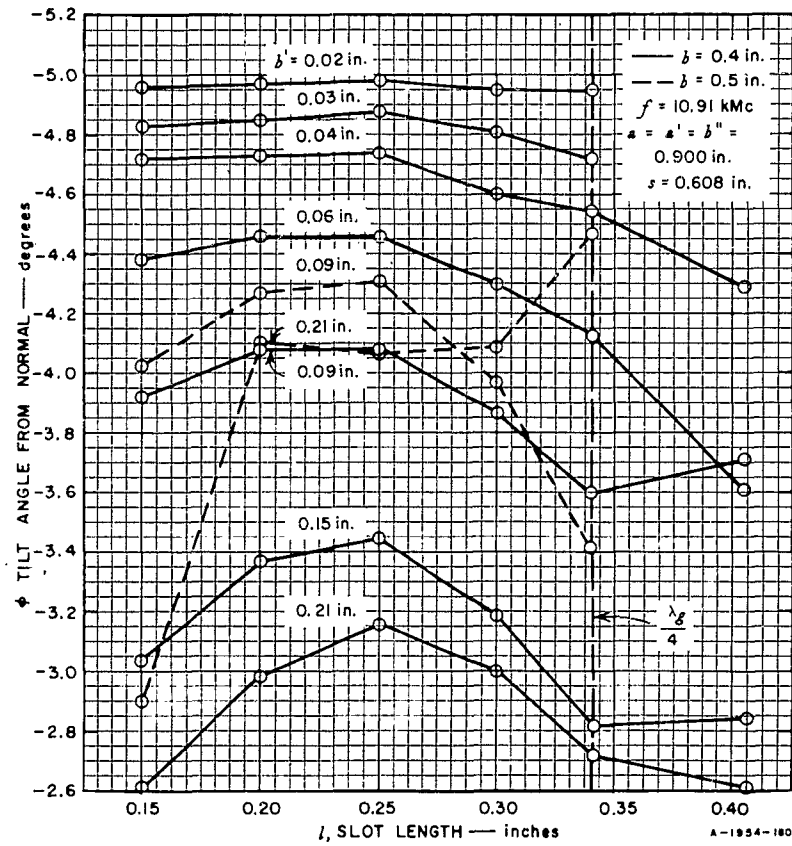


FIG. II-3  
TILT ANGLE VS. SLOT LENGTH FOR VARIOUS SLOT HEIGHTS,  $b'$



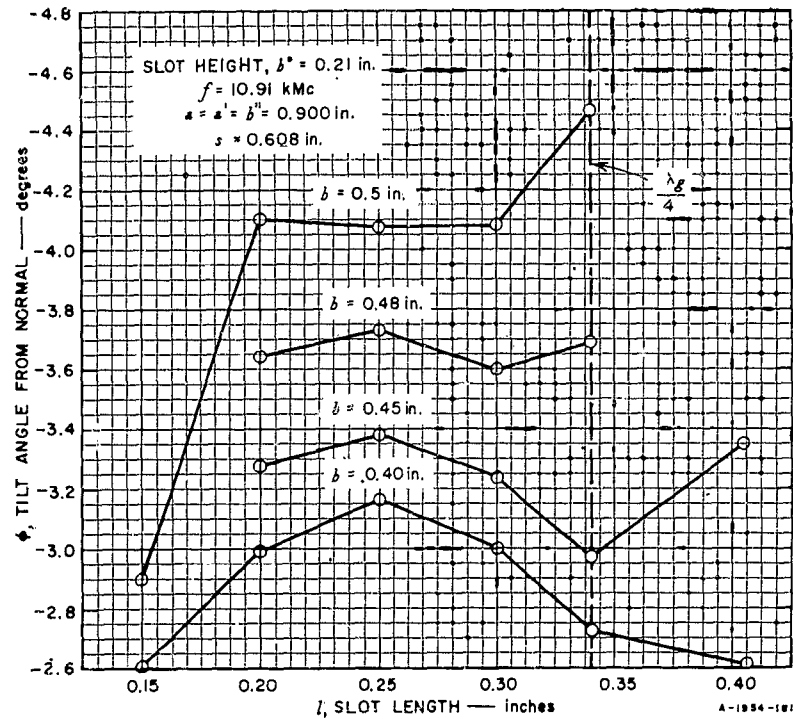


FIG. II-4

TILT ANGLE VS. SLOT LENGTH FOR VARIOUS MAIN WAVEGUIDE HEIGHTS,  $b$ .

at 0.608 inch. In Fig. II-4, a similar family of curves is plotted keeping the slot height,  $b'$ , fixed and varying the main waveguide height,  $b$ . From these two figures it is apparent that the angle of the radiation from the X-band test sections becomes very insensitive to slot length,  $l$ , in the vicinity of  $l = 0.25$  inch, for all slot heights over the range tested. For this reason,  $l$  was fixed at this value for subsequent tests. From these two figures it is also apparent that the larger the main waveguide height, the more nearly the velocity of propagation as measured by  $\phi$  approaches that in unperturbed waveguide at this frequency, corresponding to a tilt angle of 5.19 degrees for both figures. Another advantage of the larger height is that the losses in the main waveguide are reduced. For these reasons, the height of the main waveguide was fixed at 0.500 inch.

With the dimensions  $a$ ,  $a'$ ,  $b$ , and  $b''$  fixed, it becomes necessary to vary the slot spacings,  $s$ , along the array in order to maintain the phase velocity, or beam tilt angle, constant along the array. To determine  $s$ ,

another set of 24-slot X-band test sections was built and tested in the same manner. The results of these tests are shown in Fig. II-5, in which the tilt angle,  $\phi$ , is plotted as a function of the slot spacing,  $s$ , for various slot heights,  $b'$ . From these data any array with the tilt angle varying from about  $-4.9$  to  $-5.6$  degrees can be designed. A tilt angle of  $-5.25$  degrees was arbitrarily selected, and the final design data, obtained by averaging the data in Fig. II-5, is shown in Fig. II-6, in which the slot height,  $b'$ , is shown as a function of the slot spacing,  $s$ , with the other dimensions as shown on the figure. The only experimental point that does not fall on the smooth curve is the point where  $b' = 0.02$  inch. In view of the consistency of the remaining points in approaching the theoretical point  $s = 0.6073$  inch as  $b'$  approaches zero, the design curve was extended as shown by the dashed portion of the curve in Fig. II-6, essentially ignoring the point for  $b' = 0.02$  inch. This theoretical end point

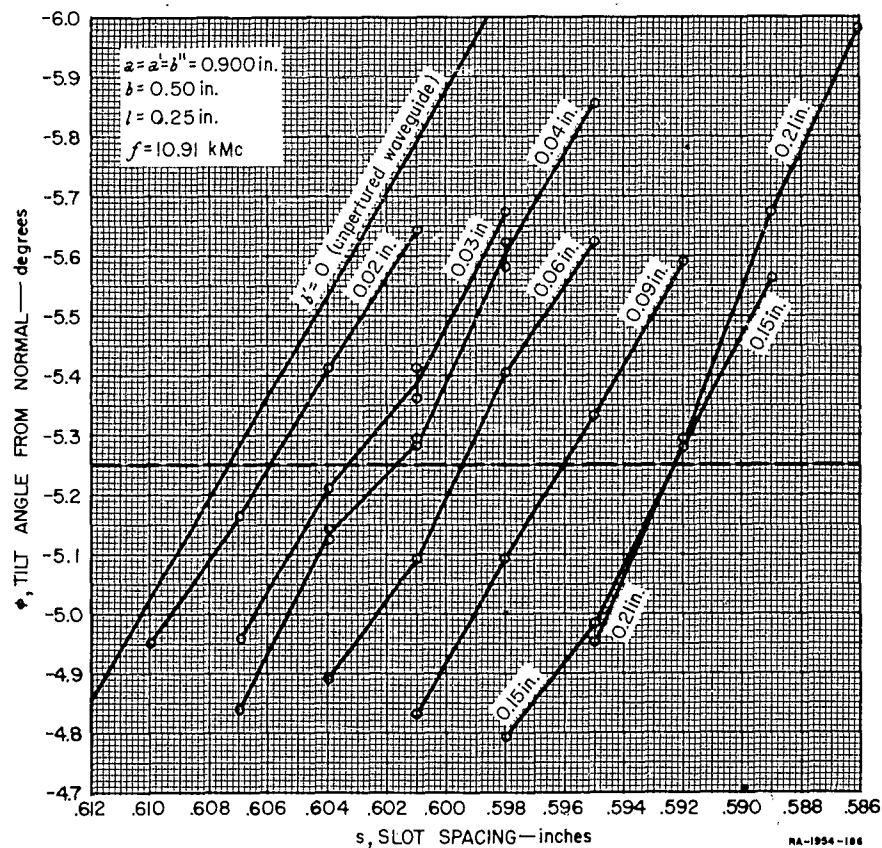


FIG. II-5  
TILT ANGLE VS. SLOT SPACING FOR VARIOUS SLOT HEIGHTS,  $b'$

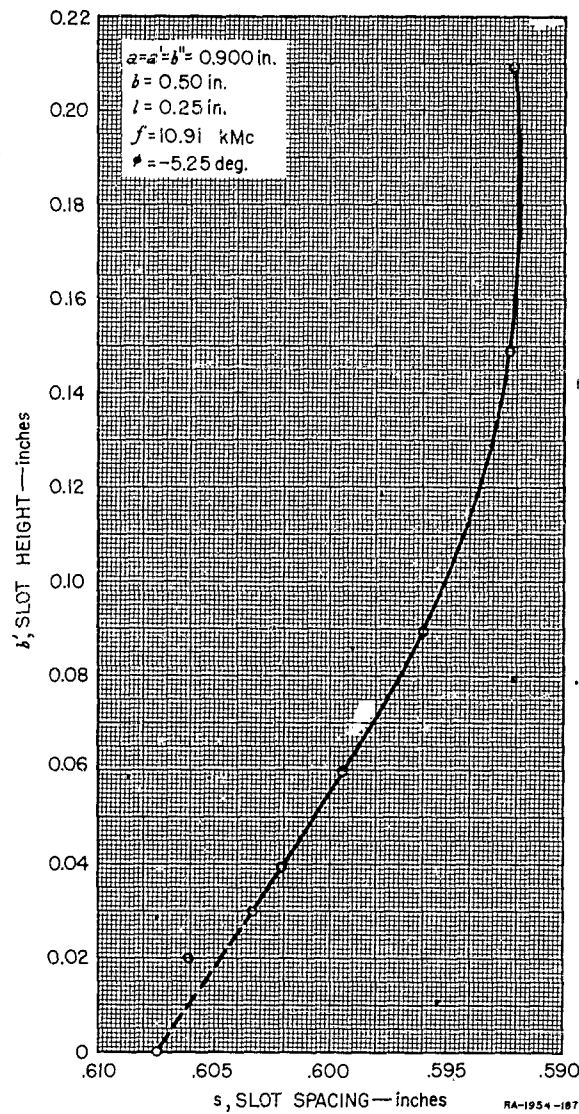


FIG. II-6  
 SLOT HEIGHT VS. SLOT SPACING FOR TILT ANGLE OF  
 -5.25 DEGREES

is found from the known phase velocity in unperturbed waveguide and the spacing required of infinitesimally small slots to produce radiation at  $\phi = -5.25$  degrees.

It is now necessary to determine the power coupled out of the array per slot from the radiation patterns used to accumulate the data in Fig. II-5. As mentioned before, this information can be obtained from the relative amplitudes of the two lobes from each test section when the test section is terminated in a short circuit. Since one lobe is from the wave traveling forward in the array, and the other from the wave reflected from the short circuit (neglecting reflections from the individual slots), the relative power level of the smaller to the larger lobe is given by

$$\frac{P_1}{P_2} = \left( 1 - \frac{P}{P_0} \right)^n$$

where  $P/P_0$  is the ratio of the power coupled out by one slot to the power incident on that slot and  $n$  is the total number of slots along the array. The measured data were corrected for the loss in the unperturbed guide by subtracting 0.1 db from each value of  $P_1/P_2$  expressed in db. Although patterns were not measured at the exact slot spacings required for a tilt angle of  $-5.25$  degrees, they were measured on either side of the proper values of  $\phi$ , as shown in Fig. II-5, and the values of  $P/P_0$  for the required spacings can be found accurately by interpolating between these measured points. The final values of  $P/P_0$  found in this way are shown in Fig. II-7 as a function of slot height  $b'$ . As in Fig. II-6, the value for  $b' = 0.02$  inch seems to be out of line with remaining points, so the curve is extended as shown by the dashed portion.

It is interesting to compare this experimental data with a curve of  $P/P_0$  calculated for a normal Purcell array given by the approximate formula derived by Purcell.<sup>3,4</sup> This formula (given in Refs. 1, 3, and 4) reduces to the simpler expression

$$\frac{P}{P_0} = \frac{128}{\pi^4} \frac{(b')^2}{sb} \frac{\lambda_g}{\lambda} \left( \frac{\lambda_g}{2a} \right)^2 \left[ \frac{\cos \frac{\pi a}{\lambda_g}}{1 - \left( \frac{2a}{\lambda_g} \right)^2} \right]^2$$

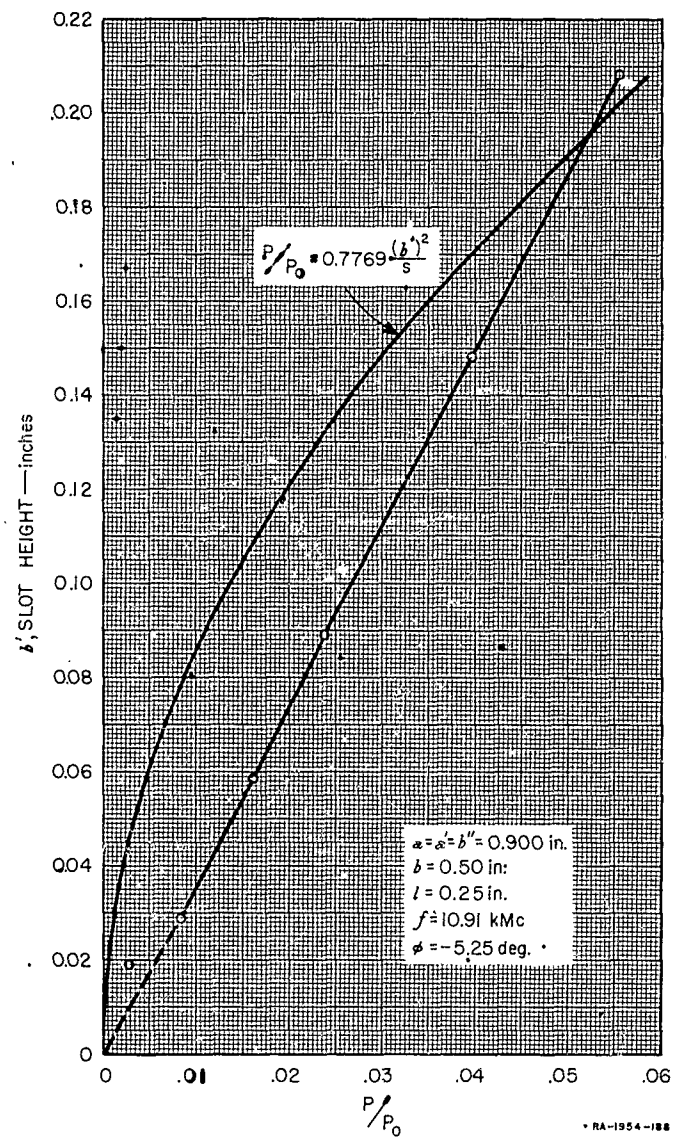


FIG. 11-7  
SLOT HEIGHT VS. POWER COUPLED OUT PER SLOT

for  $a = a' = b''$  and  $d \approx a$ . For the constants shown in Fig. II-7, this further reduces to

$$\frac{P}{P_0} = 0.7769 \frac{(b')^2}{s}$$

which is shown in Fig. II-7 along with the experimental data. It is apparent that the agreement between the two curves is not satisfactory for design purposes, and emphasizes the necessity for the experimental accumulation of design data and the need for a more refined theory.

Figures II-6 and II-7, then, contain all the data necessary to design the 5-foot modified Purcell array at  $K_u$ -band. The scale factor was arbitrarily selected as 0.900:0.280, the ratio of the widths of RG-52/U and RG-96/U waveguides. This makes the scaled-up design frequency 35.07 kMc.

Using this data and the design procedure described in the Second Annual Report,<sup>1</sup> a modified Purcell array was designed to have a Taylor aperture distribution for a -25 db side lobe level (Fig. II-3, Ref. 1) and to radiate a beam 5.25 degrees toward the feed end of the array measured from the normal to the array.

The important parameters and dimensions of the final array are the following:

Design frequency: 35.07 Gc

Main waveguide width:  $a = 0.280$  inch

Main waveguide height:  $b = 0.155$  inch

Length from outer edges of first to last slots: 60.194 inches

Total number of slots: 320

Slot width:  $a' = 0.280$  inch

Slot length:  $l = 0.077$  inch.

The slot heights,  $b'$ , and slot spacings,  $s$ , are shown in Figs. II-8 and II-9, respectively.

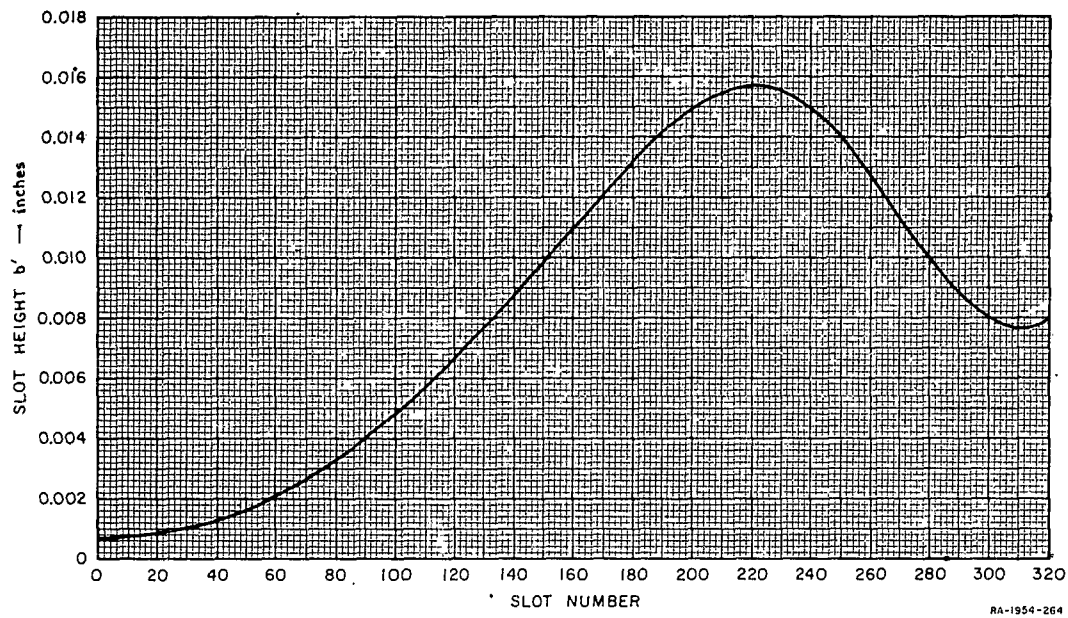


FIG. II-8  
SLOT HEIGHT VS SLOT NUMBER FOR FINAL ARRAY

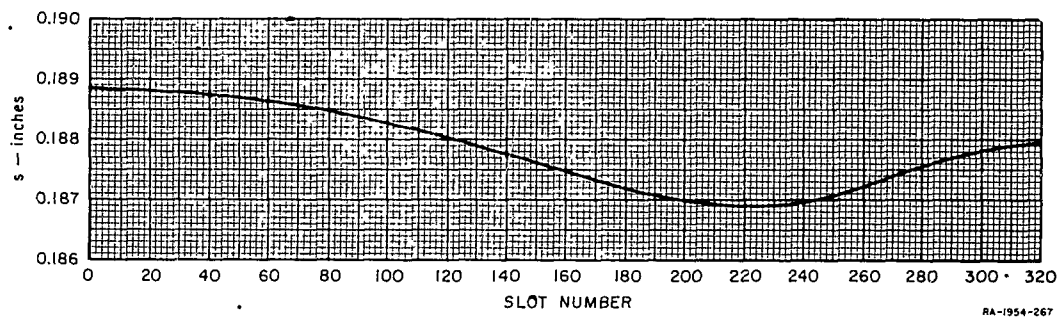


FIG. II-9  
SLOT SPACING VS SLOT NUMBER FOR FINAL ARRAY

## 2. CONSTRUCTION

The large holding fixture shown in Fig. II-1 was machined from a 2½- by 3-inch bar of 2024T4 Aluminum alloy, which is sufficiently stable for the purpose, yet sufficiently strong to support the many threading operations required.

All of the shaded bars shown in Fig. II-1 were made of oil-hardening tool steel except the one with the milled slots, which was called "Speed Treat" steel. This one bar was rough ground and then normalized before being finish ground to a +0.004-inch dimension. After a second normalizing, the slots were machined, the excess removed, and then finish ground to size.

The upper and lower bars between which the slotted bar is sandwiched were precision ground flats, 1¼ inch by ½ inch in cross section.

All of the steel surfaces were given a copper flash followed by a 0.0002-inch plate of silver, and the mating surfaces hand-honed to remove any residual uneven plating, and to ensure minimum RF losses in the completed antenna.

Nickel-plated steel screws were used throughout to help eliminate some of the possible corrosion problems.

The *E*-plane horn indicated in Fig. II-1 extended out 12<sup>5</sup>/<sub>8</sub> inches from the beginning of the flared region, producing an *E*-plane radius,  $R_e$ , of 13.75 inches and an *E*-plane aperture of 3<sup>7</sup>/<sub>16</sub> inches, from which the *E*-plane gain factor can be computed as a function of frequency.

## 3. TESTS

The completed antenna was mounted on a radiation pattern measuring range as shown in the photograph in Fig. II-10, and *H*-plane patterns were taken over the frequency band from about 28 to 37 Gc. Typical patterns are shown in Figs. II-11 and II-12. Note that, in common with all slotted waveguide arrays, the beam direction changes with frequency, scanning away from the normal and toward the feed end of the array as the frequency is lowered. The measured beam positions as a function of frequency are plotted in Fig. II-13, along with the design beam position at the design frequency. Note that the agreement is quite good, indicating that the control of the phase velocity along the array was entirely adequate.



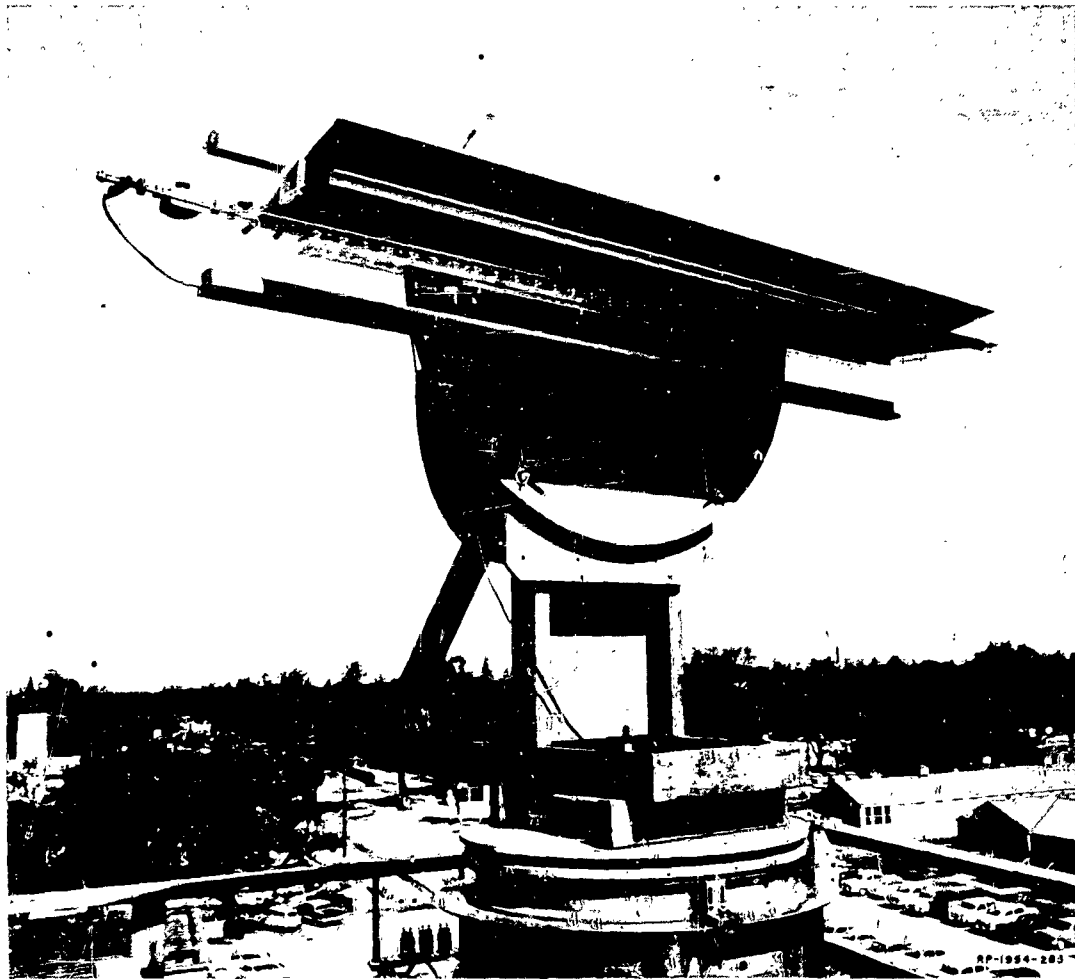


FIG. 11-10  
MODIFIED PURCELL ARRAY ON PATTERN RANGE

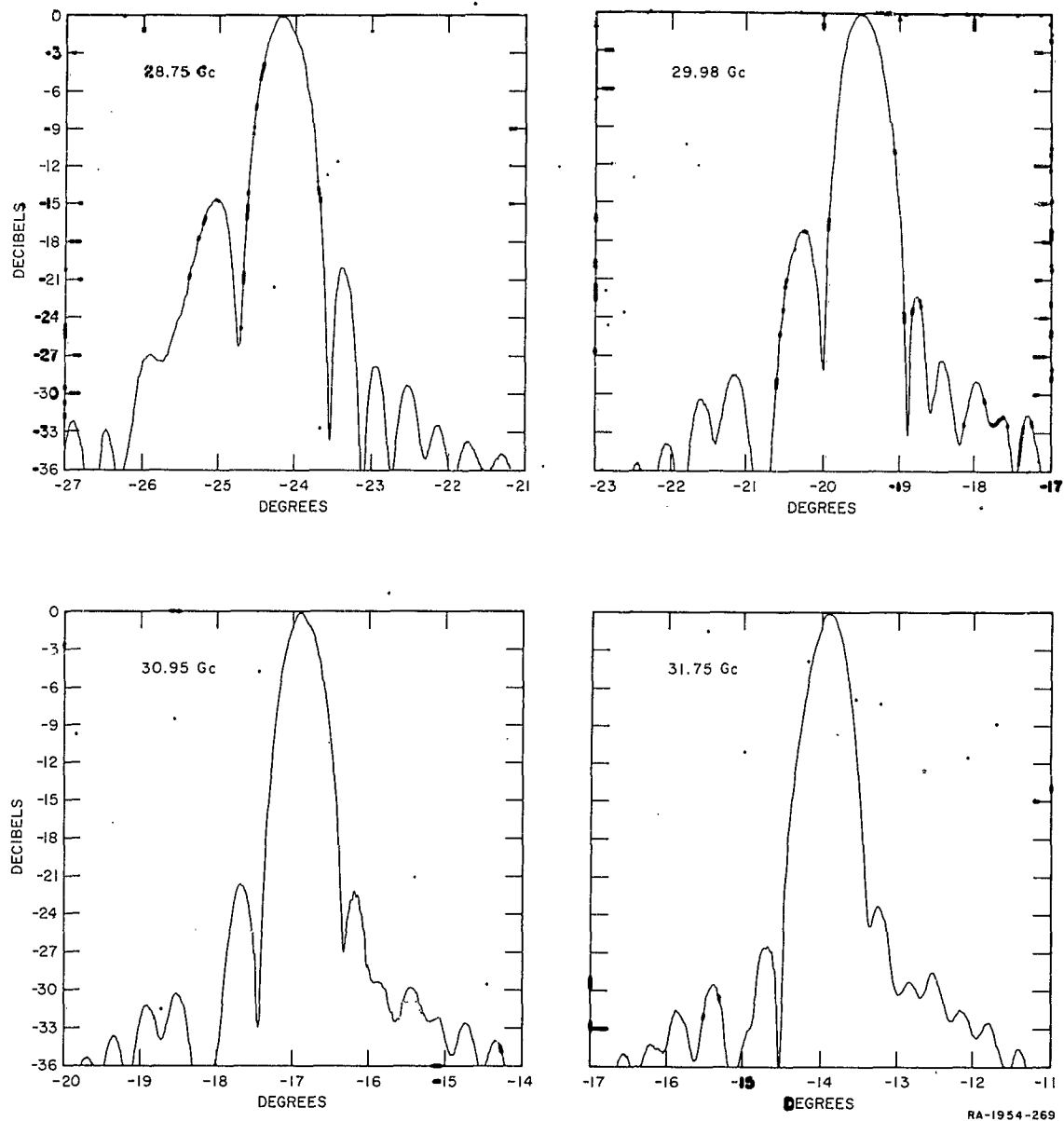


FIG. II-11  
TYPICAL RADIATION PATTERNS - 28.75 TO 31.75 Gc

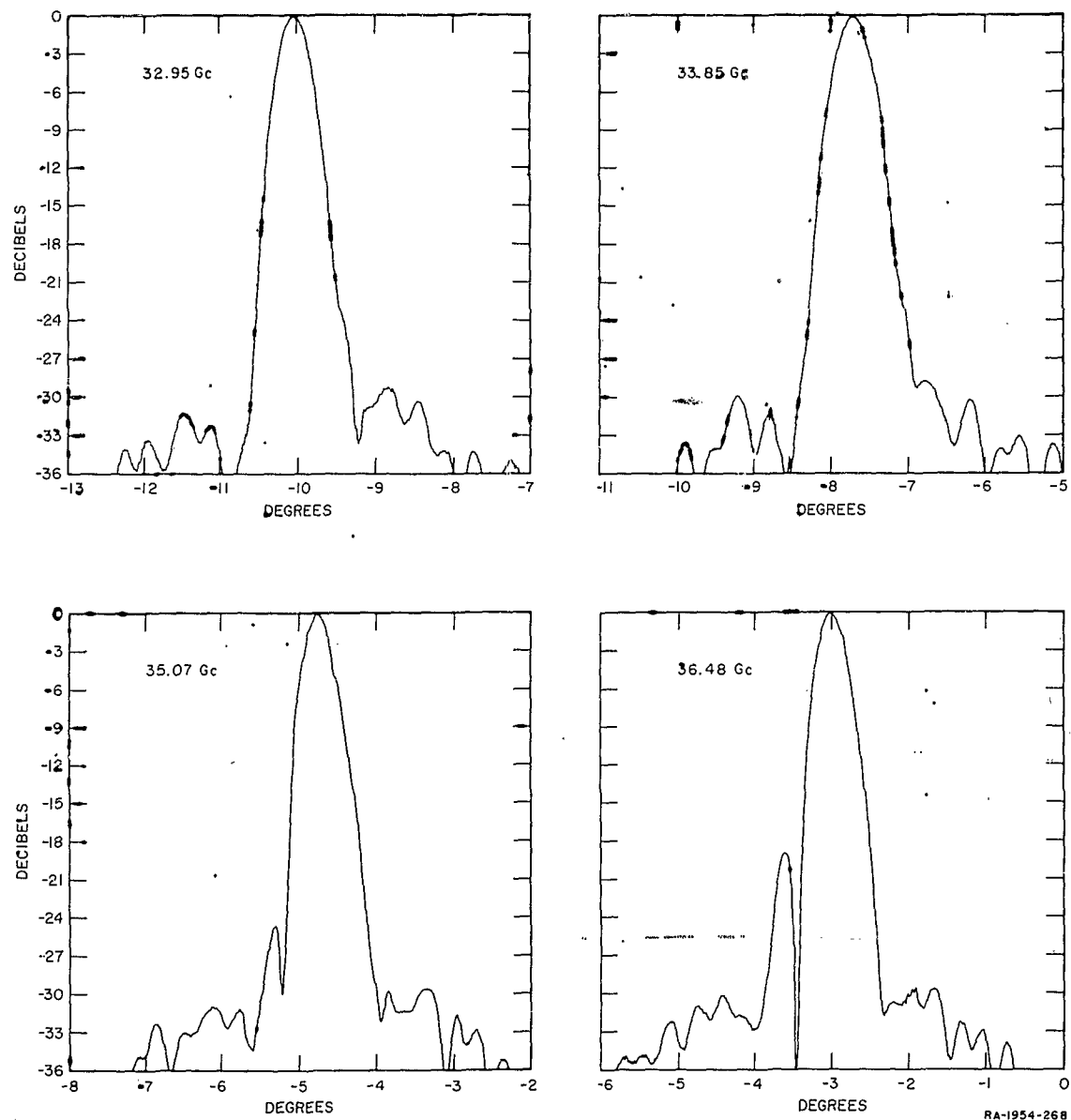


FIG. 11-12  
TYPICAL RADIATION PATTERNS - 32.95 TO 36.48 Gc

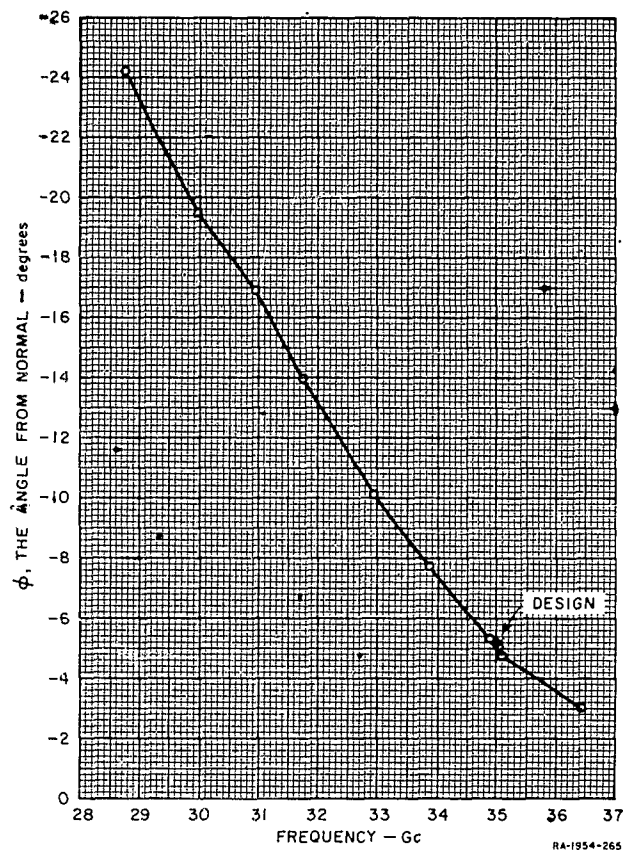


FIG. 11-13  
MEASURED BEAM POSITIONS  
AS A FUNCTION OF FREQUENCY

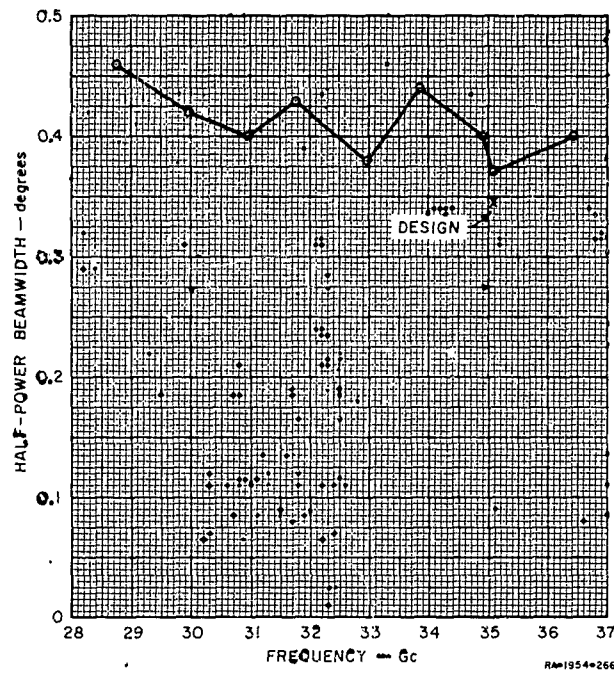


FIG. 11-14  
MEASURED BEAMWIDTH VS FREQUENCY

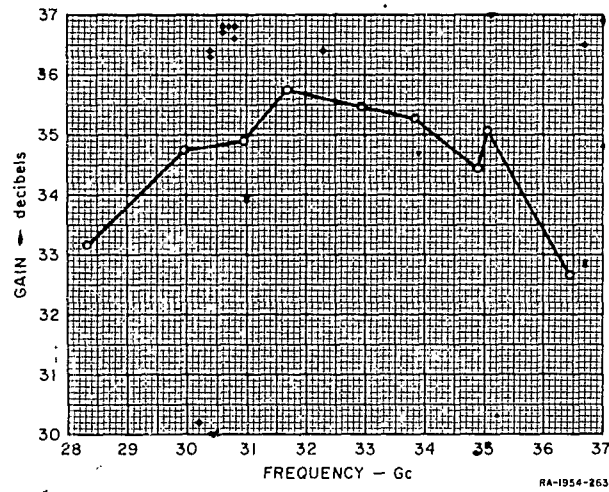


FIG. 11-15  
MEASURED GAIN VS FREQUENCY

The 3-db beamwidths of the main lobe do not change greatly over the same frequency band. These measured beamwidths are plotted in Fig. II-14, along with the theoretical beamwidth at the design frequency. The scatter in the experimental points is undoubtedly due to experimental errors in measuring such very narrow beams, but a general trend toward larger beamwidths at lower frequencies is still apparent. This increase in beamwidth is due both to the decrease in the frequency and to a decrease in the length of the projected aperture as the beam scans away from the normal to the aperture.

The gain of the modified Purcell array was also measured as a function of frequency by comparing it with that of a gain-standard horn with a computed gain of the order of 30 db. These gain measurements are plotted in Fig. II-15. It is here that the first discrepancy between the design parameters and the measured parameters becomes apparent. The theoretical directivity of such an array is given by

$$G = \frac{4\pi A}{\lambda^2} G_E G_H F$$

where

$\lambda$  is the free-space wavelength (0.3365 inch at 35.07 Gc)

$A$  is the area of the projected aperture  
( $3.4375 \times 60 \times \cos 5.25^\circ$  square inches)

$G_E$  is the  $E$ -plane gain-factor for the flared horn (0.695)

$G_H$  is the  $H$ -plane gain-factor for the 25 db Taylor distribution (0.90—see Ref. 5)

$F$  is the fraction of the input power to be radiated by the antenna (0.90 in this case).

This formula yields a directivity of 41 db, and allowing approximately 0.6 db for RF losses within the antenna (losses associated with propagation along a waveguide half the length of the array and out the slots<sup>2</sup>), a gain of 40.4 db.

The discrepancy of over 5 db has been attributed to the fact that the coupling coefficients of the slots are slightly less than anticipated, rather than to unsuspected RF losses or radiation in spurious directions.

The reasoning behind this proceeds as follows. First, the measured insertion loss of the antenna between input and output terminals is only 3.5 db at the design frequency. Furthermore, the input VSWR of the antenna is about 3.1 when a short-circuit is placed on the output end, corresponding to a matched attenuator of about 3.3 db. Allowing about 1.2 db for the dissipative losses from the input to the short circuit at the output end leaves about 2.2 db of attenuation due to radiation along the array. This corresponds to about 40 percent of the input power being radiated rather than the 90 percent design figure. This accounts for 3.5 db of the missing gain. The remaining loss in gain can then be attributed to the fact that the amplitude distribution along the array is asymmetric, or peaked up toward the load end of the antenna, and is more sharply tapered at each end of the array for the reasons described below. This distribution accounts for the lower-than-expected side lobes at the design frequency (see Fig. II-12), the filled-in nulls in the side-lobe region, and the slightly greater beamwidth. A certain amount of loss must also be allowed for the finite tolerances with which this antenna could be constructed, although it is felt that these losses are small as evidenced by the clean radiation patterns.

The fact that no appreciable power was being radiated in spurious directions due to higher-order modes being excited in the parallel-plane transmission line was confirmed by a careful search for spurious lobes in the complete hemisphere of the radiation pattern.

There are several causes for the discrepancy between the actual and the expected coupling coefficients in the final array. In the first place, an array that is as long as this one turns out to be extremely sensitive to small, cumulative errors in the coupling coefficients. Thus, an error of only 0.1 db in the measurements of the insertion loss of the 24-slot X-band test sections would result in an error of over 1.3 db in the final, 320-slot array. It is felt that the measuring technique itself was accurate within  $\pm 0.05$  db, but that the estimate of the RF losses in the X-band test sections could well be off by considerably more than this, particularly for the smaller slot sizes. The loss estimated for all the 18-inch-long X-band test sections in reducing the experimental data to produce the curve in Fig. II-7 was 0.1 db. Three of the four waveguide walls were silver-plated for these tests, but the fourth was aluminum alloy and all of the slots were milled in an aluminum alloy strip. For small

slot depths, the loss in propagating from the feeding waveguide to the parallel-plate transmission line could be appreciable, particularly since some reactive currents are involved between the two ends of the slot. Losses in the short circuits at the end of each test section must also be taken into account in the measurements. Thus, a total error of only 0.3 db in underestimating the total losses in these test sections would account for over half of the discrepancy in the final array.

The remaining discrepancy may be accounted for if the "unruly" experimental point shown in the lower left-hand corner of Fig. II-7 actually represents the true behavior of the slot coupling coefficients. A very appreciable portion of the slots in the final array, especially toward the feed end of the array, were designed using the data in the dashed portion of the curve in Fig. II-7. If the experimental point actually represents good data, then these slots have much smaller coupling coefficients than expected, and the amplitude distribution will be more tapered than expected. Evidence that this actually occurs is found in the radiation pattern at the design frequency (Fig. II-12) where the side lobes beyond the first are appreciably lower than those expected from a 25-db Taylor distribution (see Fig. II-2 of Ref. 1).

It is felt, then, that this experimental model of the modified Purcell array has demonstrated the following:

- (1) That the most severe cumulative tolerance problem, that of maintaining the phase velocity constant along the array, can readily be handled in the modified Purcell array by virtue of its mechanical simplicity and ruggedness.
- (2) That the problem of obtaining an adequate amplitude distribution along the aperture needs some further tests, particularly for the smaller slot sizes, but that the precision required in these tests is entirely within the current state of the art.

### C. ANALYSIS OF ARRAY JUNCTIONS

In this section some theoretical results are presented of the electrical performance of the modified Purcell array. This analysis was undertaken both because of the rather poor agreement between the experimental measurements and the approximate theory, and because a suitable analytical technique has been developed on another project in the



Microwave Group of Stanford Research Institute.\* This analysis can be accomplished by separating the problem into two parts. In the first part the junction of the feed waveguide and a slot is considered; the equivalent circuit of this junction is presented in this section. In the second part the junction of the slots and the parallel plate region is considered. Analytical results have not yet been obtained for the second part, but the same analytical technique can be applied to the second part that is applied to the first part. When the equivalent circuit for the junctions at each end of the slot is known, the power radiated by the slot and the phase velocity in the feed waveguide can be calculated.

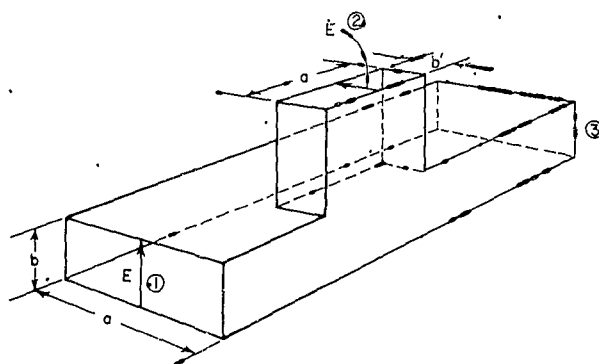


FIG. II-16  
JUNCTION BETWEEN FEED WAVEGUIDE AND SLOT

The junction between the feed waveguide and a slot is shown in Fig. II-16. For the junction between a single slot and the feed waveguide to accurately represent the junctions between many slots and the feed waveguide, the interaction between the disturbing fields of adjacent slots must be small. In a modified Purcell array many wavelengths long, the cross sections of the slots are small, and it is assumed here that the interactions between slots are small.

The equivalent circuit of the junction of Fig. II-16 is shown in Fig. II-17. This equivalent circuit is of the same form that is obtained for the *H*-plane rectangular waveguide *T*-junction in the *Waveguide Handbook*.<sup>6</sup> At the indicated terminal planes the equivalent circuit is a parallel connection of transmission lines, an ideal transformer, and a shunt susceptance. The characteristic admittances of the waveguides forming the junction are defined to be

$$Y_0 = \frac{1}{\eta} \frac{\lambda}{\lambda_g} \frac{a}{2b}, \quad \frac{Y'_0}{Y_0} = \frac{b}{b'}$$

\* This technique will be described in a subsequent report to be issued by SRI under another contract.

where  $\eta = 120\pi$  ohms is the impedance of free space, and  $\lambda$  and  $\lambda_g$  are the free-space and guide wavelengths, respectively.

Formulas for the exact equivalent-circuit parameters of this junction require the inversion of an infinite matrix; however, the equivalent-circuit parameters may be calculated to any desired accuracy by using a matrix

of sufficient size. These formulas for the equivalent circuit parameters were programmed on the Burroughs 220 computer at Stanford University to obtain numerical data.\* The numerical data for the equivalent circuit of the junction are presented in graphical form in Figs. II-18 and II-19 and tabulated in Table II-1. It is estimated that the data are accurate to at least 1/2 percent, based upon calculations using different sizes of matrices. The particular frequency and waveguide sizes were chosen to match those of the modified Purcell array reported in the previous section of this report. The program for the Burroughs 220 computer has been written so that the equivalent circuit parameters at other frequencies and for other waveguide sizes can be easily calculated

TABLE II-1  
EQUIVALENT CIRCUIT PARAMETERS  
OF JUNCTION WITH  
 $a = 0.900$  inch,  $b = 0.400$  inch  
and  $f = 10.91$  Gc

$\frac{b'}{b}$	$\frac{d}{a}$	$\frac{d'}{a}$	$\frac{B}{Y_0}$	$\frac{Y_0'}{n^2 Y_0}$
0.0	0.0	0.3760	-0.0	0.0
0.0625	0.0044	0.3261	-0.0403	0.0226
0.125	0.0080	0.3023	-0.0789	0.0423
0.1875	0.0113	0.2881	-0.1150	0.0598
0.250	0.0142	0.2808	-0.1476	0.0759
0.375	0.0189	0.2786	-0.1986	0.1058
0.500	0.0222	0.2840	-0.2323	0.1315

\* Acknowledgements are gratefully made to F. Kaye Tomlin who programmed the Burroughs 220 computer to obtain the numerical data.

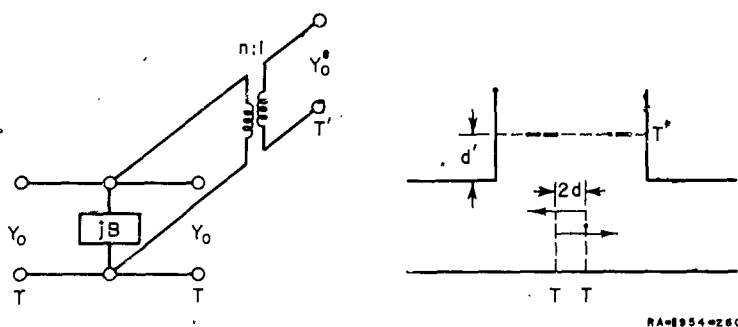


FIG. II-17  
EQUIVALENT CIRCUIT OF JUNCTION

To check the theoretical data, measurements were made upon an experimental model of the junction, with  $b'/b = 0.5$ . To measure the position of the terminal plane,  $T$ , a moving short circuit was placed in Arm 3 and moved until minimum signal was transmitted between Arms 1 and 2; the position of the short circuit so found is an integral number of half-guide wavelengths from the terminal

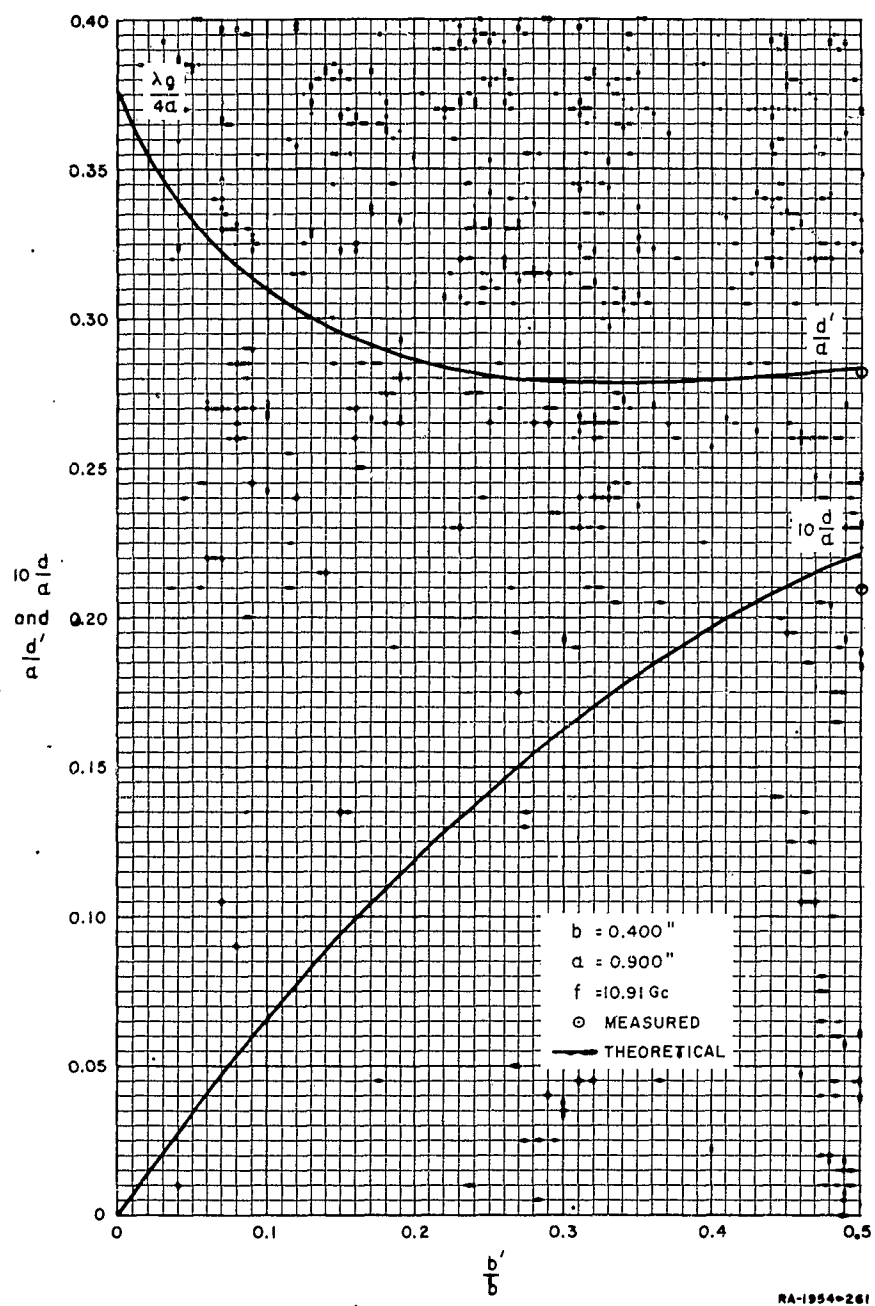


FIG. II-18  
TERMINAL-PLANE POSITIONS OF JUNCTION

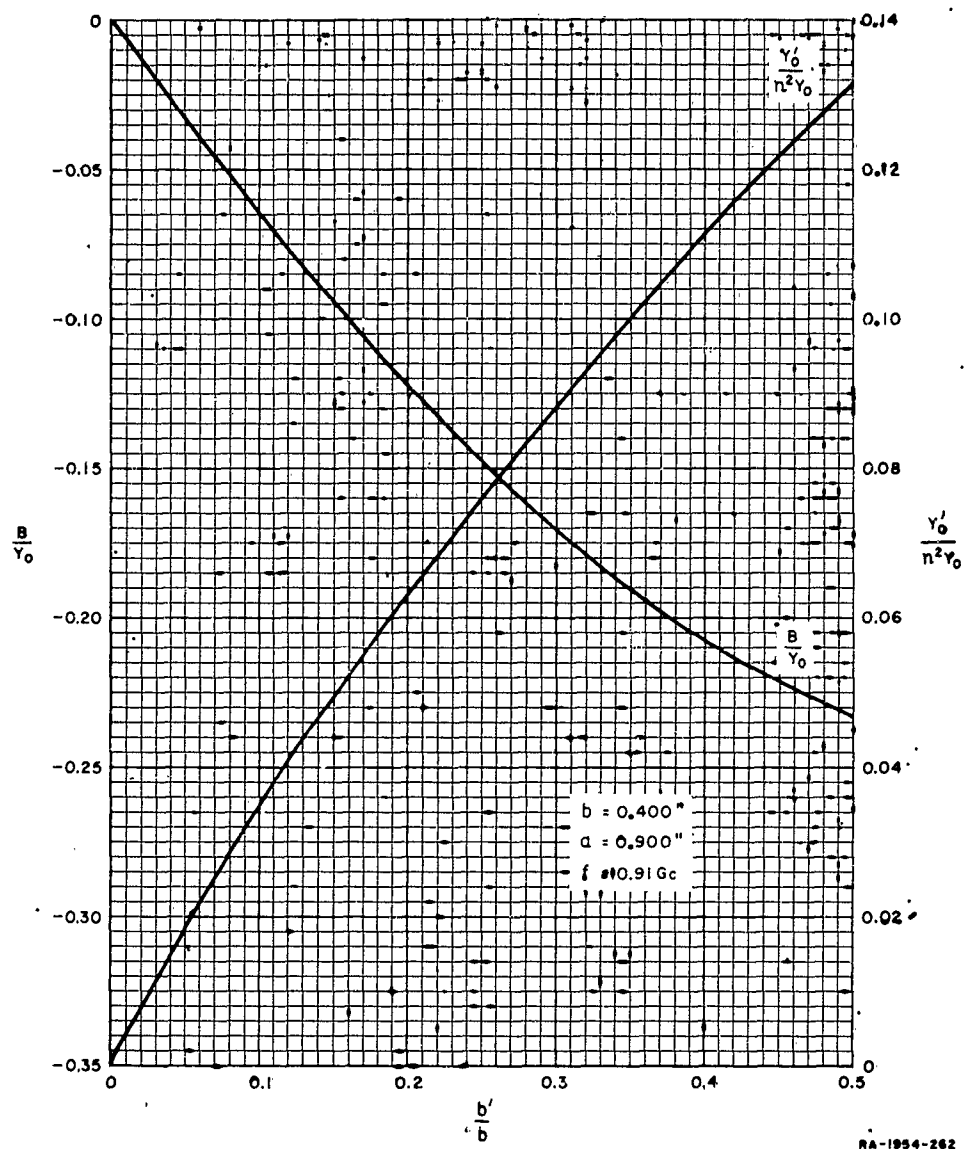


FIG. 11-19  
EQUIVALENT CIRCUIT PARAMETERS OF JUNCTION

plane,  $T$ . Similarly, to measure the position of the terminal plane,  $T'$ , a moving short circuit was placed in Arm 2 and adjusted so that minimum signal was transmitted between Arms 1 and 3. As shown in Table II-2 the measured and theoretical positions of the terminal planes agree very well. As a further check the voltage standing wave ratio looking into Arms 1 and 2 with matched terminations at the other arms was measured; also, the insertion loss between Arm 1 and Arms 2 and 3 was measured with matched terminations in all arms. The measured and theoretical VSWR and insertion loss agree quite closely.

TABLE II-2  
MEASURED AND THEORETICAL PARAMETERS OF JUNCTION  
FOR  
 $f = 10.91$  Gc,  $a = 0.900$  inch,  $b = 0.400$  inch

	$\frac{d}{a}$	$\frac{d'}{a}$	(VSWR) <sub>1</sub>	(VSWR) <sub>2</sub>	(I.L.) <sub>12</sub>	(I.L.) <sub>13</sub>
Measured	0.021	0.283	1.29	14.6	-9.7 db	-0.60
Theoretical	0.0222	0.2840	1.284	15.4	-9.41 db	-0.60

When the above equivalent circuit for the junction between the feed waveguide and the slot is combined with the equivalent circuit for the junction between the slots and the parallel plate region, the electrical performance of the modified Purcell array can be predicted very accurately.

## REFERENCES

1. R. C. Honey, L. A. Robinson, J. K. Shimizu, and W. J. Getsinger, "Antenna Design Parameters," Second Annual Report, Contract DA 36-039 SC-73106, SRI Project 1954, Stanford Research Institute, Menlo Park, California (January 1959).
2. R. C. Honey, L. A. Robinson and J. K. Shimizu, "Antenna Design Parameters," Third Annual Report, Contract DA 36-039 SC-73106, SRI Project 1954, Stanford Research Institute, Menlo Park, California (January 1960).
3. W. Sichak, E. M. Purcell, "Cosec<sup>2</sup> Antennas with a Line Source and Shaped Cylindrical Reflector," MIT Rad. Lab. Report 624, pp. 7-13, Massachusetts Institute of Technology, Cambridge, Massachusetts (November 1944).
4. S. Silver, *Microwave Antenna Theory and Design*, Rad Lab Series Vol. 12, pp. 328-337 (McGraw-Hill Book Company, Inc., New York City, 1949).
5. R. C. Hansen, "Gain Limitations of Large Antennas," IRE Transactions on Antennas and Propagation, V. AP-8, n. 5, pp. 490-495 (September 1960).
6. N. Marcuvitz, *Waveguide Handbook*, MIT Rad. Lab. Series Vol. 10, pp. 355-360 (McGraw-Hill Book Company, Inc., New York City, 1951).

### III INVESTIGATIONS OF LINEAR ARRAYS

#### A. LINEAR ARRAYS WITH VARIABLE INTERELEMENT SPACINGS

##### 1. INTRODUCTION

Linear arrays with variable interelement spacings have received increasing attention in recent years.<sup>1-8\*</sup> The reason for this interest is primarily that a considerable saving in the number of array elements is possible in large directional antenna arrays where high resolution rather than high gain is most important. Furthermore, by changing the interelement phase, the main beam of the radiation pattern can often be steered through a wider angle and over a much larger frequency bandwidth than is possible with equispaced arrays. Both equally and unequally spaced linear arrays are very simple to analyze. Well-developed methods are also available for designing linear antenna arrays with equispaced elements that will produce a desired space factor with reasonable accuracy. Most of these methods, theoretical as well as experimental, make use of the fact that the space factor of an array of equispaced elements can be expressed as a polynomial, the coefficients of which are used to determine the array excitation coefficients. Dolph<sup>9</sup> designed a theoretical optimum broadside array with equispaced elements making use of the properties of the Tchebyscheff polynomials. DuHamel<sup>10</sup> extended Dolph's method to the case of an end-fire array with equispaced elements. For an arbitrary pattern, Woodward and Lawson<sup>11</sup> have given a method of designing a linear array of equispaced elements which will produce a space factor that exactly equals a desired space factor in a number of directions in space which are chosen equidistant in  $\sin \theta$ ,  $\theta$  being the angle between the normal to the array axis and the direction of observation.

The space factor of an array of equispaced elements is a periodic function. It is thus generally necessary to choose the interelement spacing not larger than one-half wavelength in order to avoid more than one period of the space factor appearing in visible space. In special cases, where more than one period of the space factor can be allowed in

---

\* References are listed at the end of the section.

visible space, a larger spacing can be chosen. For example, the spacing can be close to one wavelength for a broadside array before several pencil beams will appear.

Spacings of less than one-half wavelength are not very practical: with such small spacings, the coupling between the elements of the array will be strong, and the prescribed excitation coefficients of the array may be hard to realize. Therefore, a linear array of equispaced elements can seldom be used to cover a large bandwidth.

For arrays with variable interelement spacings, a prescribed space factor can be approximated more closely than with constant spacings. The reason for this is that, by choosing the spacings as independent variables, an additional degree of freedom is gained which can be used to control the radiation pattern. This has been discussed by Unz.<sup>1</sup> Very often, however, a good approximation to a space factor that is given in advance can still only be obtained when the average interelement spacing is not larger than one-half wavelength. As an example, an array where the elements are spaced according to the zeros of a Legendre polynomial of the same order as the number of elements can be made to approximate a given space factor very closely; however, the average interelement spacing must be less than one-half wavelength.<sup>3</sup>

When the array is to be used as a directional antenna with high resolution rather than high gain, the unequally spaced array will, however, often be much superior to the equispaced array. The unequally spaced array requires fewer elements to produce a certain resolution, and the main beam can be steered over a larger frequency bandwidth than is possible with an equispaced array. However, there is a lower limit to the side-lobe level attainable.

None of the theoretical methods of synthesis mentioned above can be used for variable element spacings, since these methods take as their starting point space factors that can be expressed as polynomials. An analysis of various directional arrays with variable spacings has been made by King, Packard, and Thomas.<sup>2</sup> In that analysis, all elements are excited identically, and the average element spacing is larger than one wavelength.

Directional arrays with variable spacings have been investigated by a perturbation method by R. F. Harrington,<sup>8</sup> with the purpose of reducing

the side-lobe level of an array with constant excitations. The side-lobe reduction achieved by Harrington is only effective when the average element spacing is less than some maximum value between one-half and one wavelength.

Since no adequate theory exists for designing directional linear arrays with large variable interelement spacings, some experiments have been performed using analog and digital computer techniques to get some insight in the properties of these arrays. The results of these experiments will be reported and discussed. Only symmetric linear arrays with a constant magnitude of excitation have been studied. The excitation of the elements was chosen to be constant, since that will result in the maximum gain from a given number of elements, neglecting mutual effects.

## 2. GENERAL

Restricting the analysis to arrays with odd numbers of elements, the space factor of a symmetric linear array with  $2N + 1$  elements radiating broadside is given by

$$G(\theta) = \sum_{n=0}^N \epsilon_n A_n \cos(kz_n \sin \theta) \quad , \quad (\text{III-1})$$

where  $A_n$  is the real excitation of the  $n$ th element pair away from the center element, and  $z_n$  is the distance from the elements of this pair to the center element as shown in Fig. III-1.  $\epsilon_n$  is Neumann's number defined by

$$\epsilon_n = \begin{cases} 1 & \text{for } n = 0 \\ 2 & \text{for } n > 0 \end{cases}$$

The excitations  $A_n$  are normalized so that the space factor has its maximum value, unity, in the broadside direction  $\theta = 0$ , i.e.,

$$\sum_{n=0}^N \epsilon_n A_n = 1$$

The angle  $\theta$  is the angle between the direction of observation and the broadside direction;  $k = 2\pi/\lambda$  is the intrinsic propagation constant; and  $\lambda$  is the free-space wavelength.



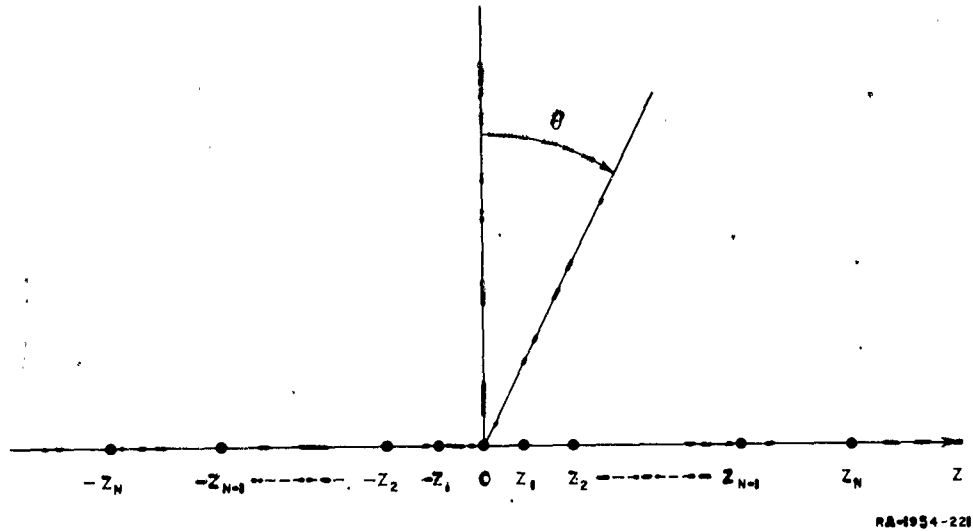


FIG. III-1  
SYMMETRIC LINEAR ARRAY WITH  $2N + 1$  ELEMENTS

To steer the main beam to a direction  $\theta = \theta_0$ , the phase of excitation of the elements shall vary linearly along the array axis so that the excitation of the  $n$ th element pair becomes  $A_n e^{\pm j k z_n \sin \theta_0}$  with the time factor  $e^{j \omega t}$ . The space factor will then be given by

$$G(\theta) = \sum_{n=0}^N \epsilon_n A_n \cos [k z_n (\sin \theta - \sin \theta_0)] \quad (\text{III-2})$$

Except for a translation of  $\sin \theta_0$  along a  $\sin \theta$  axis, this space factor is the same as that for the broadside array. Therefore, the beam-steering properties of the array can be seen immediately, once the broadside radiation pattern is known. As we shall see below, steerability is achieved at the expense of bandwidth.

The computations reported in the following are applied directly to broadside arrays. The synthesized radiation patterns have been plotted as a function of  $d_{av}/\lambda \sin \theta$ , where  $d_{av}$  is the average interelement spacing in the array. If the maximum value of  $d_{av}/\lambda \sin \theta$  that can be used before a side lobe will exceed the synthesized side-lobe level is  $w_0$ , and if the

main lobe is to be steered within the range  $-\theta_0 \leq \theta \leq \theta_0$  in space, then it is necessary that

$$\frac{d_{av}}{\lambda} (1 + \sin \theta_0) \leq w_0 .$$

The shortest wavelength at which the array can be operated,  $\lambda_{min}$ , is therefore given by

$$\frac{d_{av}}{\lambda_{min}} (1 + \sin \theta_0) = w_0 . \quad (\text{III-3})$$

Theoretically, the array can be operated at any wavelength exceeding  $\lambda_{min}$ . However, if some of the spacings in the array are smaller than one-half wavelength, difficulties will be encountered in realizing the array due to mutual coupling between elements. Therefore, we shall define a largest operating wavelength,  $\lambda_{max}$ , of the array by the relation

$$\lambda_{max} = 2d_{min} \quad (\text{III-4})$$

where  $d_{min}$  is the smallest spacing between adjacent elements in the array. Define the maximum bandwidth of the array by

$$B = \frac{\lambda_{max}}{\lambda_{min}} ,$$

and, with reference to Eq. (III-3), the steerability of the array by

$$1 + \sin \theta_0 ,$$

which increases from one to two when the beam steering range about the broadside direction is increased from zero to cover the whole visible space. The product of the bandwidth and the steerability [see Eq. (III-3)] is then given by

$$B(1 + \sin \theta_0) = \frac{2w_0}{d_{av}/d_{min}} . \quad (\text{III-5})$$

$w_0$  may also be interpreted as the maximum average interelement spacing, measured in wavelengths, that can be used in a broadside array before side lobes stronger than the synthesized side-lobe level appear in space. Since the right-hand side of this equation is a constant that is characteristic of the array, steerability is achieved at the expense of narrowed bandwidth, and vice versa. The product of bandwidth and steerability increases as the ratio between the average and the smallest interelement spacing decreases. This does not mean that the array with constant interelement spacings is better than an array with variable interelement spacings, since  $w_0$  can be made much larger for an array with variable interelement spacings than for an array with constant interelement spacings. Actually, the maximum value of  $w_0$  for an array with constant interelement spacings is only slightly less than 1. The product of bandwidth and steerability is, therefore, only slightly less than 2 for the array with constant interelement spacings. Since a product of 2 is required to steer the main beam through all directions of space at a single frequency, this array cannot even be used to obtain complete steerability at one frequency. Most of the arrays synthesized in the following have bandwidth-steerability products much larger than 2 and hence will have complete steerability over a finite bandwidth.

Given the width of the main lobe of the radiation pattern and the number of elements of a broadside array, the computations described below will determine

- (1) The total length of the array required to produce the given width of the main lobe
- (2) The element positions with an attempt to minimize the side-lobe level.

The beamwidth of the main lobe is rather insensitive to changes of the element positions and to the total number of elements; it depends primarily on the total length of the array. Unless the excitations of the elements are strongly tapered, and the interelement spacings vary wildly, the following formula can be used with reasonable accuracy for determining the total length,  $L$ , of a broadside array required to produce a 3-db beamwidth,  $\Delta\theta$ , where it is assumed that  $\Delta\theta \ll 1$  radian

$$\frac{L}{\lambda} \approx \frac{1}{\Delta\theta} \quad \text{(III-6)}$$

When the array length has been chosen, the distance of the end elements to the array center is

$$z_N = \frac{L}{2}$$

Broadside arrays with variable interelement spacings are of great practical importance when the average spacing is larger, preferably much larger than one wavelength. For such arrays, the number of elements used in conventional arrays to obtain given directional characteristics can be markedly reduced. Therefore, only arrays with large average interelement spacings will be considered. Because the elements are assumed to be spaced much more than one wavelength apart, the achievable side-lobe level will be expected to have a lower limit. This can perhaps best be understood by considering first a broadside array of equispaced omnidirectional elements. To avoid strong grating lobes in the radiation pattern, the spacing between neighboring elements must be smaller than about one wavelength. If the spacing in the equispaced broadside array is allowed to exceed one wavelength, the beamwidth of the main beam becomes smaller. However, at the same time a number of grating lobes with the same level as the main lobe appear in space. These grating lobes can be suppressed to some extent without influencing the level of the main lobe and without influencing appreciably the beamwidth of the main beam by suitably rearranging the elements of the array. However, the lobes outside of the main beam cannot be suppressed to an arbitrarily low level. The lowest obtainable side-lobe level depends in particular on the number of elements used in the array; the larger the number of elements, the lower the theoretical limit of the side-lobe level. This theoretical limit of the side-lobe level can be predicted very easily for the case of a very long array. For such arrays, the beamwidth of the main lobe depends essentially upon the length of the array and only slightly on the number of elements in the array and on the way the elements have been arranged. As the length of an array with a constant number of elements is increased, the power radiated into the main lobe decreases and very soon becomes negligible compared to the power radiated in the side lobes.<sup>12</sup> Consequently, the average gain in the side-lobe region is very nearly unity. The lowest level to which the highest side lobe can be suppressed depends on the arrangement of the elements in the

array. If the array could be designed to have equal side lobes, the lowest obtainable side-lobe level would be  $-(G - 3)$  db, where  $G$  is the gain of the array in the principal direction, when it is assumed that the space factor oscillates rapidly in the side-lobe region. When all elements are given the same excitation and mutual couplings are neglected the array gain equals the number of array elements. The theoretical lower limit for the side-lobe level then is

$$B = -10 \log \left( \frac{M}{2} \right) \text{ db} \quad (\text{III-7})$$

where  $M$  is the number of array elements. According to this formula, lower side-lobe levels can be obtained with more elements in an array. However, the optimum space factor of an unequally spaced array will usually not have equal side lobes, but will contain a number of side lobes that are stronger than the rest. For this reason, the minimum obtainable side-lobe level is higher than given by Eq. (III-7), although it has not been possible to predict just how much higher.

Equation (III-7) is an approximate expression for the theoretical lower limit of the side-lobe level. A more accurate expression will now be derived. Assume that each element of an array of  $M$  elements is fed by the power  $P$ . Neglecting mutual effects, and assuming each element to be an isotropic radiator, the power gain of the array is  $M$ . The power radiated per steradian in the principal direction then is

$$S = \frac{M^2 P}{4\pi}$$

According to Eq. (III-6), the 3-db beamwidth of the main lobe is approximately  $\lambda/L$  when  $L \gg \lambda$  where  $L$  is the array length. The power radiated in the main lobe therefore is approximately

$$P_0 = M^2 P \frac{\lambda}{2L}$$

The power radiated into the side-lobe region is thus

$$P_s = MP - P_0 = MP \left( 1 - M \frac{\lambda}{2L} \right) = MP \left( 1 - \frac{\lambda}{2d_{av}} \right)$$

where  $d_{av}$  is the average interelement spacing in the array. The average power density in the side-lobe region accordingly is

$$10 \log \left( \frac{M}{1 - \frac{\lambda}{2d_{av}}} \right) \text{ db}$$

less than the power density in the principal direction. When the space factor oscillates rapidly in the side-lobe region we conclude that the theoretical lower limit of the side-lobe level is

$$B = -10 \log \left( \frac{M}{2} \right) - 10 \log \left( \frac{1}{1 - \frac{\lambda}{2d_{av}}} \right) \text{ db} \quad (\text{III-8})$$

It will be noted that Eqs. (III-7) and (III-8) give the same result for  $d_{av} \gg \lambda$ , and that Eq. (III-8) predicts a lower side-lobe level for smaller spacings.

### 3. ARRAY COMPUTATIONS

#### a. GENERAL

In the computations described below the positions of the elements of an array have been changed in an attempt to further reduce the side-lobe level. Unfortunately, the problem of finding optimum arrays with variable interelement spacings, i.e., arrays for which the side-lobe level cannot be reduced by making small changes of the positions of the elements (excluding end elements), does not have a unique solution, but there are numerous "optimum" solutions which lead to different element arrangements and to different side-lobe levels. Which one of these solutions will be found in the computations will depend upon the initial array chosen, i.e., the array with which one starts the computations. The computations will systematically change the element positions in such a way as to further reduce the side-lobe level. As the maximum side-lobe level is reduced during the computations, more and more side lobes approach close to this level. However, there will probably be a limit to the number of side lobes reaching the maximum side-lobe level. It is reasonable to expect that if there are  $N$  element positions which are varied to

improve the over-all side-lobe level, then one can improve the side-lobe level only as long as the radiation pattern contains less than about  $N$  side lobes reaching the maximum side-lobe level. When about  $N$  side lobes have reached the maximum side-lobe level, it is unlikely, although not impossible, that any improvement of the radiation pattern can be obtained by further small changes in the element positions.

#### b. COMPUTATIONS WITH ANALOG COMPUTER

Analog machines have sometimes been used to synthesize linear and planar arrays.<sup>13,14,15</sup> An analog computer is particularly suitable for the design of symmetric linear arrays and compares favorably with a digital computer. According to Eq. (III-4), the space factor of a symmetric, linear, unequally spaced array is a sum of cosine-functions. In the analog computer, these cosine-functions can be simulated by harmonic but nonharmonically related electrical oscillations. By combining the oscillations according to the space factor Eq. (III-1), and displaying the resulting time function on the screen of a cathode-ray oscillograph, it is a simple matter to observe the radiation pattern of an unequally spaced linear array

Let the time function formed by the analog computer be

$$V(t) = \sum_{n=0}^N V_n \cos(\omega_n t) \quad (\text{III-9})$$

where  $V_n$  is the amplitude and  $\omega_n$  the angular frequency of the  $n$ th oscillation. The relations expressing the analog between the space factor Eq. (III-1), and the time function, Eq. (III-9), are immediately seen to be

$$V_n = \epsilon_n A_n \quad (\text{III-10})$$

and

$$\omega_n t = k z_n \sin \theta \quad (\text{III-11})$$

Introducing the frequency  $f_n$  rather than the angular frequency  $\omega_n$ , Eq. (III-11) is reduced to

$$f_n t = \frac{z_n}{\lambda} \sin \theta \quad (\text{III-12})$$

The computations are started at the time  $t = 0$  with all oscillations in the same phase. The time function, Eq. (III-9), is displayed in a time interval  $T$  that, according to Eq. (III-12), is related to the maximum used frequency  $f_N$  and the array length  $L$  as follows

$$f_N T = \frac{z_N}{\lambda} = \frac{L}{2\lambda} \quad (\text{III-13})$$

From Eq. (III-12) it is then deduced that

$$\frac{t}{T} = \sin \theta \quad (\text{III-14})$$

and

$$\frac{f_n}{f_N} = 2 \frac{z_n}{L} \quad (\text{III-15})$$

When the analog computer is capable of computing the space factor several times per second, the element positions and excitations can be varied manually, and, by observing the effects on the radiation pattern, it is expected that a near-optimum array can soon be found.

Since a fast analog computer was not available, only a few arrays were synthesized by analog-computer techniques. Results obtained for an eleven-element array with an average spacing of three wavelengths were slightly improved by a digital computer. These results will be presented in Part A-3-c.

#### c. COMPUTATIONS WITH DIGITAL COMPUTER

Although the array synthesis problem is particularly well suited for an analog computer, it may be worthwhile also to attempt solving the problem with a digital computer. The use of a digital computer for array synthesis problems may become more expensive than the use of an analog computer; however, the digital computer can solve the problem with much higher accuracy. This is of particular value in the final stages of the computations where a reasonably good array has already been obtained and it is desired to further improve this array by very small changes in the element positions. In these final steps of the



computations the element positions are changed in a very systematic way, and the logic used in the code for a digital computer becomes correspondingly simple.

The time used by the digital computer to compute one radiation pattern to determine the side-lobe level depends on the number of elements in the array, on the array length, and on the number of element positions that are being changed between consecutive computations of two patterns. As an example, the optimum positions of one pair of elements of a 51-element array with average spacing  $3\lambda$  were determined by the computer in an average time of about six minutes. The time used by a fast analog computer to display the same pattern could probably be reduced to less than ten seconds, depending on the accuracy called for. In the initial steps of the computations where very high accuracy is not required, and where the element positions may have to be changed a considerable number of times, often in a very unsystematic way, a fast analog computer should, therefore, be considered superior to a digital computer.

The computations described below were made on a Burroughs 220 computer available in Stanford Research Institute. When an initial array is fed into the computer, the machine computes the side-lobe level of the pattern of this array. One of the elements of the array is then moved to one side of its initial position, first in coarse steps of about one-sixth of a wavelength, then in fine steps of about one-sixtieth of a wavelength; the side-lobe level is computed after each change of element position, until the position giving the lowest side-lobe level has been found. Hereafter, the element is moved to the other side of its initial position in a similar way to find the best element position on this side of the initial position. (One or both of these better positions may eventually coincide with the initial position.) Henceforth, the computer compares the side-lobe levels for these two positions of the element and rejects the position giving the higher side-lobe level. With the better element position, the computer proceeds to perform the same type of changes of the position of the next element of the array, and so forth. When the positions of all elements except for the center element and the end elements have been successively changed, a new loop of computations is started. Computations are continued until the improvement of the side-lobe level obtained for the last loop is smaller than a certain number. The number of computational loops needed to arrive at the best array was in no case more than four.

Computations were made with the objective of synthesizing symmetrical arrays with 11, 21, and 51 elements each. The elements were given the same excitation, and the average spacing was held constant and equal to 2 or 3 wavelengths during the computations. The initial arrays fed into the computer are summarized in Table III-1. A description of these arrays will be given below.

The synthesized radiation patterns for broadside operation are shown in Figs. III-2 to III-10. In these figures, the side lobes are shown on the same side. The patterns are normalized to unity and are plotted as functions of  $d_{av}/\lambda \sin \theta$ . After the best positions of the elements of an array

TABLE III-1  
INITIAL ARRAYS USED IN COMPUTATIONS  
WITH DIGITAL COMPUTER

INITIAL ARRAY NO.	DESCRIPTION
1	Uniform array
2	Array found with analog computer
3	Controlled cosines array
4	Legendre array.

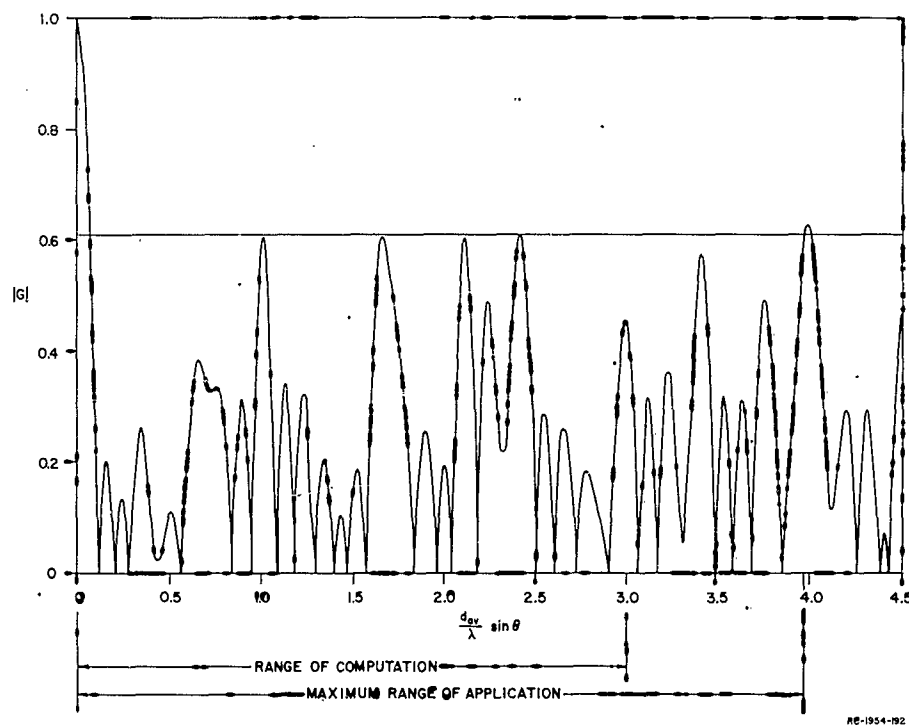
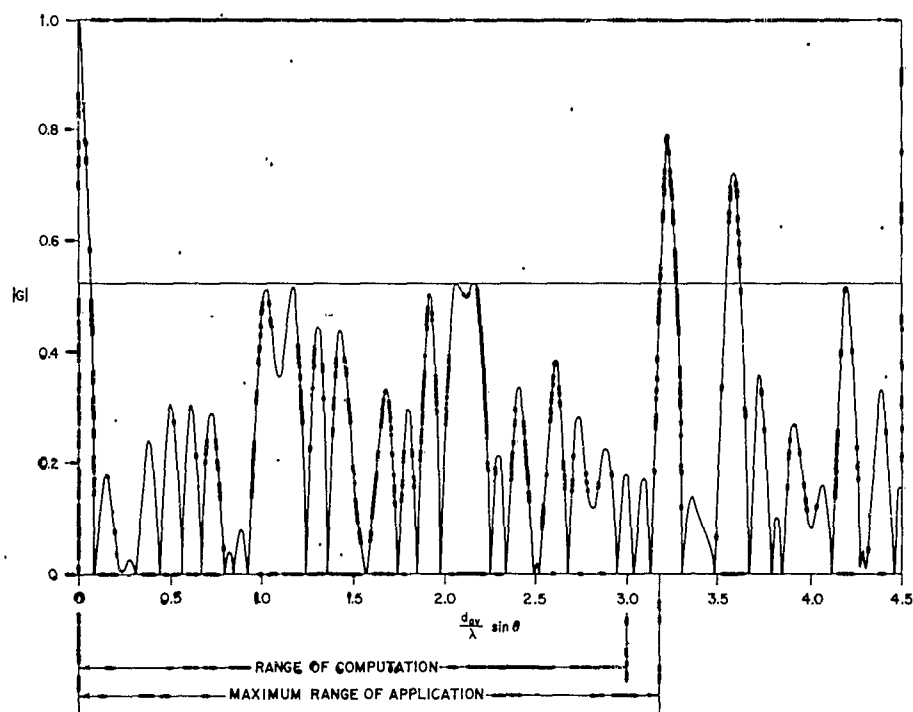


FIG. III-2  
SPACE FACTOR OF 11-ELEMENT ARRAY SYNTHESIZED  
FROM INITIAL ARRAY 1- $d_{av} = 3\lambda$



NC-1954-194

FIG. 111-3  
SPACE FACTOR OF 11-ELEMENT ARRAY SYNTHESIZED  
FROM INITIAL ARRAY  $2-d_{av} = 3\lambda$

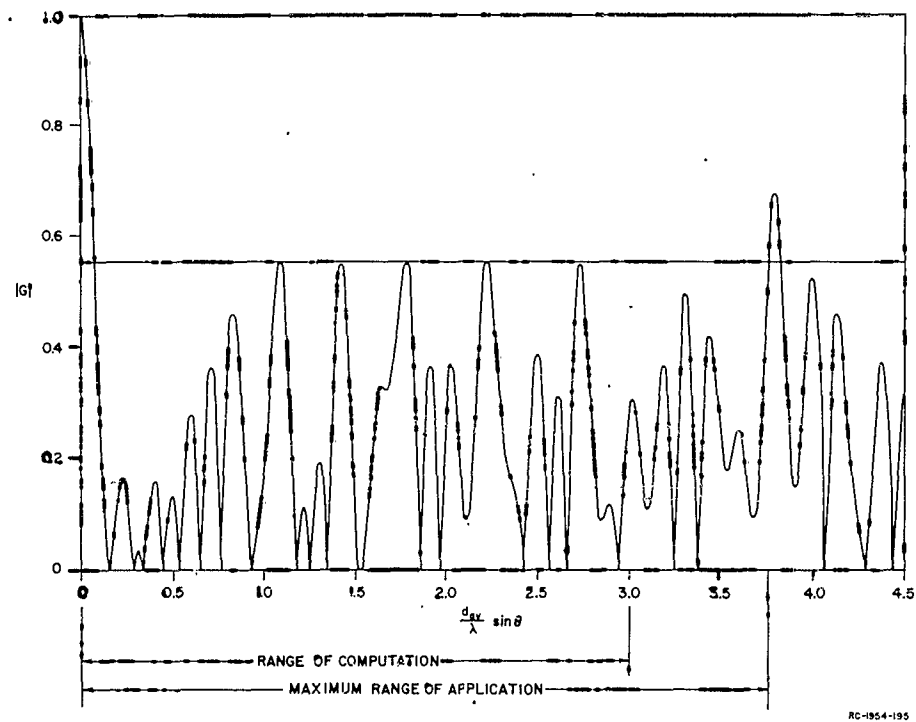


FIG. 111-4  
 SPACE FACTOR OF 11-ELEMENT ARRAY SYNTHESIZED  
 FROM INITIAL ARRAY 3— $d_{av} = 3\lambda$

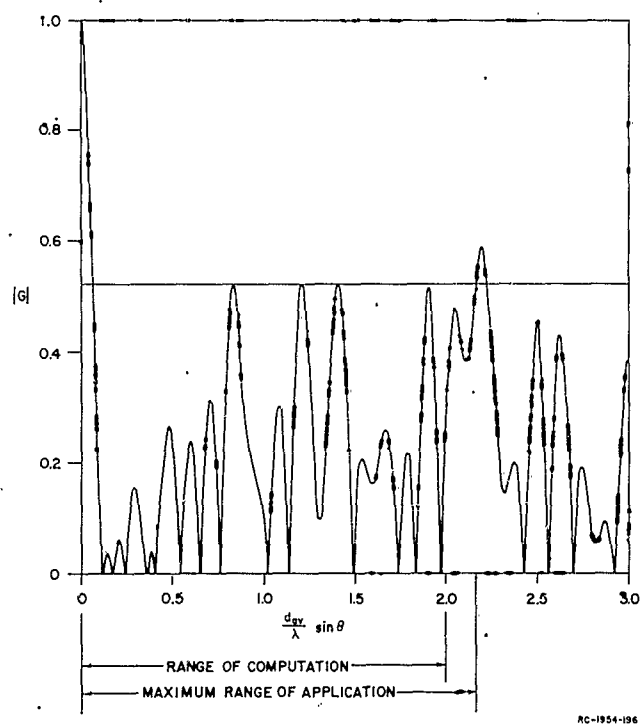
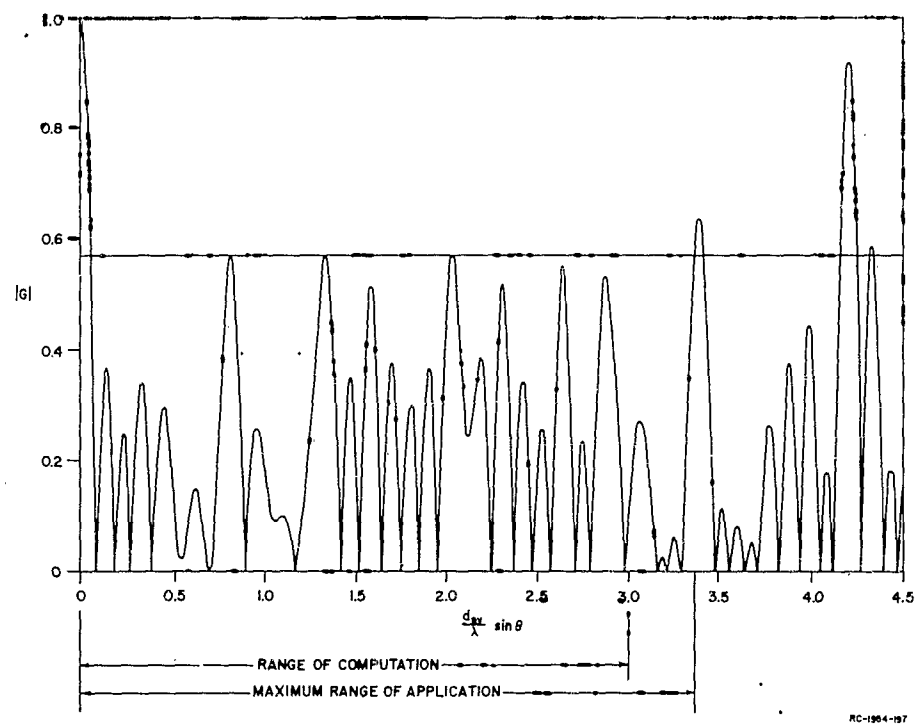
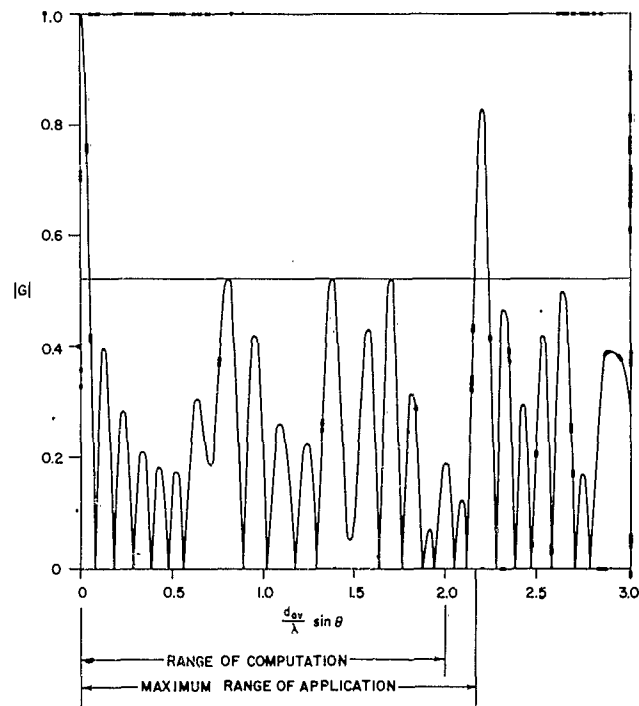


FIG. 111-5  
 SPACE FACTOR OF 11-ELEMENT ARRAY SYNTHESIZED  
 FROM INITIAL ARRAY  $3-d_{av} = 2\lambda$



RC-1964-197

FIG. III-6  
SPACE FACTOR OF 11-ELEMENT ARRAY SYNTHESIZED  
FROM INITIAL ARRAY  $4-d_{av} = 3\lambda$



RC-1954-198

FIG. III-7  
SPACE FACTOR OF 11-ELEMENT ARRAY SYNTHESIZED  
FROM INITIAL ARRAY 4— $d_{av} = 2\lambda$

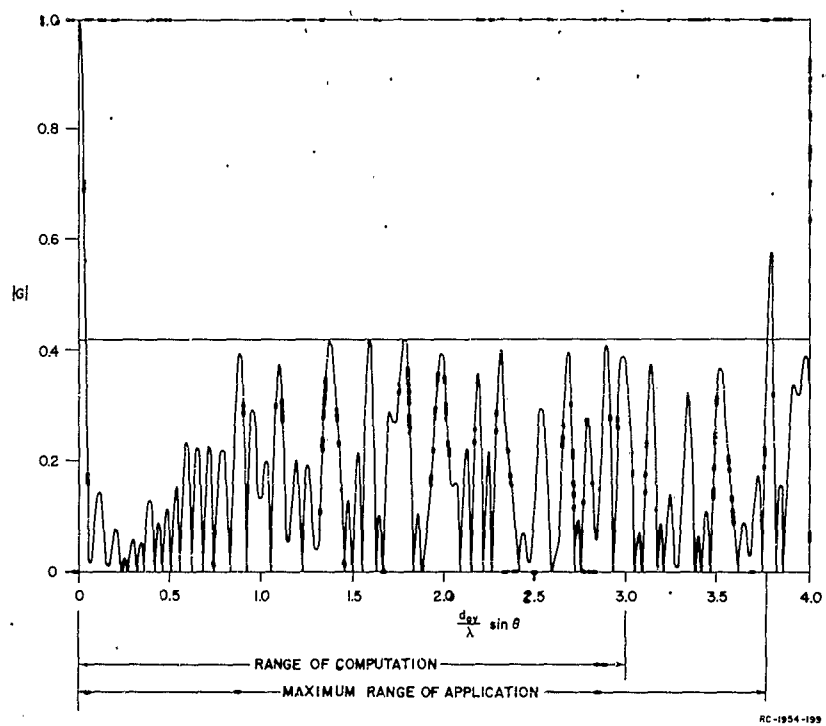


FIG. III-8  
 SPACE FACTOR OF 21-ELEMENT ARRAY SYNTHESIZED  
 FROM INITIAL ARRAY 3  $\rightarrow d_{av} = 3\lambda$



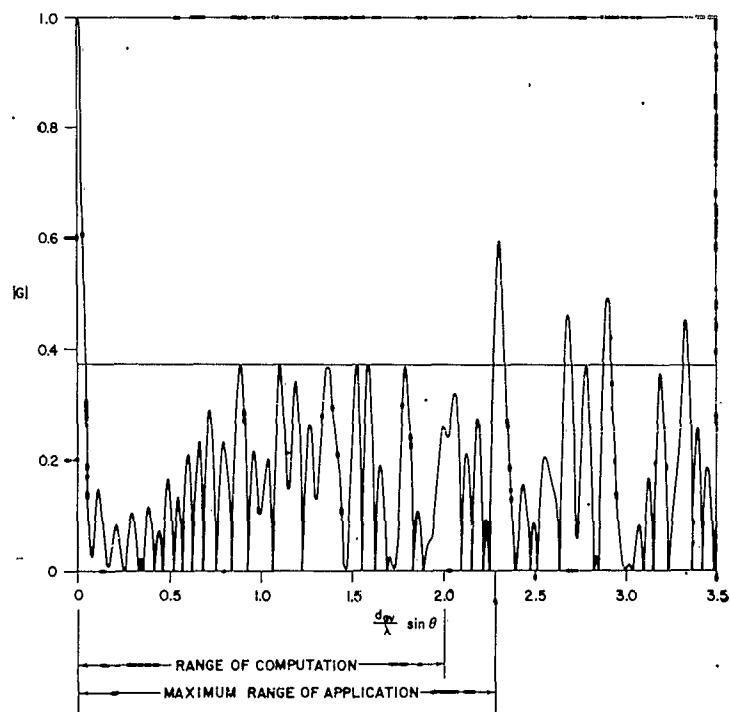


FIG. III-9  
 SPACE FACTOR OF 21-ELEMENT ARRAY SYNTHESIZED  
 FROM INITIAL ARRAY 3— $d_{av} = 2\lambda$

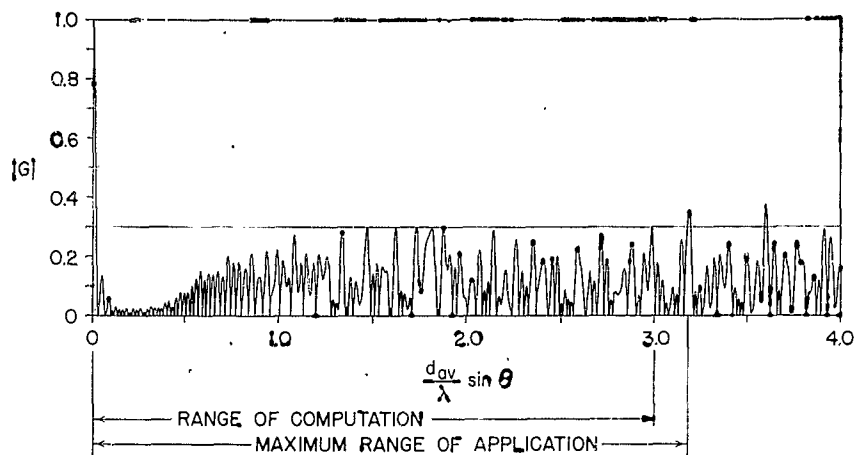


FIG. III-10  
SPACE FACTOR OF 51-ELEMENT ARRAY SYNTHESIZED  
FROM INITIAL ARRAY 3— $d_{av} = 3\lambda$

were determined, the final radiation pattern was computed over a larger range of  $d_{av}/\lambda \sin \theta$  than was used in synthesizing the array. As shown in the figures, the arrays can in most cases be used over a somewhat larger range than the range of computation without increasing the synthesized side-lobe level.

The data of the initial arrays and of the arrays synthesized from the initial arrays are presented in Tables III-2 and III-3 for 11-element arrays, in Tables III-4 and III-5 for 21-element arrays, and in Tables III-6 and III-7 for a 51-element array. All element positions in Tables III-2, III-4 and III-6 are normalized to unity for the end elements. Also in these tables, the maximum array length, the maximum average spacing and the minimum spacing that can be used before the side-lobe level will exceed the synthesized side-lobe level, can be found. The average spacing associated with the initial arrays in these tables shall be interpreted as the average spacing for which computations were made. The minimum spacing determines the maximum product of bandwidth and steerability, Eq. (III-5), for which the side-lobe level of the array will not exceed the synthesized level and no spacing will be smaller than one-half wavelength. This product is listed in Tables III-3, III-5, and III-7. The properties of the broadside array, as characterized by the 3-db beamwidth of the main lobe, the side-lobe level, and the approximate gain are

TABLE III-2  
11-ELEMENT ARRAYS SYNTHESIZED WITH DIGITAL COMPUTER

ARRAY	ARRAY LENGTH IN WAVELENGTHS	AVERAGE SPACING IN WAVELENGTHS	MINIMUM SPACING IN WAVELENGTHS	NORMALIZED ELEMENT POSITIONS						RAD. PATTERN FIG. NO.
				$z_0$	$z_1$	$z_2$	$z_3$	$z_4$	$z_5$	
Initial Array 1	--	3.0	--	0.000	0.200	0.400	0.600	0.800	1.000	--
Synthesized Array	38.3	3.83	1.91	0.000	0.248	0.348	0.607	0.822	1.000	2
Initial Array 2	--	3.0	--	0.000	0.178	0.383	0.561	0.682	1.000	--
Synthesized Array	31.6	3.16	1.85	0.000	0.179	0.384	0.560	0.677	1.000	3
Initial Array 3	--	3.0	--	0.000	0.128	0.282	0.462	0.692	1.000	--
Synthesized Array	37.5	3.75	2.02	0.000	0.108	0.264	0.460	0.694	1.000	4
Initial Array 3	--	2.0	--	0.000	0.128	0.282	0.462	0.692	1.000	--
Synthesized Array	21.6	2.16	1.11	0.000	0.179	0.282	0.460	0.684	1.000	5
Initial Array 4	--	3.0	--	0.000	0.276	0.531	0.746	0.907	1.000	--
Synthesized Array	33.5	3.35	1.62	0.000	0.292	0.480	0.761	0.903	1.000	6
Initial Array 4	--	2.0	--	0.000	0.276	0.531	0.746	0.907	1.000	--
Synthesized Array	21.3	2.13	0.98	0.000	0.283	0.546	0.747	0.908	1.000	7

TABLE III-3  
RADIATION PATTERN DATA OF 11-ELEMENT ARRAYS SYNTHESIZED WITH DIGITAL COMPUTER

ARRAY	AVERAGE SPACING IN WAVELENGTHS	BANDWIDTH x STEERABILITY $B(1 + \sin \theta_0)$	SIDE-LOBE LEVEL		3 db BEAMWIDTH OF MAIN LOBE	GAIN db	DOLPH-ARRAY WITH SAME PATTERN DATA		RAD. PATTERN FIG. NO.
				db			Number of Elements	Gain db	
Initial Array 1	3.0	--	1.000	0	--	--	--	--	--
Synthesized Array	3.83	3.8	0.608	-4.3	1.2°	10.4	29	7.0	2
Initial Array 2	3.0	--	0.541	-5.3	--	--	--	--	--
Synthesized Array	3.16	3.7	0.522	-5.6	1.5°	10.4	25	8.0	3
Initial Array 3	3.0	--	0.723	-2.8	--	--	--	--	--
Synthesized Array	3.75	4.0	0.558	-5.1	1.4°	10.4	26	7.7	4
Initial Array 3	2.0	--	0.723	-2.8	--	--	--	--	--
Synthesized Array	2.16	2.2	0.526	-5.6	2.4°	10.4	16	7.8	5
Initial Array 4	3.0	--	0.764	-2.3	--	--	--	--	--
Synthesized Array	3.35	3.2	0.571	-4.9	1.2°	10.4	30	7.5	6
Initial Array 4	2.0	--	0.628	-4.0	--	--	--	--	--
Synthesized Array	2.13	1.9	0.523	-5.6	1.9°	10.4	19	7.9	7

TABLE III-4  
21-ELEMENT ARRAYS SYNTHESIZED WITH DIGITAL COMPUTER

ARRAY	ARRAY LENGTH IN WAVELENGTHS	AVERAGE SPACING IN WAVELENGTHS	MINIMUM SPACING IN WAVELENGTHS	$z_0$	$z_1$	$z_2$	NORMALIZED ELEMENT POSITIONS					$z_8$	$z_9$	RAD. PATTERN FIG. NO.
							$z_3$	$z_4$	$z_5$	$z_6$	$z_7$			
Initial Array 3	--	3.0	--	0.000	0.0525	0.1087	0.1761	0.2536	0.3416	0.4403	0.5544	0.6838	0.8180	--
Synthesized Array	75.6	3.78	1.82	0.000	0.0483	0.1077	0.1767	0.2530	0.3422	0.4520	0.5549	0.6828	0.8180	8
Initial Array 3	--	2.0	--	0.000	0.0525	0.1087	0.1761	0.2536	0.3416	0.4403	0.5544	0.6838	0.8180	--
Synthesized Array	45.6	2.28	0.93	0.000	0.0408	0.1013	0.1761	0.2546	0.3416	0.4398	0.5565	0.6812	0.8196	9

TABLE III-5  
RADIATION PATTERN DATA OF 21-ELEMENT ARRAYS SYNTHESIZED WITH DIGITAL COMPUTER

ARRAY	AVERAGE SPACING IN WAVELENGTHS	BANDWIDTH $\times$ STEERABILITY $B(1 + \sin \theta_0)$	SIDE-LOBE LEVEL		3 db BEAMWIDTH OF MAIN LOBE	GAIN db	DOLPH-ARRAY WITH SAME PATTERN DATA		RAD. PATTERN FIG. NO.
				db			Number of Elements	Gain db	
Initial Array 3	3.0	--	0.547	-5.2	--	--	--	--	--
Synthesized Array	3.78	3.6	0.425	-7.4	0.74°	13.2	53	10.0	8
Initial Array 3	2.0	--	0.547	-5.2	--	--	--	--	--
Synthesized Array	2.28	1.8	0.374	-8.5	1.25°	13.2	31	10.4	9

TABLE III-6  
51-ELEMENT ARRAY SYNTHESIZED WITH DIGITAL COMPUTER

ARRAY	ARRAY LENGTH IN WAVELENGTHS	AVERAGE SPACING IN WAVELENGTHS	MINIMUM SPACING IN WAVELENGTHS	NORMALIZED ELEMENT POSITIONS												RAD. PATTERN FIG. NO.	
				$z_0$	$z_1$	$z_2$	$z_3$	$z_4$	$z_5$	$z_6$	$z_7$	$z_8$	$z_9$	$z_{10}$	$z_{11}$		$z_{12}$
Initial Array 3 Synthesized Array	159.5	3.0 3.19	1.50	0.0000	0.0207	0.0414	0.0643	0.0869	0.1098	0.1346	0.1614	0.1903	0.2215	0.2546	0.2899	0.3250	..
				0.0000	0.0229	0.0417	0.0656	0.0869	0.1098	0.1346	0.1610	0.1906	0.2222	0.2537	0.2899	0.3250	10
				$z_{13}$	$z_{14}$	$z_{15}$	$z_{16}$	$z_{17}$	$z_{18}$	$z_{19}$	$z_{20}$	$z_{21}$	$z_{22}$	$z_{23}$	$z_{24}$	$z_{25}$	
				0.3622	0.4017	0.4408	0.4844	0.5280	0.5754	0.6273	0.6792	0.7330	0.7909	0.8530	0.9233	1.0000	
				0.3622	0.4020	0.4421	0.4870	0.5280	0.5777	0.6276	0.6792	0.7336	0.7915	0.8536	0.9227	1.0000	

TABLE III-7  
RADIATION PATTERN DATA OF 51-ELEMENT ARRAY SYNTHESIZED  
WITH DIGITAL COMPUTER

ARRAY	AVERAGE SPACING IN WAVELENGTHS	BANDWIDTH $\times$ STEERABILITY $B(1 + \sin \theta_0)$	SIDE-LOBE LEVEL		3 db BEAMWIDTH OF MAIN LOBE	GAIN db	DOLPH-ARRAY WITH SAME PATTERN DATA		RAD. PATTERN FIG. NO.
			db	db			Number of Elements	Gain db	
Initial Array 3 Synthesized Array	3.0	--	0.356	9.0	--	--	--	--	--
	3.19	3.0	0.300	10.5	0.37°	17.1	128	--	10

also presented in these tables. To further emphasize the advantages of using variable interelement spacings, we list also the number of elements and the gain of a Dolph-Tchebyscheff array that has constant spacings slightly smaller than one wavelength, and produces the same beamwidth and the same side-lobe level as the synthesized arrays.

The initial eleven-element arrays fed into the digital computer were chosen to try out several characteristic types of element arrangements. Initial Array 1 is the uniformly spaced array which has 0-db side lobes. The pattern of the array synthesized from this initial array is shown in Fig. III-2.

Initial Array 2 is an array found with the analog computer. The side-lobe level of this array was improved by 0.3 db by the digital computer, see Fig. III-3. This array is the best of all the eleven-element arrays investigated. The interelement spacings of the array are seen to vary in an unsystematic way along the array axis.

Initial Array 3 is an array designed by a method of "controlled cosines," as suggested by King, Packard, and Thomas.<sup>2</sup> The spacings of this array increase from the center toward the end elements of the array. Computations on eleven-element arrays were made for average spacings  $3\lambda$  and  $2\lambda$ , see Figs. III-4 and III-5. As expected, a lower side-lobe level can be obtained with the smaller average spacing. The side-lobe levels of these arrays are not too much different from those of the arrays synthesized from Initial Array 4, which has its elements placed according to the zeros of a Legendre polynomial of eleventh order, see Figs. III-6 and III-7. However, the beamwidth is smaller for the Legendre arrays. This is characteristic of arrays whose interelement spacings decrease from the center toward the ends of the array.

From the experiments with eleven-element arrays, no clear indication has been obtained as to which element arrangements might lead to great improvements of the side-lobe level.

King, Thomas, and Packard<sup>2</sup> designed a 21-element array whose average interelement spacing for broadside operation can be as high as nearly 4 wavelengths, with a side-lobe level of -5.2 db. This array was designed according to a method of "controlled cosines." By using this array as the initial array for the digital computer, it was possible to obtain a side-lobe level of -7.4 db with an average spacing of 3.8 wavelengths, see Fig. III-8. When computations are started with an average

spacing of 2 wavelengths, the side-lobe level can be reduced to -8.5 db, see Fig. III-9.

The result of computations on a 51-element array is shown in Fig. III-10. With an average spacing of 3.2 wavelengths, the side-lobe level could be reduced to -10.5 db.

As expected from Eqs. (III-7) and (III-8), it is found that lower side-lobe levels can be obtained if more elements are included in an array. The best of the arrays described above have side-lobe levels of -5.6 db for an 11-element array, -8.5 db for a 21-element array, and -10.5 db for a 51-element array. For comparison the theoretical lower limits of the side-lobe level as predicted from Eq. (III-8) are -8.1 db, -10.8 db, and -14.5 db, respectively. It should again be pointed out that these theoretical limits are unattainable since they assume that all side lobes are of equal amplitude.

#### 4. CONCLUSIONS

The following conclusions can be drawn from the computations of the space factor of symmetric linear arrays having constant excitations and variable interelement spacings.

The side-lobe level depends primarily on the number of elements in the array and only very little on the average spacing when the average spacing exceeds about 2 wavelengths.

The 3-db beamwidth of the main lobe depends primarily on the length of the array.

Comparisons of variable spacing arrays with Dolph-Tchebyscheff arrays producing the same beamwidth and side-lobe levels show that the variable-spacing arrays have significantly fewer elements, at least for the moderate side-lobe levels considered in this study.

The product of bandwidth and steerability can be made much larger than for conventional equispaced arrays.

The problem of synthesizing an array with variable interelement spacings to reduce the side-lobe level so that small changes of the array element positions will not improve the side-lobe level further does not have a unique solution; instead, there are numerous solutions with different side-lobe levels.

In the initial steps of the synthesis of an array with variable interelement spacings, the main problem is to find some array whose side-lobe level can be improved more than, or as much as, any other array by small changes of the array element positions. The solution of this problem should preferably be approached by theory, although no theory has yet been developed. Lacking this theory, a fast analog computer is recommended to find approximate solutions. The final steps of the synthesis problem should preferably be solved by a digital computer.

## B. LINEAR ARRAYS WITH CONSTANT INTERELEMENT SPACINGS

### 1. INTRODUCTION

An important (and unsolved) problem in the theory of linear antennas is the following. Let a number of identical radiators be symmetrically spaced along a line. Suppose that each radiator is energized with the same frequency and phase. How should the amplitudes be related for maximum broadside directivity (see Fig. III-11)?

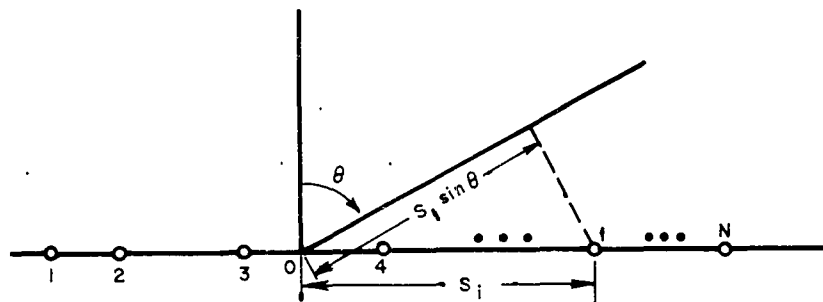


FIG. III-11  
THE FAR FIELD

If the phases are allowed not to be equal, but all are required to be either in step or exactly 180 degrees out of step [every phase is either  $\phi(t)$  or  $180^\circ + \phi(t)$ ] the problem is more tractable. Solutions to the problem when the number of equally spaced radiators is odd and spacing and wavelength are fixed can be found in a number of articles.<sup>16-24</sup> In this part, however, the problem will be made more precise mathematically, the solution will be rederived, and the best constant spacing will be found for maximum directivity. The solution to the problem for an even number



of radiators is considerably different from the solution for an odd number of radiators. This difference is pointed out by Riblet;<sup>17</sup> some authors, including some text-book authors, seem to be unaware of this difference.

## 2. THE FAR FIELD

### a. GENERAL

The desired far-field pattern is pictured in Fig. III-12. A certain small positive angle  $\epsilon$  is given; the problem is to make the far-field amplitude as close to zero as possible in all directions outside  $|\theta| \leq \epsilon$ , while keeping the amplitude 1 in the direction  $\theta = 0$ .

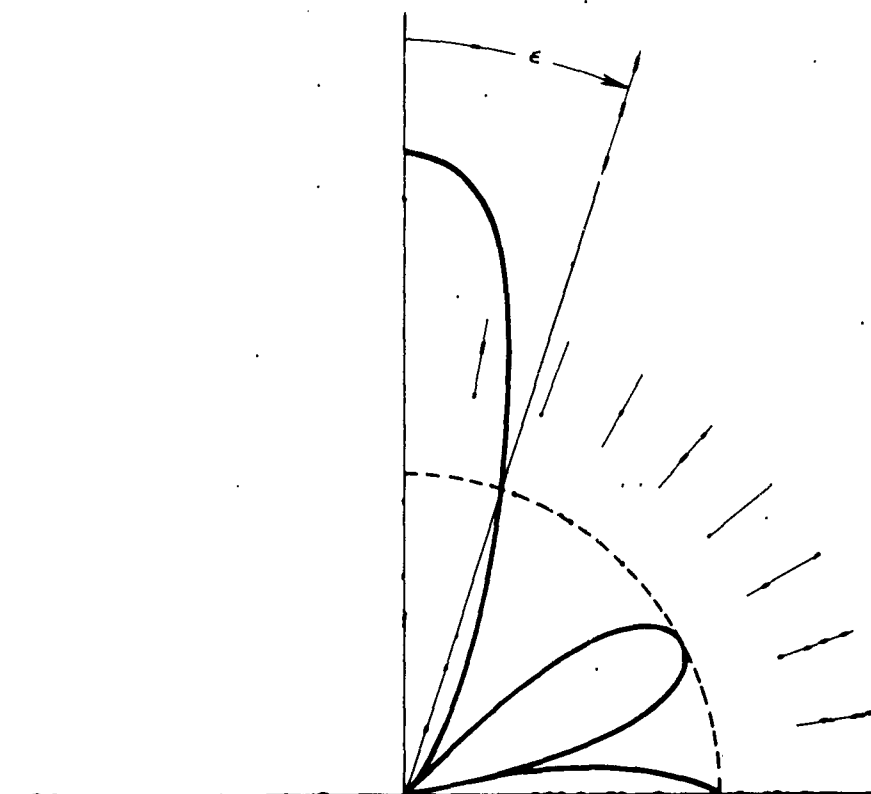


FIG. III-12  
DESIRED FAR-FIELD PATTERN

Suppose each of  $N$  sources (Fig. III-11) is emitting a sinusoidal signal at frequency  $f$ . At time  $t$ , the instantaneous amplitude of the signal received from the  $p$ th source at distance  $R_p$  from that source is

$$\operatorname{Re} A'_p \exp [j 2\pi f(t - R_p/c)] ,$$

where  $c$  is the speed of wave propagation. The instantaneous amplitude of the far field of the linear array in the direction  $\theta$  is then

$$\begin{aligned} \operatorname{Re} \sum_{p=1}^N A'_p \exp \{j 2\pi f[t - (R - d_p \sin \theta)/c]\} \\ = \operatorname{Re} \exp [j 2\pi f(t - R/c)] \sum_{p=1}^N A'_p \exp (j 2\pi f d_p \sin \theta/c) , \end{aligned}$$

where  $d_p$  is the distance of the  $p$ th source from the origin 0 on the line of sources and  $R$  is the distance of the far-field point from the origin.

The maximum amplitude of the far-field signal is

$$|G| = \left| \sum_{p=1}^N A'_p \exp [j 2\pi(d_p/\lambda) \sin \theta] \right| ,$$

where  $c/f$  has been replaced by its equal, the wavelength  $\lambda$ . Quantity  $G$  is the "radiation pattern" for an array of isotropic radiators or the "space factor" for other types of radiators and is the quantity being optimized here.

The array is assumed to be symmetrical; that is

$$d_p = -d_{N-p+1} ,$$

$$A'_p = A'_{N-p+1} .$$

If  $N$  is even,

$$|G| = \left| 2 \sum_{p=1}^{N/2} A'_p \cos [2\pi(d_p/\lambda) \sin \theta] \right| ,$$

while if  $N$  is odd,

$$|G| = \left| A'_{(N+1)/2} + 2 \sum_{p=1}^{(N-1)/2} A'_p \cos [2\pi(d_p/\lambda) \sin \theta] \right|$$

Finally, if the sources are all in phase, the  $A'_p$  are all positive multiples of the same complex number of magnitude unity, so that  $|G|$  is the magnitude of the real function

$$(N \text{ even}) \quad G = \sum_{p=1}^n A_p \cos (kd_p \sin \theta) \quad , \quad N = 2n$$

$$(N \text{ odd}) \quad G = \frac{1}{2} A_{n+1} + \sum_{p=1}^n A_p \cos (kd_p \sin \theta) \quad , \quad N = 2n + 1$$

with

$$A_p = 2|A'_p| \quad ,$$

and  $k$  the intrinsic propagation constant,  $k = 2\pi/\lambda$ . The symmetries of the sine and cosine functions show that  $G$  is determined if  $G$  is known for  $0 \leq \theta \leq \pi/2$ .

It is now assumed that the sources are equally spaced. This means, after a renumbering of the radiators from the center out, for  $N$  odd

$$d_p = pd_1 \quad , \quad p = 1, 2, \dots \quad ,$$

but for  $N$  even,

$$d_p = (2p - 1)d_1 \quad , \quad p = 1, 2, \dots \quad ,$$

as shown in Fig. III-13.

#### b. THE CASE FOR $N$ ODD

The problem when  $N$  is odd may be stated as follows (Fig. II-12). Choose positive constants  $A_0, A_1, \dots, A_n$  so that  $(1/2)A_0 + A_1 + \dots + A_n = 1$  and so that

$$G = \frac{1}{2} A_0 + \sum_{p=1}^n A_p \cos (pkd_1 \sin \theta)$$

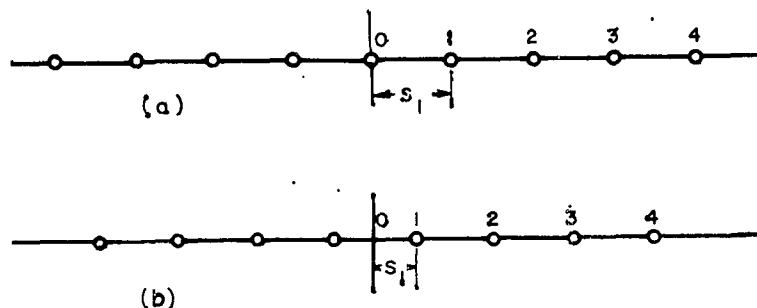


FIG. III-13  
 SYMMETRICALLY PLACED, EQUALLY SPACED RADIATORS  
 (a) ODD NUMBER OF RADIATORS,  $N = 9$   
 (b) EVEN NUMBER OF RADIATORS,  $N = 8$

is as close to zero as possible for  $\theta$  between  $\epsilon$  and  $\pi/2$  inclusive. The problem is not solved below; instead the  $A_p$  are permitted to be positive or negative, so that the radiators are all in phase or 180 degrees out of phase. The formulation of the problem is nevertheless slightly more precise than appears in Refs. 16-24. Moreover, the spacing  $d_1$  is found which corresponds to lowest side-lobe level; it is

$$d_1 = \lambda / (1 + \sin \epsilon) .$$

#### i. Preliminary Reductions

Since  $\sin \theta$  increases on  $\epsilon \leq \theta \leq \pi/2$  one may use

$$z = kd_1 \sin \theta$$

as an independent variable:

$$G = \frac{1}{2} A_0 + \sum_{p=1}^n A_p \cos pz . \quad (\text{III-16})$$

The interval of minimization is  $kd_1 \sin \epsilon \leq z \leq kd_1$ .

If an integral multiple of  $2\pi$  lies on this interval, then at such a point  $z = 2\pi q$  and

$$G = \frac{1}{2} A_0 + \sum_{p=1}^n A_p = 1 \text{ by assumption}$$

Thus no reduction of  $\max |G|$  below its value at  $\theta = 0$  is achieved. For  $kd_1$  to minimize  $|G|$ ,  $kd_1$  must satisfy the inequalities

$$2\pi q < kd_1 \sin \epsilon < kd_1 < 2\pi(q + 1)$$

for some integer  $q$ .

From the first and last of these inequalities

$$2\pi q < kd_1 \sin \epsilon < 2\pi(q + 1) \sin \epsilon$$

or

$$q < (q + 1) \sin \epsilon$$

If  $\sin \epsilon < 1/2$ , as it will be in any practical case,  $q$  is necessarily zero and

$$0 < kd_1 \sin \epsilon < kd_1 < 2\pi \quad (\text{III-17})$$

Since  $\cos pz$  may be written as a polynomial of degree  $p$  in  $\cos z$ ,  $G$  may be written as a polynomial of degree  $n$  in  $\cos z$ :

$$G = B_0 + \sum_{p=1}^n B_p (\cos z)^p$$

For any  $kd_1$  satisfying Eq. (III-17), the maximum  $M$  and minimum  $m$  values of  $\cos z$  on  $kd_1 \sin \epsilon \leq z \leq kd_1$  satisfy

$$-1 \leq m \leq \cos z \leq M < 1 \quad (\text{III-18})$$

An appropriate linear transformation spreads the interval  $(m, M)$  over  $(-1, 1)$ :

$$x = \frac{2 \cos z - M - m}{M - m}$$

or

$$\cos z = \frac{1}{2} [(M - m)x + M + m]$$

Function  $G$  is thus a polynomial of degree  $n$  in  $x$ :

$$G = C_0 + \sum_{p=1}^n C_p x^p \quad (III-19)$$

Furthermore, the point  $x_0$ , where  $z = 0$ , lies outside the interval  $(-1, 1)$ . For,

$$x_0 = \frac{2 - M - m}{M - m}$$

where, by Eq. (III-18),

$$\begin{aligned} x_0 &> \frac{2M - M - m}{M - m} \\ &= 1 \end{aligned}$$

#### ii. Solution to the Problem

For any  $kd_1$  satisfying Eq. (III-17), it has been shown that  $G$  is a polynomial of degree  $n$  in  $x$  with as small a maximum absolute value as possible on  $-1 \leq x \leq 1$  while taking the value  $G = 1$  at  $x = x_0$ . As proved in Appendix A, the solution for  $G$  in this form is unique and is given by the Tchebyscheff polynomial

$$T_n(x) = 2^{1-n} \cos(n \arccos x) = 2^{-n} (x + \sqrt{x^2 - 1})^n + 2^{-n} (x - \sqrt{x^2 - 1})^n$$

$$G = T_n(x)/T_n(x_0) \quad (III-20)$$

The coefficients  $C_p$  in Eq. (III-19) for  $G$  are thus obtained. Following through the transformations gives the  $A_p$  wanted.

The preliminary result is

$$\begin{aligned} \frac{T_n(x)}{T_n(x_0)} &= \frac{1}{T_n(x_0)} \sum_{r=0}^{[n/2]} \sum_{l=0}^{n-2r} \sum_{q=0}^l \frac{(n-r)!}{r!(n-2r-l)!q!(l-q)!} (-1)^r \frac{n}{n-r} 2^{n-2r-l-1} \\ &\times v^{n-2r-l} u^{2r-n} \cos(l-2q)z \end{aligned}$$

where

$$v = -(M + m)/2, u = (M - m)/2$$

$$T_n(x_0) = 2^{1-n} \cosh(n \operatorname{arccosh} x_0).$$

By changing the order of summations, one finds the coefficients in Eq. (III-16) to be

$$A_p = \frac{1}{T_n(x_0)} \sum_{r=0}^{[(n-p)/2]} \sum_{\substack{l=p \\ l-p \text{ even}}}^{n-2r} D_{n,r,l,p} (-1)^r \frac{n}{n-r} 2^{n-2r-l} v^{n-2r-l} u^{2r-n}, \quad (\text{III-21})$$

where

$$D_{n,r,l,p} = \frac{(n-r)!}{r!(n-r-l)! [1/2(l-p)]! [1/2(l+p)]!}$$

The symbol  $[(n-p)/2]$  denotes the integral part of  $(n-p)/2$ , i.e.,  $(n-p)/2$  if  $n-p$  is even;  $(n-p-1)/2$  otherwise.

It remains to choose  $kd_1$  to reduce  $\max |G|$  on  $\epsilon \leq \theta \leq \pi/2$  as much as may be. The final form, Eq. (III-20), shows that the value of  $kd_1$  which minimizes  $|G|$  is that for which  $|T_n(x_0)|$  is as large as possible. Since  $|T_n(x)|$  is an increasing function on  $1 \leq x$ ,  $|T_n(x_0)|$  is maximized if  $x_0$  is. Thus  $kd_1$  is to be chosen so that

$$x_0 = \frac{2 - M - m}{M - m} \quad (\text{III-22})$$

is as large as may be.

$M$  and  $m$  are functions of  $kd_1$  on  $0 < kd_1 < 2\pi$ :

$$m = \begin{cases} \cos kd_1 & 0 < kd_1 \leq \pi \\ -1 & \pi \leq kd_1 < 2\pi \end{cases}$$

(The constant value of  $m$  on the second range is due to the fact that, with  $\sin \epsilon < 1/2$ ,  $\pi < kd_1 < 2\pi$  implies  $kd_1 \sin \epsilon < \pi < kd_1$ )

$$M = \begin{cases} \cos (kd_1 \sin \epsilon) & , \quad 0 < kd_1 \leq b \\ \cos kd_1 & , \quad b \leq kd_1 < 2\pi \end{cases}$$

where  $b$  is the solution of

$$\cos (b \sin \epsilon) = \cos b ,$$

$$b = \frac{2\pi}{1 + \sin \epsilon}$$

One may note that  $\pi < b < 2\pi$ .

Substituting these values for  $m$  and  $M$  into Eq. (III-22) gives

$$x_0 = \begin{cases} \frac{2 - \cos (kd_1 \sin \epsilon) - \cos kd_1}{\cos (kd_1 \sin \epsilon) - \cos kd_1} & , \quad 0 < kd_1 \leq \pi \\ \frac{3 - \cos (kd_1 \sin \epsilon)}{\cos (kd_1 \sin \epsilon) + 1} & , \quad \pi \leq kd_1 \leq b \\ \frac{3 - \cos kd_1}{\cos kd_1 + 1} & , \quad b \leq kd_1 < 2\pi \end{cases}$$

These forms may be written

$$x_0 = \begin{cases} \frac{2(1 - \cos kd_1)}{\cos (kd_1 \sin \epsilon) - \cos kd_1} - 1 & \text{on } 0 < kd_1 \leq \pi \\ \frac{4}{\cos (kd_1 \sin \epsilon) + 1} - 1 & \text{on } \pi \leq kd_1 \leq b \\ \frac{4}{\cos kd_1 + 1} - 1 & \text{on } b \leq kd_1 < 2\pi \end{cases}$$

As  $kd_1$  increases on the respective ranges, the first form increases (see the lemma in Appendix A); the second form also increases, and the third form decreases, the latter two statements being obvious. Thus, since  $x_0$  is continuous, it is a maximum for  $kd_1 = b = 2\pi/(1 + \sin \epsilon)$ .



iii. The Case for  $n = 1$  ( $N = 3$ )

With  $n = 1$ , the optimum  $y$  is

$$G = \frac{x}{x_0}$$

where

$$kd_1 = \frac{2\pi}{1 + \sin \epsilon}$$

$$M = \cos kd_1$$

$$m = -1$$

$$x = \frac{2 \cos z + 1 - \cos kd_1}{1 + \cos kd_1}$$

$$z = kd_1 \sin \theta$$

and

$$x_0 = \frac{3 - \cos kd_1}{1 + \cos kd_1}$$

Explicitly

$$G = \frac{(1 - \cos kd_1) + 2 \cos (kd_1 \sin \theta)}{3 - \cos kd_1}$$

Since the constant term and the coefficient of  $\cos z$  in the form for  $G$  are positive, this solution of the related problem for  $n = 1$  is also the solution of the given optimum antenna problem for  $n = 1$ .

c. THE CASE FOR  $N$  EVEN

For  $N$  even,  $N = 2n$ , the problem is suggested by Figs. III-12 and III-13(b). The mathematical formulation is as follows: given a positive angle  $\epsilon$ ,  $0 < \epsilon < \pi/2$ , find real (positive) constants  $A_p$ ,  $p = 1, 2, \dots, n$  so that

$$A_1 + A_2 + \dots + A_n = 1$$

and so that

$$G = \sum_{p=1}^n A_p \cos (kd_p \sin \theta)$$

is as near zero as possible for values of  $\theta$  between  $\epsilon$  and  $\pi/2$  inclusive. Again it is assumed that the sources are equally spaced, and the restriction that  $A_p$  be positive is lifted. Thus,

$$G = \sum_{p=1}^n A_p \cos [(2p-1) kd_1 \sin \theta]$$

i. *Preliminary reductions* are similar to those in the case for  $N$  odd. Set  $z = kd_1 \sin \theta$ , then

$$G = \sum_{p=1}^n A_p \cos [(2p-1) z] ; \quad (\text{III-23})$$

the interval of minimization is  $kd_1 \sin \epsilon \leq z \leq kd_1$ . By expanding  $\cos [(2p-1) z]$ , one sees that  $G$  is a polynomial in  $\cos z$

$$G = \sum_{p=1}^{N-1} B_p (\cos z)^p = \sum_{p=1}^{N-1} B_p \bar{x}^p, \quad \bar{x} = \cos z ; \quad (\text{III-24})$$

but now,  $G$  must be an odd polynomial [if even indices occur in Eq. (III-24), Eq. (III-24) cannot be reduced to Eq. (III-23)]. A linear transformation of the  $\bar{x}$ -coordinate, like  $\bar{x} = (2 \cos z - M - m)/(M - m)$ , is not indicated, since such a transformation would change Eq. (III-24) into another polynomial, and by this change conceal the fact that Eq. (III-24) is an odd polynomial.

It is again desirable to denote the maximum and minimum values of  $\cos z$  on the interval  $kd_1 \sin \epsilon \leq z \leq kd_1$  by  $M$ ,  $m$ , and to remark that

$$-1 \leq m \leq \cos z \leq M < 1$$

There are four cases:

- (i)  $m = -1$
- (ii)  $-1 < m \leq 0 < M$  or  $-1 < m < 0 \leq M$ ,
- (iii)  $-1 < m < M < 0$ ,
- (iv)  $0 < m < M$ .

## ii. Solution to the Problem

In the case where  $m = -1$ ,  $G$  takes the value  $-1$  in the interval  $kd_1 \sin \epsilon \leq z \leq kd_1$ , since

$$G|_{\cos z = -1} = -G|_{\cos z = -1} = -G|_{\theta=0} = -1.$$

Hence no directivity can be achieved. This case occurs when and only when  $kd_1 \geq \pi$ , i.e., when the spacing is one wavelength or more.

In the second case the solution turns out to be a Tchebyscheff polynomial; in the third and fourth cases, the solution is found in terms of elliptic functions.

Now consider the second case in detail. The abstract problem is the following. Find an odd polynomial in  $\bar{x}$ , of degree  $N-1$ , which has the value 1 at  $\bar{x} = 1$ , and which is as near to 0 as possible for  $m \leq \bar{x} \leq M$ . The solution is  $G = T_{N-1}(\bar{x}/D)/T_{N-1}(1/D)$ , where  $D = \max(|m|, M)$ , and  $T_r(x)$  is the Tchebyscheff polynomial

$$2^{-r}(x + \sqrt{x^2 - 1})^r + 2^{-r}(x - \sqrt{x^2 - 1})^r.$$

The preceding statement is nearly obvious. Make the magnification  $x = \bar{x}/D$ ,  $x_0 = 1/D$ . Now if  $R(x)$  is any odd polynomial,

$$\max_{0 \leq x \leq 1} |R(x)| = \max_{-1 \leq x \leq 1} |R(x)|.$$

Corollary 2 of Appendix A shows that  $T_{N-1}(x)/T_{N-1}(x_0)$  is indeed the solution to the problem. When  $M$  and  $m$  have the same sign,\* the reasoning is similar, whether the sign is negative (Case iii) or positive (Case iv). [The third case,  $-1 < m < M < 0$ , can occur only if  $\cos(kd_1 \sin \epsilon) \leq 0$ ; the spacing between radiators must then be at least  $\lambda/(2 \sin \epsilon)$ , which contradicts the condition  $-1 < m$  in the practical case  $\sin \epsilon < 1/2$ . Hence attention is restricted to Case iv,  $0 < m < M < 1$ .]

In Case iv, it is convenient to make the change of variables  $x = \bar{x}/M$ ,  $x_0 = 1/M$ ,  $\mu = m/M$ . It is required to find the odd polynomial  $R(x)$

---

\* The fact that Tchebyscheff polynomials do not solve the problem in this case was pointed out by Riblet in Ref. 17.

of degree  $N - 1$  which takes the value 1 at  $x = x_0$ , and which is as close to 0 as possible on  $\mu \leq x \leq 1$ . The solution of this problem is related to the solution given by Achieser<sup>25</sup> in 1928 to a problem of Solatorev.

By employing Achieser's solution in a manner parallel to that for the Tchebyscheff case, the following result is obtained:

$$R(x) = \frac{U(x)}{U(x_0)}$$

$$x = \frac{\mu \operatorname{cn} u}{\sqrt{(\mu^2 - \operatorname{sn}^2 u)}} \quad (\text{the square root is defined as } \mu \text{ at } u = 0),$$

$$\mu = \operatorname{sn} \frac{K}{N-1}$$

$$U(x) = \frac{1}{2} L_{N-1} F(u)$$

$$L_{N-1} = \frac{1}{2^{N-2}} \left[ \frac{\Theta(0) \Theta_1(0)}{\Theta\left(\frac{K}{N-1}\right) \Theta_1\left(\frac{K}{N-1}\right)} \right]^{N-1}$$

$$F(u) = \left[ \frac{H\left(\frac{K}{N-1} + u\right)}{H\left(\frac{K}{N-1} - u\right)} \right]^{(N-1)/2} + \left[ \frac{H\left(\frac{K}{N-1} - u\right)}{H\left(\frac{K}{N-1} + u\right)} \right]^{(N-1)/2}$$

$$\begin{aligned} H(u) &= \Theta_1\left(\frac{u}{2K}\right) = 2 \left[ q^{1/4} \sin \frac{\pi u}{2K} - q^{3/4} \sin \frac{3\pi u}{2K} + \dots \right] \\ &= 2 \sum (-)^t q^{(2t-1)^2/4} \sin \frac{(2t-1)\pi u}{2K}, \end{aligned}$$

$$\begin{aligned} \Theta(u) &= \Theta_0\left(\frac{u}{2K}\right) = 1 - 2q \cos \frac{\pi u}{K} + 2q^4 \cos \frac{2\pi u}{K} - \dots \\ &\quad \mp 2q^{n^2} \frac{\cos n\pi u}{K} \pm \dots, \end{aligned}$$

$$\theta_1(u) = \theta_3 \left( \frac{u}{2K} \right) = 1 + 2q \cos \frac{\pi u}{K} + 2q^4 \cos \frac{2\pi u}{K} + \dots$$

$$q = \exp \frac{-\pi K'}{K}$$

$K$  satisfies  $\text{sn}(K, k) = 1$ , and the modulus  $k$  in this relation is determined by the equation  $\mu = \text{sn} [K/(N-1)]$ . With  $k'^2 = 1 - k^2$ ,  $K'$  is defined by  $\text{sn}(K', k') = 1$ . The graph of  $U(x)/U(x_0)$  is shown in Fig. III-14.

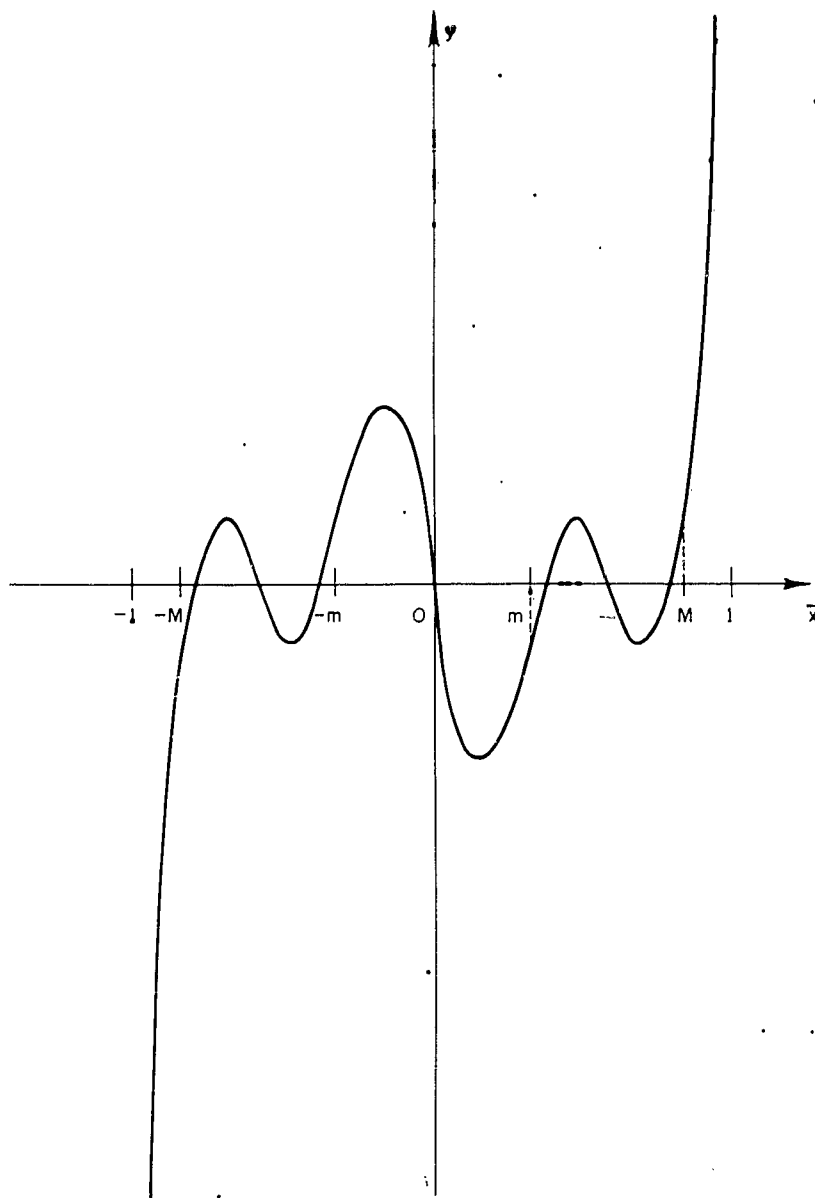


FIG. III-14

GRAPH OF THE POLYNOMIAL DEFINED BY ELLIPTIC FUNCTIONS  
(CASE iv,  $N = 8$  ILLUSTRATED.)

## REFERENCES

1. H. Unz, "Linear Arrays with Arbitrarily Distributed Elements," *Trans. IRE PGAP-8*, pp. 222-223 (March 1960).
2. D. D. King, R. F. Packard, and R. K. Thomas, "Unequally-Spaced, Broad-Band Antenna Arrays," *Trans. IRE PGAP-8*, pp. 380-384 (July 1960).
3. W. F. Gabriel and M. G. Andreasen, "Investigation of Methods of Scanning the Beams of Large Antennas," Scientific Report 12, Contract AF 19(604)-2240, SRI Project 2184, Stanford Research Institute, Menlo Park, California (September 1960).
4. R. C. Honey, L. A. Robinson, M. G. Andreasen, J. Aasted, J. K. Shimizu, "Antenna Design Parameters," Quarterly Progress Report 13, Contract DA 36-039 SC-73106, SRI Project 1954, Stanford Research Institute, Menlo Park, California (May 1960).
5. M. G. Andreasen, L. A. Robinson, R. C. Honey, and J. Aasted, "Antenna Design Parameters," Quarterly Progress Report 14, Contract DA 36-039 SC-73106, SRI Project 1954, Stanford Research Institute, Menlo Park, California (September 1960).
6. M. G. Andreasen, "Arrays with Variable Inter-element Spacings," presented at the joint URSI-IRE Meeting, Boulder, Colorado (December 1960).
7. S. S. Sandler, "Some Equivalences Between Equally and Unequally Spaced Arrays," *Trans. IRE PGAP-8*, pp. 496-500 (September 1960).
8. R. F. Harrington, "Side-Lobe Reduction by Nonuniform Element Spacings," S.U.R.I. Report No. EE 492-6008 T11, Contract AF 30(602)-1640, Syracuse University Research Institute (August 1960).
9. C. L. Dolph, "A Current Distribution for Broadside Arrays Which Optimizes the Relationship Between Beam Width and Side Lobe Level," *Proc. IRE* 34, pp. 335-348 (June 1946).
10. R. H. DuHamel, "Optimum Patterns for Endfire Arrays," *Proc. IRE* 41, pp. 652-659 (May 1953).
11. P. M. Woodward and J. D. Lawson, "The Theoretical Precision with Which an Arbitrary Radiation Pattern May Be Obtained from a Source of Finite Size," *Journal Inst. Elec. Engrs., London*, Pt. III, Vol. 95, pp. 363-369 (September 1958).
12. R. C. Hansen, "Gain Limitations of Large Antennas," *Trans. IRE PGAP-8*, pp. 490-495 (September 1960).
13. C. E. Smith and E. L. Gove, "An Electromechanical Calculator for Directional-Antenna Patterns," *Trans. Am. Inst. Elec. Engrs.* 62, pp. 78-83 (February 1943).
14. G. H. Brown and W. C. Morrison, "The RCA-Antemalyzer—An Instrument Useful in the Design of Directional Antenna Systems," *Proc. IRE* 34, pp. 992-999 (December 1946).
15. T. T. Taylor and J. R. Whinnery, "Applications of Potential Theory to the Design of Linear Arrays," *J. Appl. Phys.*, Vol. 22, pp. 19-29 (January 1951).
16. C. L. Dolph, "A Current Distribution for Broadside Arrays Which Optimizes the Relationship Between Beam Width and Side-Lobe Level," *Proc. IRE* 34, 335-348 (1946).
17. H. J. Riblet, "Discussion," *ibid.* 35, 489-492 (1947).
18. D. Barbieri, "A Method for Calculating the Current Distribution of Tchebyscheff Arrays," *Proc. IRE* 40, 78-82 (1952).
19. Robert J. Stegen, "Excitation Coefficients and Beamwidths of Tchebyscheff Arrays," *Proc. IRE* 41, 1671-1674 (1953).
20. R. H. DuHamel, "Optimum Patterns for Endfire Arrays," *Proc. IRE* 41, 652-659 (1953).
21. L. L. Bailin and M. J. Ehrlich, "Factors Affecting the Performance of Linear Arrays," *Proc. IRE* 41, 235-241 (1953).

22. G. J. van der Mass, "A Simplified Calculation for Dolph-Tchebyscheff Arrays," *J. Appl. Phys.* 25, 121-124 (1954).
23. T. T. Taylor, "Design of Line-Source Antennas for Narrow Beam Width and Low Side Lobes," *IRE Transactions on Antennas and Propagation* PGAP-3, 16-28 (1955).
24. Roger F. Harrington, "On the Gain and Beamwidth of Directional Antennas," *IRE Transactions on Antennas and Propagation* PGAP-6, 219-225 (1958).
25. N. Achieser, *Theory of Approximation*. F. Ungar, N. Y., 1956.

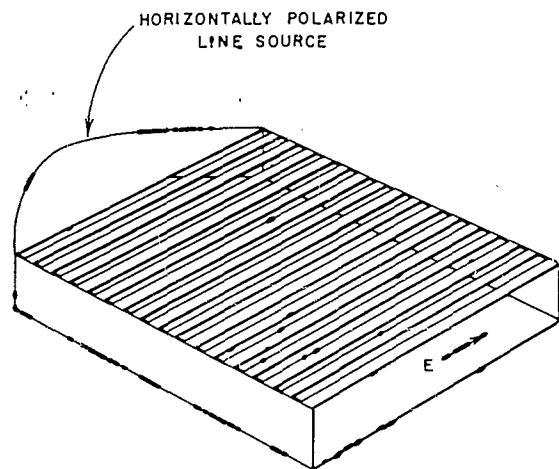


## IV VARIABLE-BEAMWIDTH LEAKY-WAVE ANTENNAS

### A. GENERAL

For some applications it is desirable to have an antenna whose radiation pattern can be changed in at least one plane. For example, in some radar systems a fan-shaped beam is desirable during the search phase, but a pencil beam is desirable during the tracking phase. An investigation was conducted to determine the variable-beamwidth capabilities of a leaky-wave antenna such as shown in Fig. IV-1. This antenna consists of an inductive sheet spaced over a solid metal wall, with a wave polarized in the plane of the antenna propagating between the two sheets. The inductive sheet may consist of an array of flat metal strips, as shown in Fig. IV-1, or it may consist of an array of round wires. The transverse-resonance condition has been used to determine the phase velocity and rate of leakage along this type of antenna, and the results have been experimentally shown to be extremely precise.<sup>1\*</sup>

This type of antenna can be designed to have a narrow *E*-plane beam by using a wide *E*-plane aperture, as shown in Fig. IV-1 or by using a narrow leaky-wave antenna as a line-source feed for a parabolic cylinder reflector. The *H*-plane radiation pattern can be controlled by the rate at which energy is allowed to leak out of the antenna, and by the phase velocity along the antenna. By suitable choice of the amplitude distribution, and by maintaining constant phase velocity along the length of the antenna, narrow *H*-plane beamwidth can



A-1592-52

FIG. IV-1  
INDUCTIVE SHEET ANTENNA

\* References are listed at the end of the section.

be obtained. The approach that will be considered here for broadening the *H*-plane radiation pattern is to produce a non-uniform phase velocity along the length of the antenna by moving the solid metal wall with respect to the inductive sheet. The resulting phase error will tend to broaden the main beam, and merge the side lobes with the main beam by filling in the nulls between lobes.

In the first calculations, no attempt was made to control the shape of the resultant broad beam. Antenna dimensions were chosen to give constant phase velocity, and to give simple arbitrary amplitude distributions along the length of the antenna. Sinusoidal and constant amplitude distributions were used. The solid wall of each antenna was then moved in simple motions with respect to the grid, and the resultant radiation patterns were then calculated. The results of these calculations are presented in Sec. IV-B. For the calculations made near the close of this study program, emphasis was placed on controlling the shape of the broad-beam radiation patterns. For these calculations, the antenna dimensions were chosen to synthesize maximally flat power patterns with half-power widths of 45 degrees. The grid-to-solid-wall spacing was then modified along the antenna to produce radiation patterns of narrower beam widths. The results of these calculations are presented in Sec. IV-C.

## B. DESIGNS BEGINNING WITH NARROW-BEAM ANTENNAS

### 1. ANTENNAS A AND B

A limited number of calculations were made for two antennas having an aperture amplitude distribution that is one-half cycle of a sine curve. Each of these antennas was designed to radiate 95 percent of the input power when radiating a pencil beam at the design frequency. The separation between the inductive sheet, consisting of a wire grid, and the solid metal wall was chosen as 0.900 inch at both ends of each antenna to match the width of standard *X*-band waveguide. The grid-to-solid-wall spacing varies along the length of each antenna as shown in Figs IV-2 and IV-3 to maintain the phase velocity constant. The center-to-center spacing required between 0.005-inch-diameter round wires to give the prescribed amplitude distribution is also shown in Figs. IV-2 and IV-3. It was anticipated that the result of moving the solid metal wall with respect to the inductive sheet would depend on the value of the phase velocity used in the design. Consequently, two design frequencies were chosen.

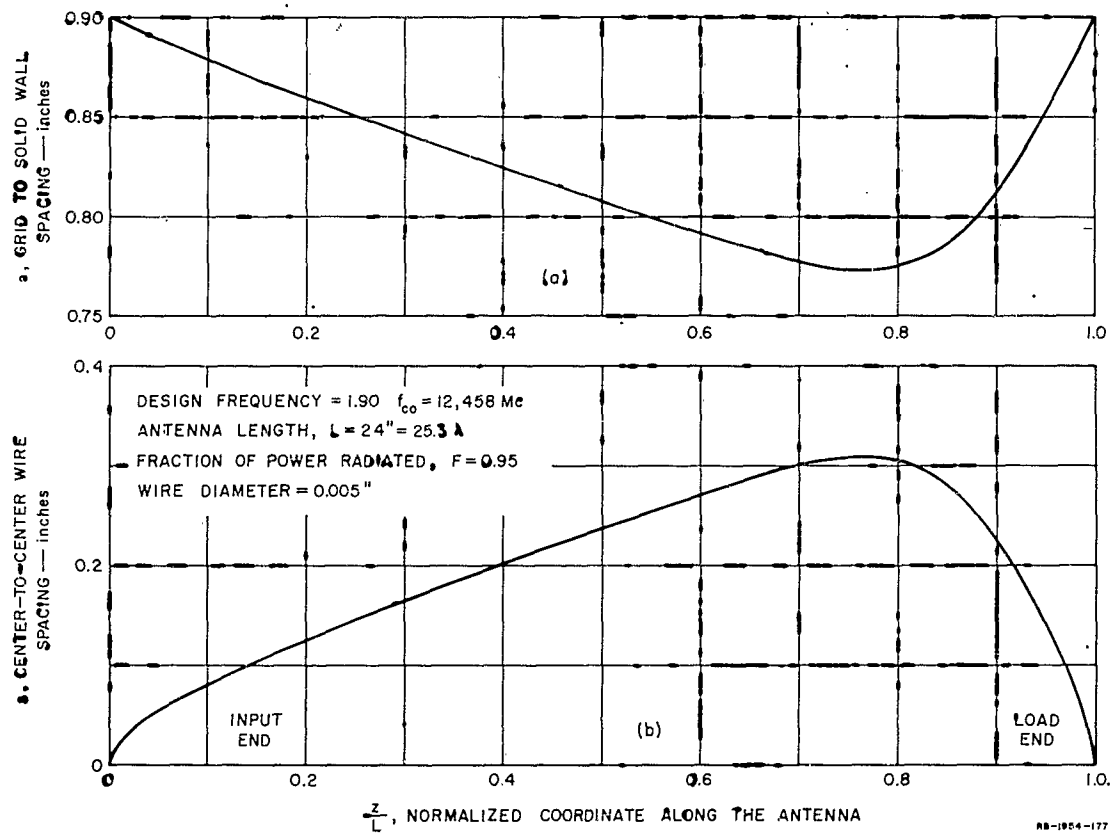


FIG. IV-2  
 DIMENSIONS OF ANTENNA A AS DESIGNED FOR CONSTANT PHASE VELOCITY

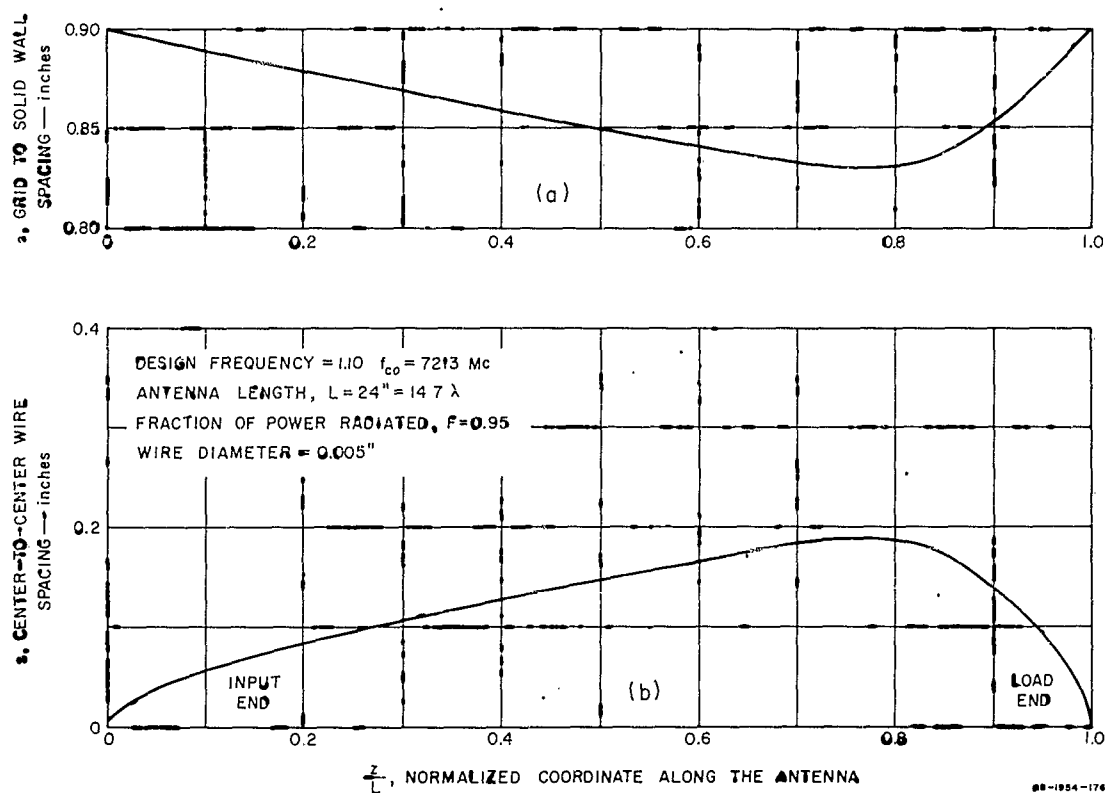


FIG. IV-3  
 DIMENSIONS OF ANTENNA B AS DESIGNED FOR CONSTANT PHASE VELOCITY

Antenna A was designed at 90 percent above the cut-off frequency,  $f_{co}$ , of the dominant mode in 0.900-inch-wide waveguide, and Antenna B was designed 10 percent above  $f_{co}$ . These frequencies were arbitrarily chosen as practical limits as determined by dissipation loss and tolerance requirements at the low frequency, and by staying 5 percent below cut-off of the  $TE_{20}$  mode at the high frequency. For  $f = 1.10 f_{co}$  and  $f = 1.90 f_{co}$ , the main beam of the  $H$ -plane radiation pattern is displaced from the broadside direction toward the output end by about 25 degrees and 58 degrees, respectively. The length of each antenna was arbitrarily chosen as 24 inches, giving a 3-db beamwidth for each antenna of 5.5 degrees when the phase velocity is constant.

Only one simple motion of the solid metal wall was considered, *i.e.*, pivoting it about one end. The input end was used as the pivot point to minimize the impedance mismatch at the input of the antenna. The  $H$ -plane radiation patterns were calculated using a digital computer to solve the equations describing the phase velocity and leakage rate along the antenna, and then to integrate the aperture fields to obtain the far-field pattern. In carrying out the integrations, points were not calculated sufficiently close together to permit the drawing of smooth radiation patterns showing side-lobe detail. Better beam-broadening results were obtained with other antennas; thus, complete patterns were never calculated for Antennas A and B. The patterns available did permit the following data to be read from them.

For Antenna A, whose design frequency is  $f = 1.90 f_{co}$ , the spacing between the output end of the solid metal wall and the inductive sheet was decreased  $0.4\lambda$  from 0.900 inch in four steps down to 0.521 inch. At this latter spacing, the dominant mode is 10 percent above cut-off at the output end of the antenna. As the spacing at the output end of Antenna A was decreased, the beamwidth increased by a factor of 1.6 at the 3-db level, and by a factor of 1.8 at the 10-db level. For Antenna B, whose design frequency is  $f = 1.10 f_{co}$ , the spacing between the output end of the solid metal wall and the inductive sheet was increased  $0.4\lambda$  from 0.900 inch in four steps up to 1.554 inches. At this latter spacing, the  $TE_{20}$  mode is only 5 percent below cut-off at the output end of the antenna. As the spacing at the output end of Antenna B was increased, the beamwidth increased by a factor of 1.8 at the 3-db level, and by a factor of 2.8 at the 10-db level. As the solid walls of both antennas were moved to broaden the main beam, the nulls between the side lobes filled in, and

the first few lobes merged with the main beam. Because of the limited number of points used in the initial calculations, further description of the side-lobe level behavior cannot be given.

By examining the amplitude and phase distributions shown in Figs. IV-4 and IV-5, it is readily seen that larger changes in beamwidth could be obtained. For the antennas described above, the amplitude distribution tapered to zero at the edges of the aperture. Thus, although motion of the solid wall introduced large phase changes across the aperture, very little power was radiated at the aperture edges where the phase error was greatest. This indicates that a uniform amplitude distribution would be more satisfactory than a tapered distribution for antennas whose beamwidth is to be variable.

As the solid wall of each of these antennas was pivoted about the input end in order to broaden the radiation patterns, the direction of the main beam also changed due to the change in average phase velocity over the central portion of each antenna, where most of the power was

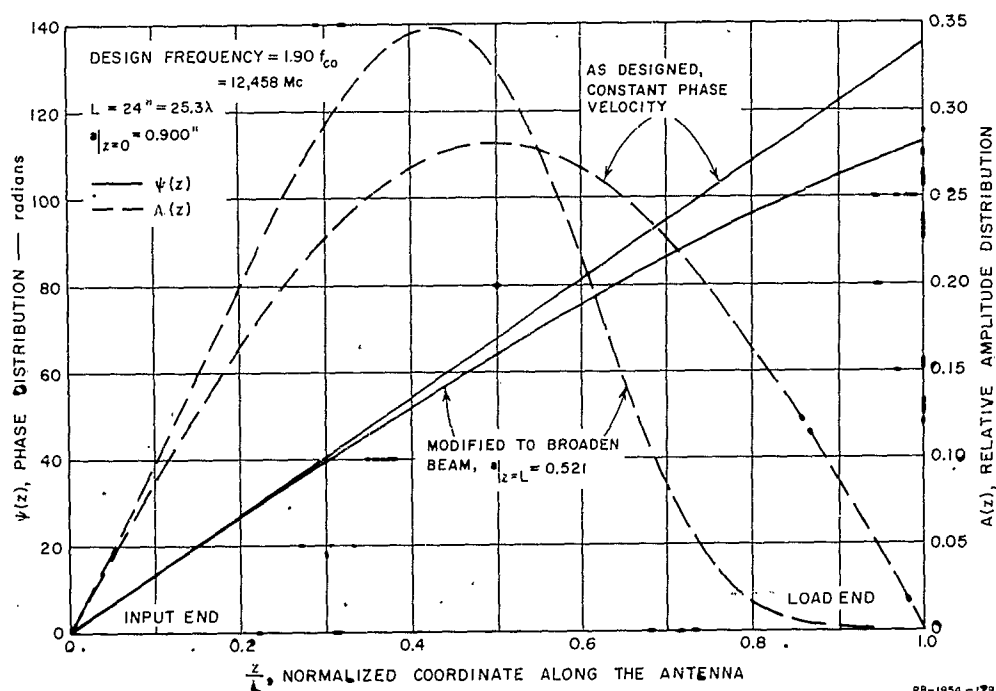


FIG. IV-4  
APERTURE DISTRIBUTIONS OF ANTENNA A

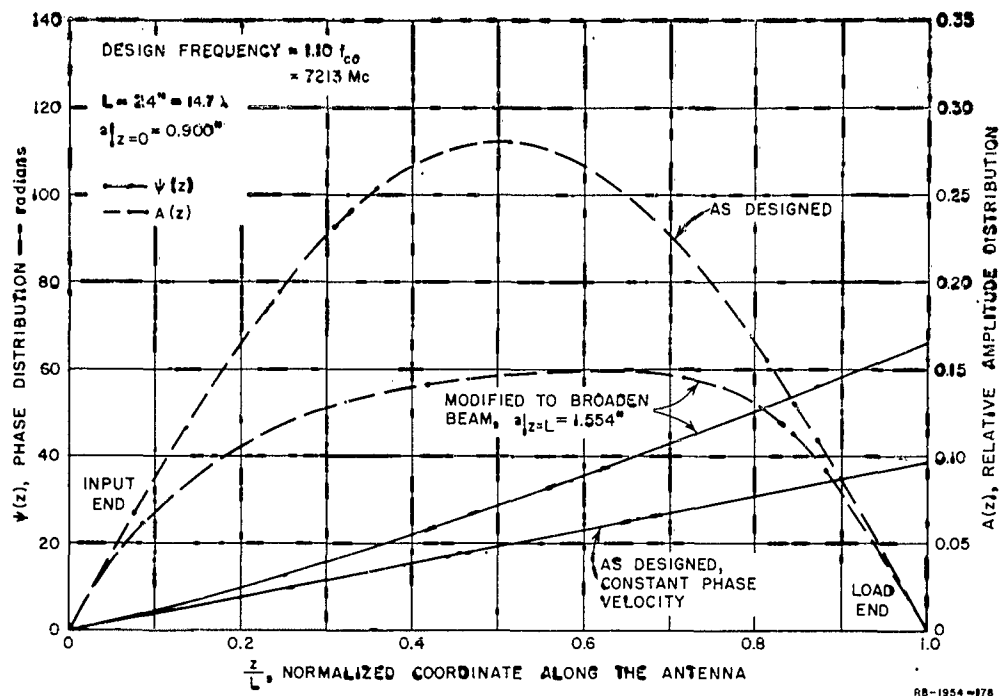


FIG. IV-5  
APERTURE DISTRIBUTIONS OF ANTENNA B

radiated.\* For Antenna A, the beam position changed from a position of 58 degrees with respect to the broadside direction to 48 degrees with respect to the broadside direction; and for Antenna B, the beam position changed from a position of 25 degrees to one of 48 degrees. If this beam-scanning that accompanies the beam-broadening is objectionable for a particular application, the beam direction could probably be kept fixed by pivoting, bending, or hinging the solid metal wall about some point other than the input of the antenna.

For both antennas, the radiated fraction of the input power changes considerably as the spacing between the inductive sheet and the solid wall is changed. As the solid wall is moved toward the inductive sheet, the amount of power radiated is increased. For Antenna A, the increase was from 95 percent to 99.99995 percent as the spacing at the output end was

\* Calculations have also been carried out for the case where the entire solid wall of Antenna B was moved the same amount in an attempt to scan the main beam without degrading the radiation pattern. In scanning the beam from a position of 25 degrees to one of 63 degrees, however, the 3-db beamwidth doubled, and the level of the first side lobe increased from -24 db to -12 db with respect to the peak of the main beam.

reduced to 0.521 inch. This effect might be used to advantage for broadening the beamwidth, since the power is radiated over a smaller effective aperture, as illustrated by Fig. IV-4. As the solid wall is moved away from the inductive sheet, on the other hand, the amount of power radiated is decreased. This is undesirable, since the power that is not radiated is dissipated in the load terminating the antenna, and thus the gain and efficiency of the antenna is reduced. When the spacing was increased to 1.554 inches at the output end of Antenna B, the radiated power dropped from 95 percent to only 33 percent of the input power. Thus, if it is desirable to increase the grid-to-solid-wall spacing over part of the antenna to produce a pattern change, the grid-to-solid-wall spacing should be decreased over some other part of the antenna in order to avoid excessive power dissipation in the load.

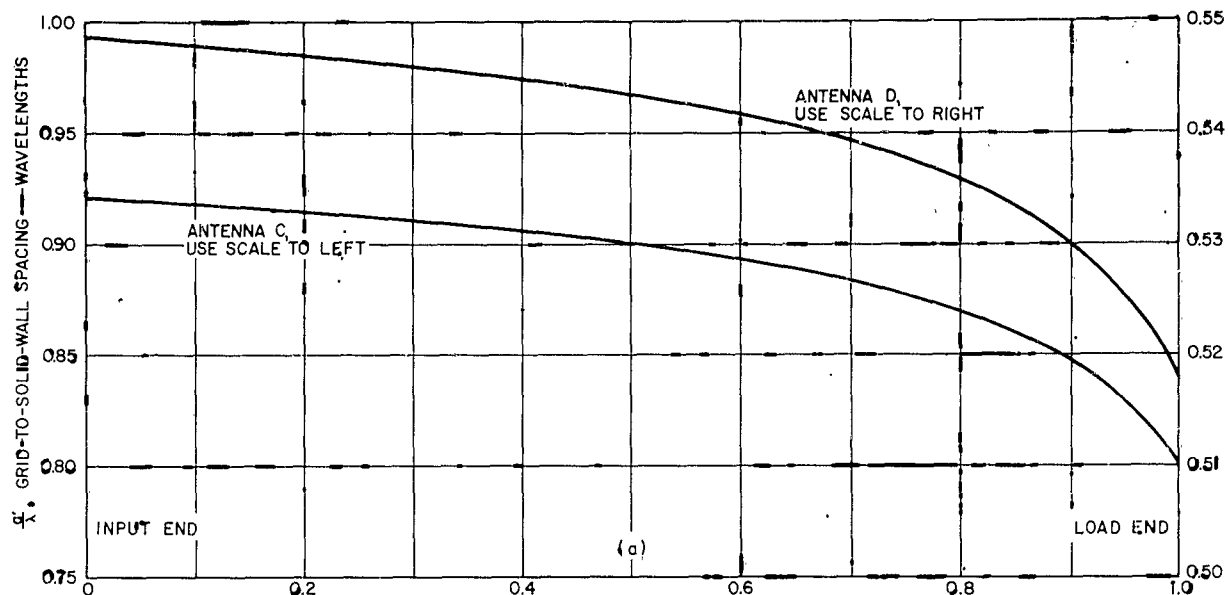
## 2. ANTENNA C

### a. GENERAL

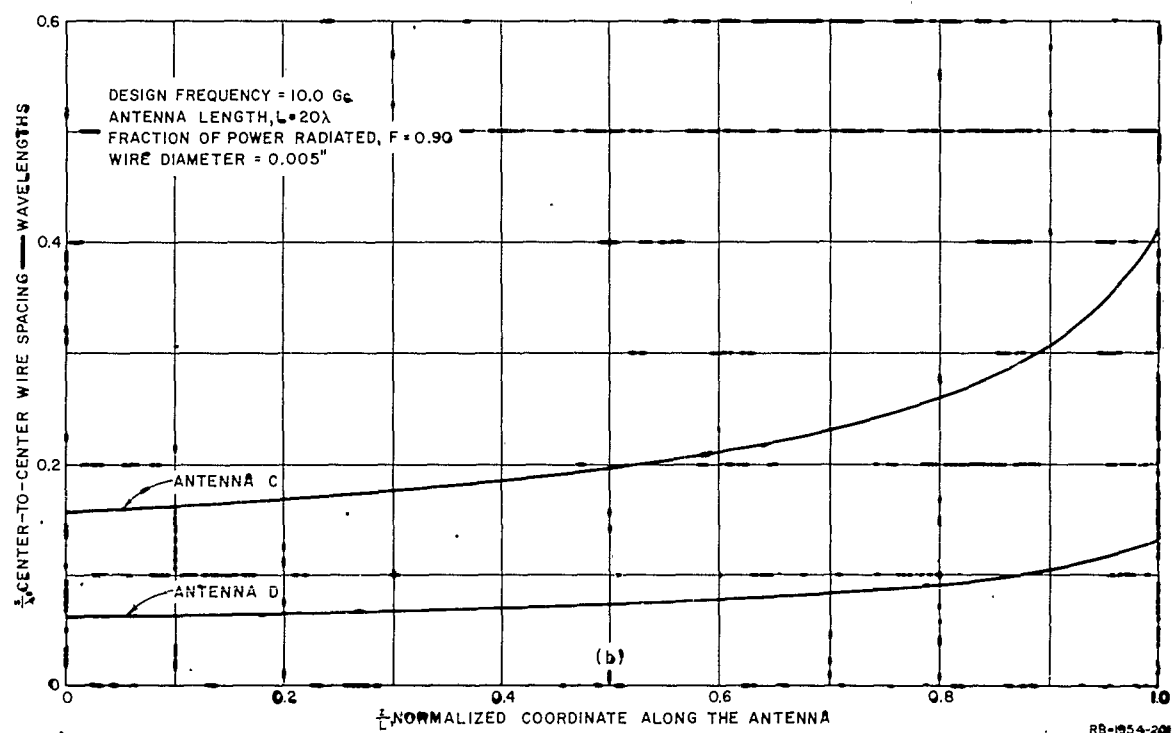
In order to have more power radiated at the ends of the antenna, where the perturbation of the phase distribution is most pronounced, two narrow-beam antennas were designed with constant-amplitude distribution along the antenna length. One of these, Antenna C, was designed with constant phase velocity as given by  $\lambda/\lambda_g = 0.86$ , which is the highest value for which complete design curves are presented in Ref. 1. The  $\lambda$  is free-space wavelength, and  $\lambda_g$  is guide wavelength of the waves propagated within the antenna. Antenna C is  $20\lambda$  long at the design frequency of 10 Gc, and is designed to radiate 90 percent of the input power. The dimensions of the antenna, as designed to radiate a narrow-beam  $H$ -plane pattern, are shown in Fig. IV-6.

When the antenna had been designed to the specifications outlined above, it was modified by moving the solid metal wall with respect to the wire grid, and the  $H$ -plane radiation pattern of the modified antenna was calculated. In carrying out these calculations, a digital computer was used to solve the transcendental equation describing this type of antenna,<sup>1</sup> and then to calculate the amplitude and phase at points every  $0.1\lambda$  along the aperture. The digital computer was then used to vectorially sum the contribution of each of these points to the radiation pattern at half-degree increments over the interval  $0 \leq \theta \leq 90$  degrees. The angle  $\theta$  is measured with respect to the broadside direction, and is positive in a direction away from the input of the antenna.





RB-1954-200



RB-1954-200

FIG. IV-6  
DIMENSIONS OF ANTENNAS C AND D AS DESIGNED FOR CONSTANT PHASE VELOCITY

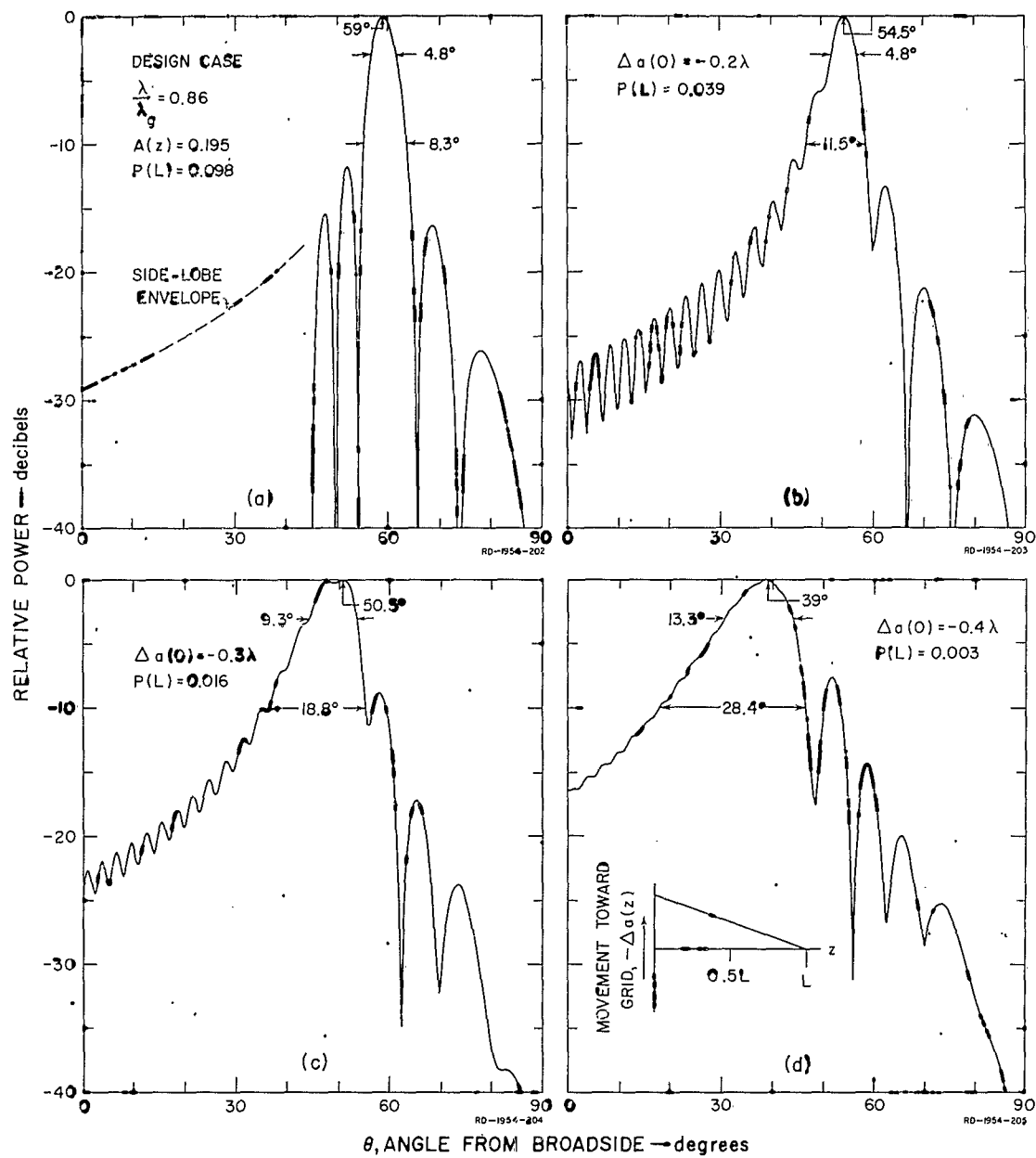


FIG. IV-7  
 RADIATION PATTERNS OF ANTENNA C WITH THE SOLID  
 WALL MOVED TOWARD THE GRID AT THE INPUT END

b. WALL MOVED TOWARD GRID AT INPUT END

The radiation pattern of Antenna C as designed with constant phase velocity is shown in Fig. IV-7(a).<sup>\*</sup> The familiar  $\sin u/u$  pattern of a uniformly illuminated aperture is modified here by the  $\cos \theta$  element pattern of the wire grid. The remaining parts of Fig. IV-7 show the patterns resulting when the grid-to-solid-wall spacing is decreased at the input end of the antenna in increments as indicated on each pattern. Also indicated on each pattern are the fraction of the input power that is dissipated in the load,  $P(L)$ , the angle at which the peak of the beam occurs, and the beamwidths at the -3 db and -10 db levels. Comparing Figs. IV-7(a) and IV-7(d), it is seen that the indicated motion of the solid metal wall increases the 3-db beamwidth by a factor of 2.8, and the 10-db beamwidth by a factor of 3.4.

For the patterns of Fig. IV-7, the grid-to-solid-wall spacing was held fixed at the load end of the antenna and the incremental change in spacing was varied linearly along the antenna, that is:

$$a(z) = a'(z) - K \left( 1 - \frac{z}{L} \right) \quad (\text{IV-1})$$

where

$a'$  = grid-to-solid-wall spacing of the antenna as designed for constant phase velocity

$a$  = grid-to-solid-wall spacing of the modified antenna

$K$  = a constant of proportionality

$z$  = coordinate along the antenna, the origin being at the input end

$L$  = total physical length of the antenna.

Since  $L \gg a$  for the antennas that will be considered, the motion described by Eq. (IV-1) corresponds very closely to pivoting the metal wall about its end located at the load end of the antenna. The minimum grid-to-solid-wall spacing considered at the input end is such that a solid-wall waveguide of the same width would be just above cut-off. A solid-wall waveguide would, presumably, be used to feed the antenna.

<sup>\*</sup> For regions where many side lobes exist separated by deep nulls, only the envelope of the side-lobe peaks is shown. This simplification does not result in significant loss of information.

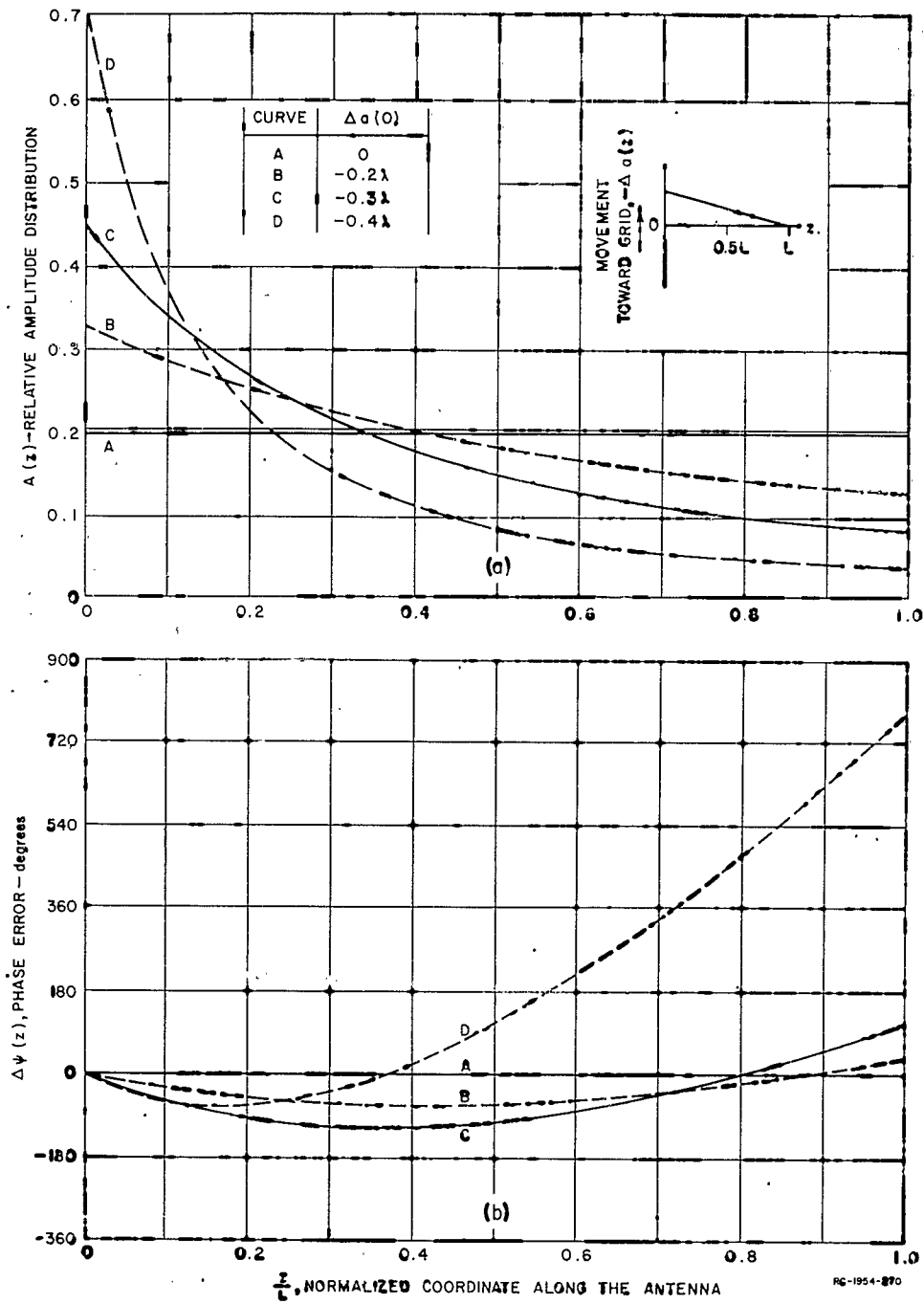


FIG. IV-8  
APERTURE DISTRIBUTIONS OF ANTENNA C WITH THE SOLID WALL  
MOVED TOWARD THE GRID AT THE INPUT END

For small motions of the solid metal wall with respect to the wire grid, the effects on the radiation pattern are probably due primarily to phase error across the antenna aperture. For large motions of the solid wall, however, changes in the amplitude distribution are also significant. The phase errors and amplitude distributions are shown in Fig. IV-8 for the wall movements for which patterns are shown in Fig. IV-7. The phase reference is taken at the input of the antenna, and each phase error curve is calculated with respect to the linear phase distribution that would produce a narrow beam in the same direction as the peak of the actual beam. Explicitly,

$$\Delta\psi(z) = \psi(z) - \frac{360^\circ}{\lambda} z \sin \theta_n \quad (\text{IV-2})$$

where

$\psi(z)$  = the phase distribution along the antenna aperture

$\theta_n$  = angle at which the peak of the radiation pattern occurs.

Equation (IV-2) neglects a small shift in the direction of the beam peak due to the element factor of the wire grid.<sup>1</sup> By defining the phase error as in Eq. (IV-2), the beam-scanning effects of moving the solid wall are at least partially separated from the beam-broadening effects.\* The curves of Fig. IV-8(a) demonstrate that as the metal wall is moved closer to the grid, the rate at which energy leaks out of the antenna increases. As a result, the amplitude distribution in the aperture of the antenna peaks up very sharply at the input end as  $a(z)$  is decreased at  $z = 0$ .

#### C. WALL MOVED TOWARD GRID AT LOAD END

Figure IV-9 shows the patterns resulting when the grid-to-solid-wall spacing of Antenna C is decreased at the load end of the antenna according to the relationship:

$$a(z) = a'(z) - K \frac{z}{L} \quad (\text{IV-3})$$

\* It will be demonstrated in the discussion of Antennas E and F that it is possible to keep the direction of the main beam nearly constant as the beam is broadened. This requires more complex movement of the solid wall than is considered above.

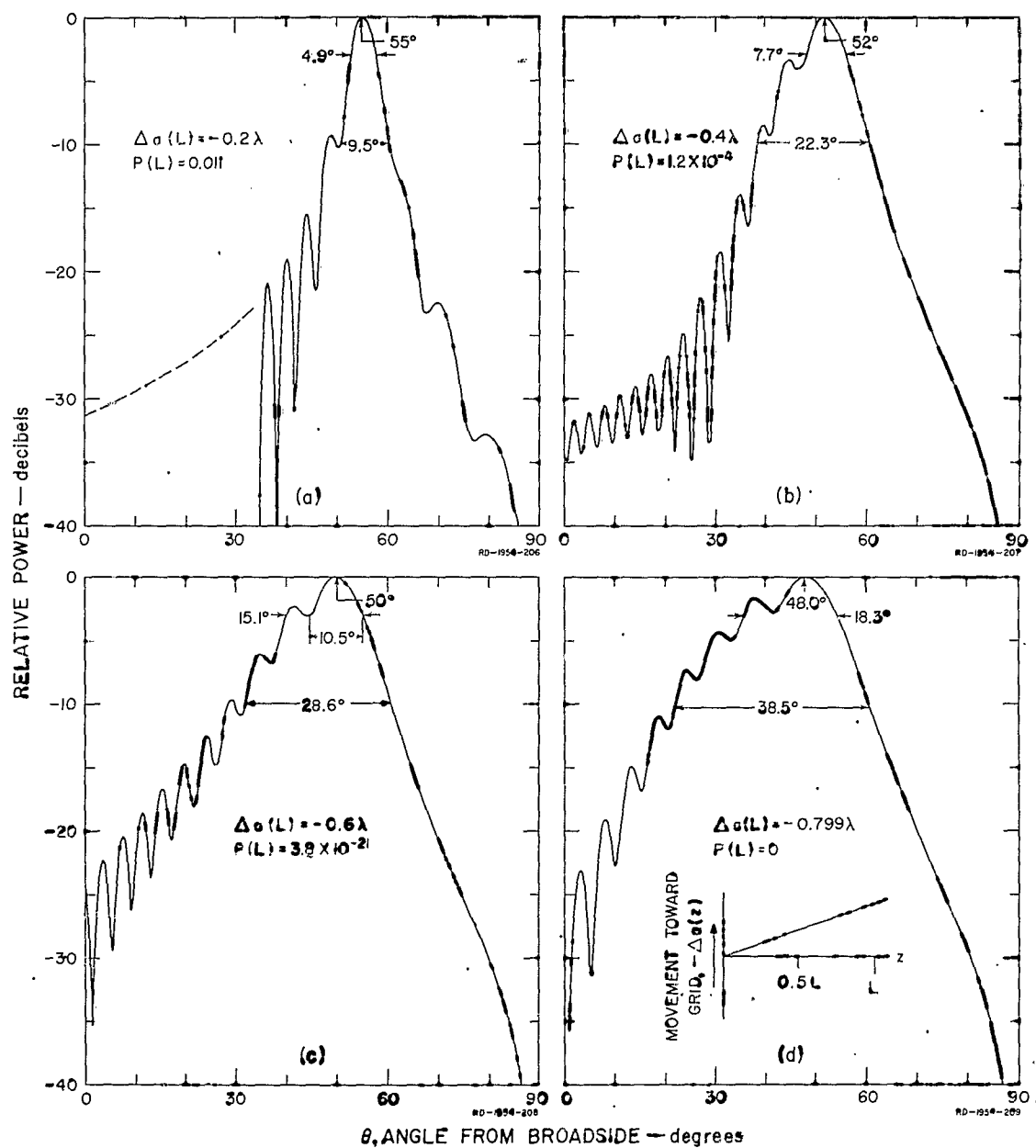


FIG. IV-9  
RADIATION PATTERNS OF ANTENNA C WITH THE SOLID WALL  
MOVED TOWARD THE GRID AT THE LOAD END

Equation (IV-3) corresponds approximately to the conditions existing when the solid metal wall is pivoted about its end at the antenna input. The pattern shown in Fig. IV-9(d) corresponds to the case where the metal plate touches the plane of the wire grid at the load end of the antenna. Comparing Figs. IV-7(a) and IV-9(d), it is seen that the indicated motion of the solid metal wall increases the 3-db beamwidth by a factor of 3.8, and the 10-db beamwidth by a factor of 4.6.

The aperture amplitude distribution and phase error corresponding to each radiation pattern of Fig. IV-9 are shown in Fig. IV-10. As  $a(z)$  is decreased at  $z = L$ , the aperture distribution peaks up smoothly near the center of the antenna. When the grid-to-solid-wall spacing is decreased sufficiently, a condition is reached that is somewhat analogous to cut-off in solid-wall waveguide, as is explained in Ref. 1. This condition might be termed pseudo-cut-off, since waves can still propagate within the antenna even though the attenuation rate rises sharply as the grid-to-solid-wall spacing is further reduced. For the antenna whose radiation pattern is shown in Fig. IV-9(d) the pseudo-cut-off point lies within the region  $0.50L < z < 0.55L$ . Beyond that region, the aperture amplitude distribution rapidly falls to a very small value as shown by Curve E in Fig. IV-10(a). This limiting of the effective radiating aperture is possibly of advantage in broadening the main beam.

#### d. WALL MOVED TOWARD GRID AT BOTH ENDS

Note from Figs. IV-7 and IV-9 that decreasing  $a(0)$  produces a smooth pattern for angles less than  $\theta_m$ , the direction of the beam peak, and that decreasing  $a(L)$  produces a smooth pattern for angles greater than  $\theta_m$ . This suggested that a smooth pattern might be obtained on both sides of  $\theta_m$  by fixing the grid-to-solid-wall spacing at some central point, and decreasing both  $a(0)$  and  $a(L)$ . This wall movement is defined by the following equations:

$$a(z) = a'(z) - K_1 \left( 0.5 - \frac{z}{L} \right) \quad (\text{IV-4})$$

for  $0 \leq z \leq 0.5L$ , and

$$a(z) = a'(z) - K_2 \left( \frac{z}{L} - 0.5 \right) \quad (\text{IV-5})$$

for  $0.5L < z \leq L$ ,

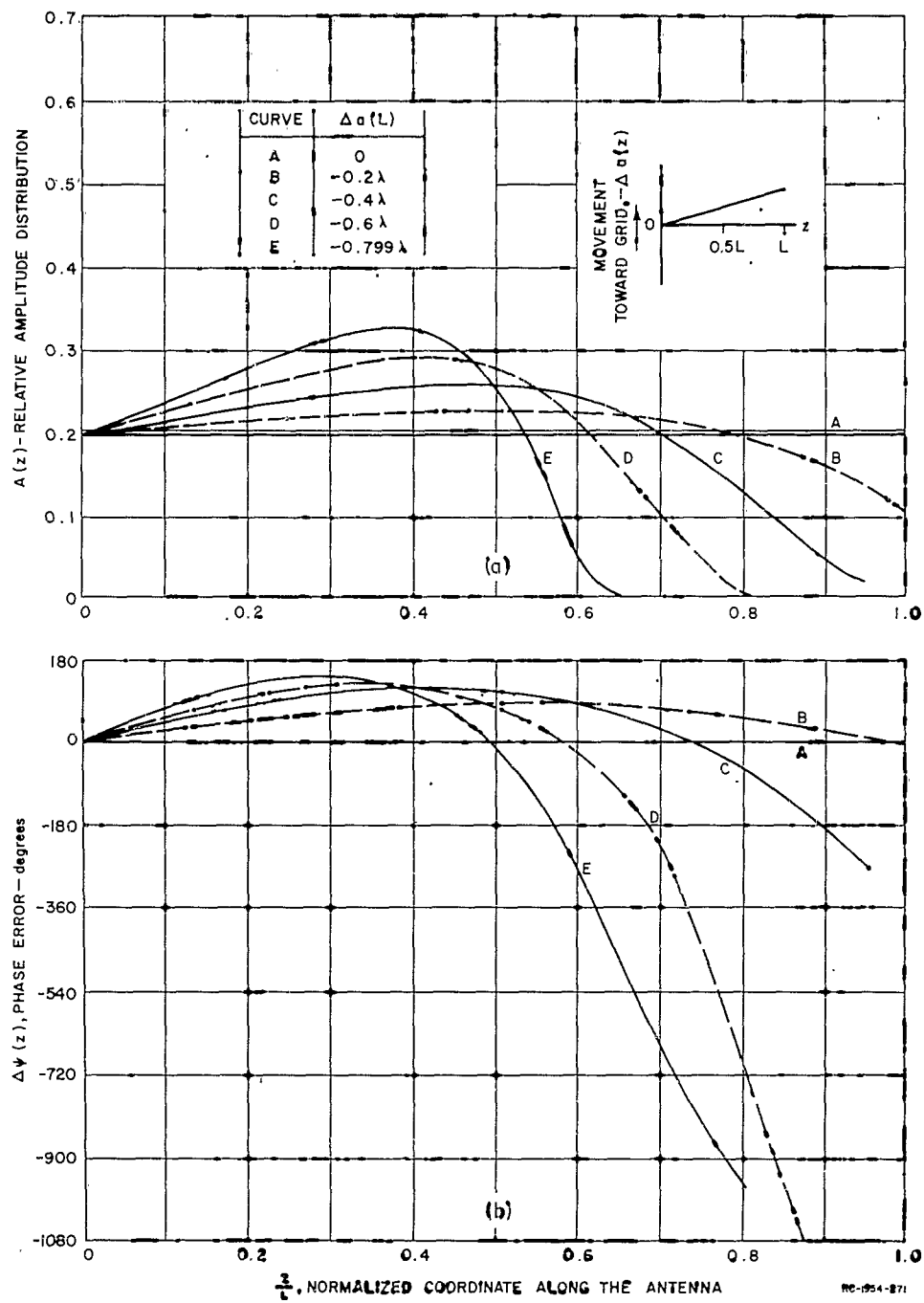


FIG. IV-10  
APERTURE DISTRIBUTIONS OF ANTENNA C WITH THE SOLID WALL  
MOVED TOWARD THE GRID AT THE LOAD END



where  $K_1, K_2$  are positive constants of proportionality. The motion defined by Eqs. (IV-4) and (IV-5) corresponds very closely to pivoting the solid wall at  $z = 0.5L$ , the solid wall being hinged at that point. The change  $\Delta a(0)$  in grid-to-solid-wall spacing at the antenna input was taken to be half the change  $\Delta a(L)$  in grid-to-solid-wall spacing at the load end of the antenna. For this ratio of  $\Delta a(0)$  to  $\Delta a(L)$ , the solid wall is touching the wire grid at the load end of the antenna when the grid-to-solid-wall spacing at the antenna input is such that a solid-wall waveguide of the same width would be just above cut-off.

It is seen from the patterns shown in Fig. IV-11 that modifications of the type described by Eqs. (IV-4) and (IV-5) are not effective in broadening the main beam of the radiation pattern. The main effect of moving the solid wall toward the wire grid at both the input and load ends is to raise the side-lobe levels, although the lobes do tend to merge for the maximum motion of the solid wall. The amplitude distributions and phase errors producing the patterns of Fig. IV-11 are shown in Fig. IV-12.

#### e. WALL MOVED TOWARD GRID AT CENTER

One final type of wall motion considered for Antenna C was motion of the center of the solid wall toward the grid, the solid wall being hinged at its center and the grid-to-solid-wall spacing remaining unchanged at both ends of the antenna. Specifically,

$$a(z) = a'(z) - K \frac{z}{L} \quad (\text{IV-6})$$

for  $0 \leq z \leq 0.5L$ , and

$$a(z) = a'(z) - K \left(1 - \frac{z}{L}\right) \quad (\text{IV-7})$$

for  $0.5L < z \leq L$ . Radiation patterns for Antenna C modified by this type of wall motion are shown in Fig. IV-13. The amplitude distributions and phase errors resulting from the wall motions of Eqs. (IV-6) and (IV-7) are plotted in Fig. IV-14. This type of wall motion increases the 3-db beamwidth only slightly, except for the largest wall movement considered. The 3-db beamwidth in Fig. IV-13(d) is larger by a factor of 3.8 than that of the antenna as designed with constant phase velocity.

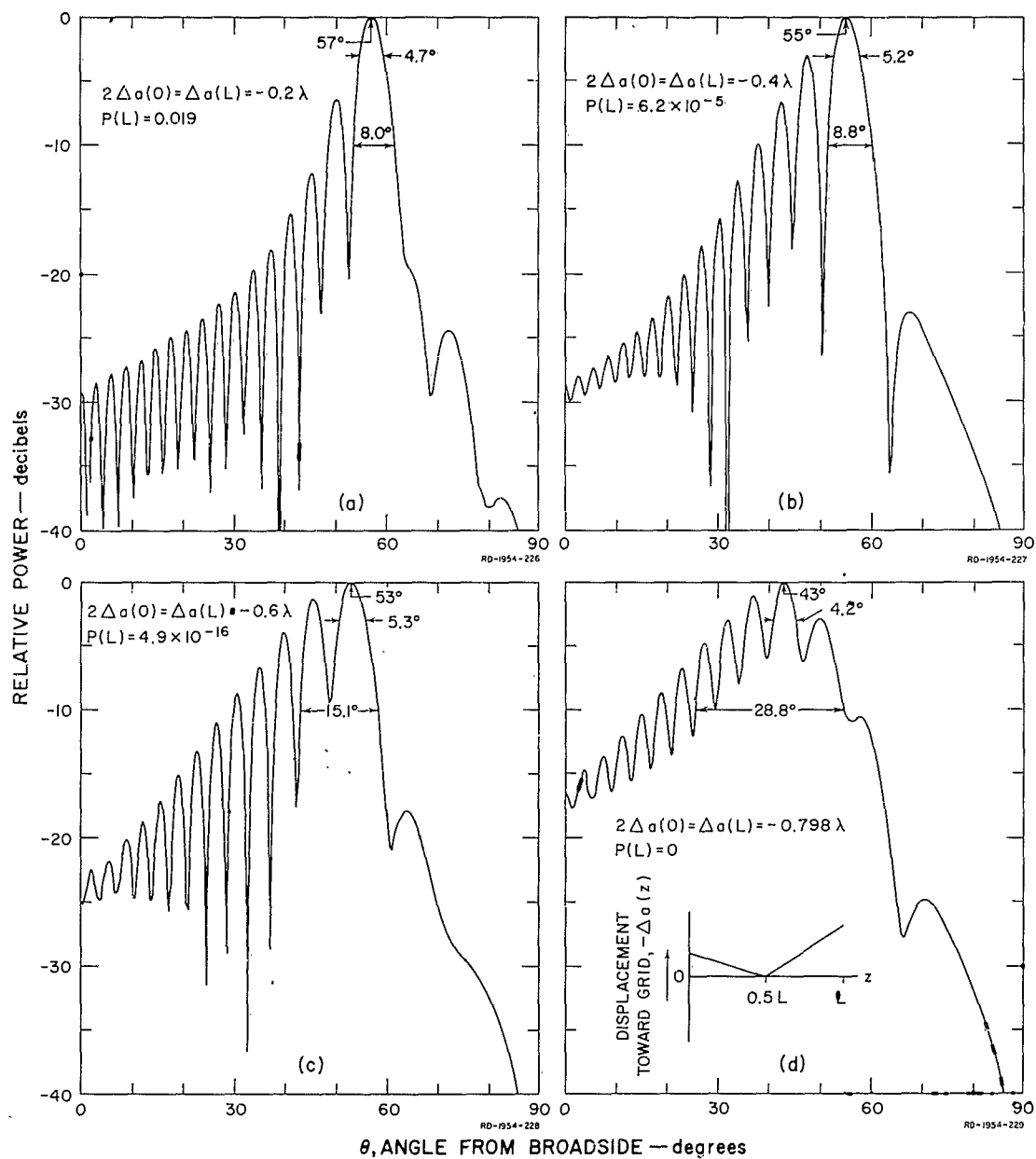


FIG. IV-11  
RADIATION PATTERNS OF ANTENNA C WITH THE SOLID WALL  
MOVED TOWARD THE GRID AT BOTH ENDS,  
THE CENTER POINT BEING FIXED

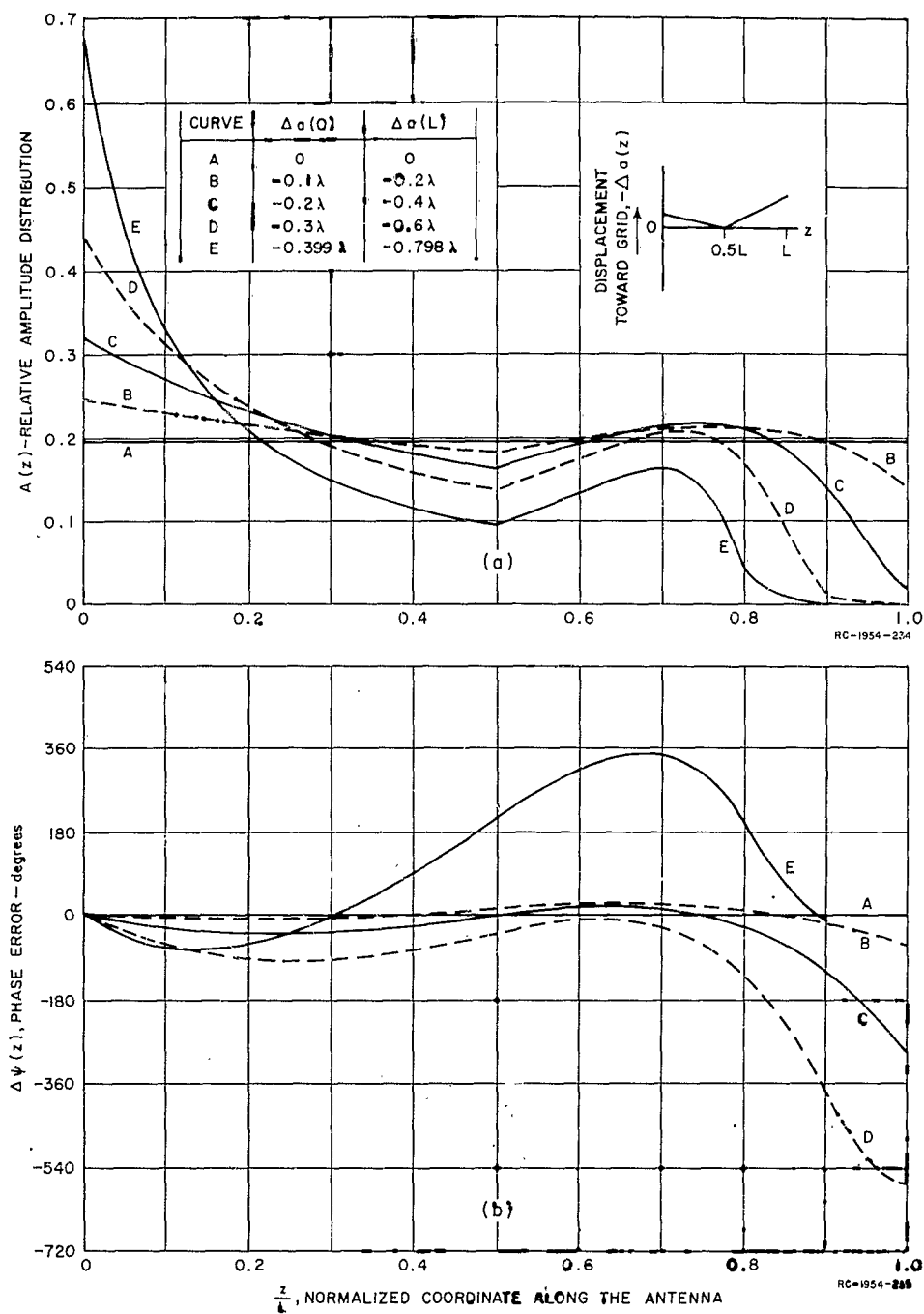


FIG. IV-12  
APERTURE DISTRIBUTIONS OF ANTENNA C WITH THE SOLID WALL  
MOVED TOWARD THE GRID AT BOTH ENDS,  
THE CENTER POINT BEING FIXED

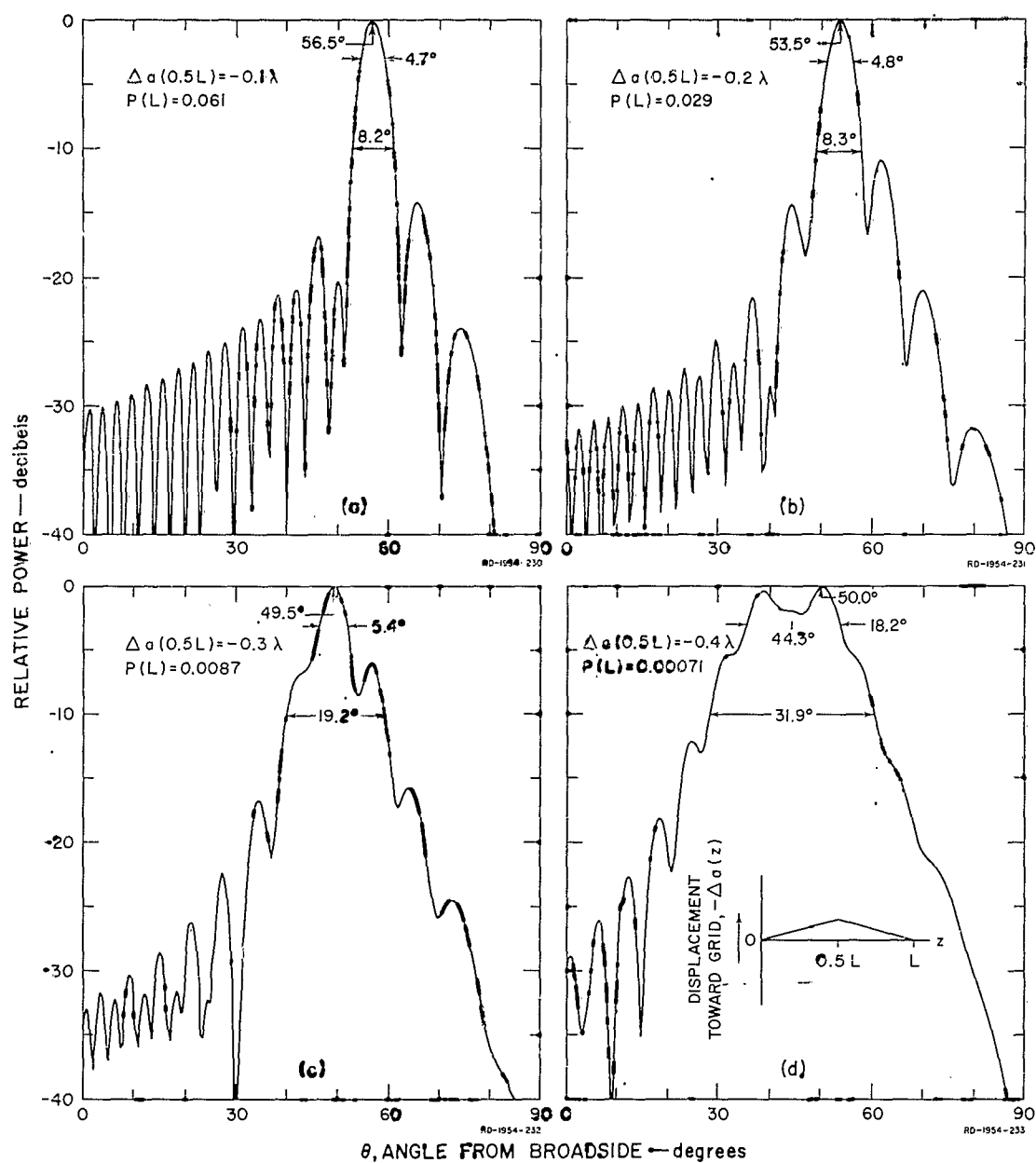


FIG. IV-13

RADIATION PATTERNS OF ANTENNA C WITH THE SOLID WALL  
MOVED TOWARD THE GRID AT THE CENTER POINT,  
BOTH ENDS BEING FIXED

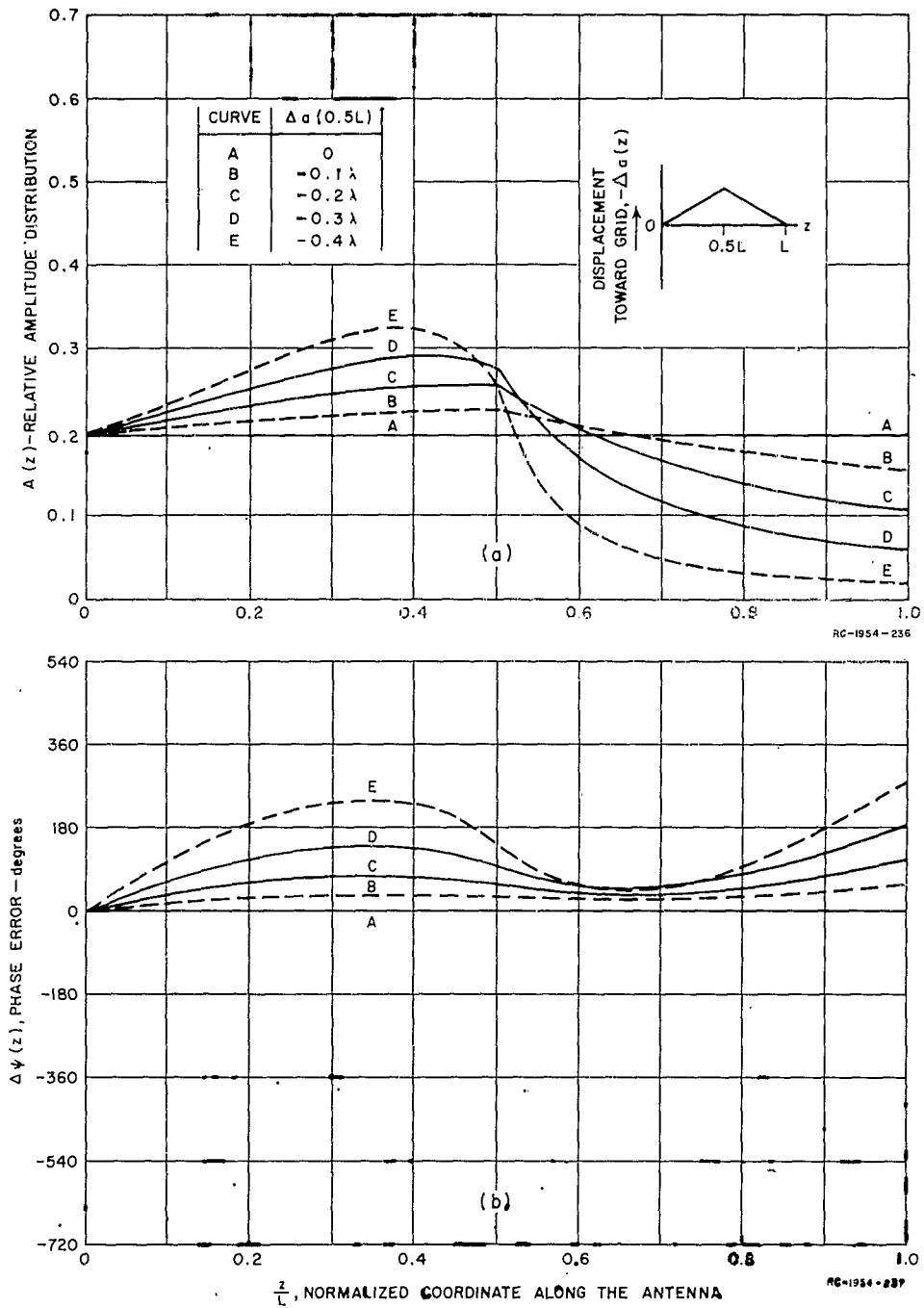


FIG. IV-14  
APERTURE DISTRIBUTIONS OF ANTENNA C WITH THE SOLID WALL  
MOVED TOWARD THE GRID AT THE CENTER POINT,  
BOTH ENDS BEING FIXED

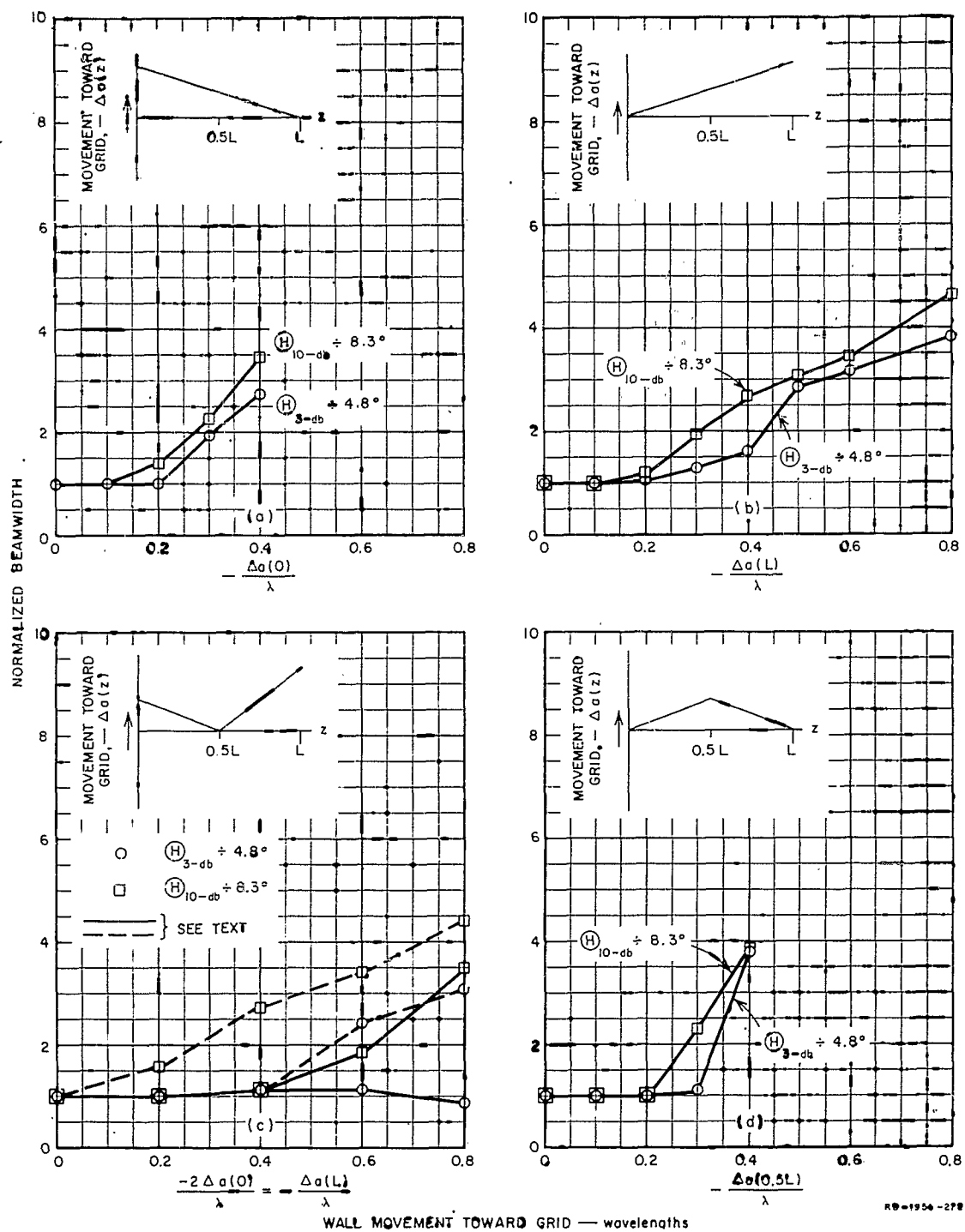


FIG. IV-15

BEAM BROADENING RESULTING FROM MOVEMENT OF THE SOLID WALL  
OF ANTENNA C TOWARD ITS GRID

#### f. COMPARISON OF WALL MOVEMENTS

The beam broadening resulting from the various wall movements tried with Antenna C is summarized in Fig. IV-15. In each part of this figure, the total beamwidth measured at the -3-db level,  $\Theta_{3db}$ , and the total beamwidth measured at the -10-db level,  $\Theta_{10db}$ , are divided by the respective values for the antenna as designed for constant phase velocity. The solid curves are each based on the beamwidths measured between the points where the radiation pattern first drops below the -3-db or -10-db level, as given by the notations on the radiation patterns. For some of the radiation patterns, the pattern crosses the -3-db and -10-db levels more than once, particularly for the patterns of Fig. IV-11. If  $\Theta_{3db}$  and  $\Theta_{10db}$  are measured between the most widely spaced points where the pattern crosses the respective level in Fig. IV-11, the dashed curves of Fig. IV-15(c) result.

It is seen from Fig. IV-15 that, for the wall movements tried with Antenna C, wall movement up to  $0.2\lambda$  does not produce significant broadening of the beam. Once the beam does start to broaden, the beamwidth is a linear function of wall movement, to a crude approximation. One factor limiting the beam broadening is the amount of wall motion that is physically possible. Movement of the wall toward the grid at the input end is limited by the requirement that the solid-wall waveguide feeding the antenna be above cut-off. Movement of the wall toward the grid at the load end of the antenna without bending the wall is limited to the case where the solid wall touches the wire grid. Further movement of the wall, once the wall touches the grid at the load end, could be obtained by hinging the wall at some central point. The wall could then be moved until the hinge point touched the grid; however, calculations have not been made for this latter wall motion.

The largest increases in the beamwidth of Antenna C were obtained with the wall motions corresponding to Figs. IV-15(b) and IV-15(d), both increasing  $\Theta_{3db}$  by a factor of 3.8. Comparing parts (b) and (d) of Fig. IV-15, it is seen that for a given wall movement at  $z = 0.5L$ , the beamwidth increases more uniformly with wall movement when the load end of the wall is free to move than when it is fixed. Thus, further calculations using the wall movement defined by Eqs. (IV-6) and (IV-7), but with hinge points other than  $z = 0.5L$ , were not considered.

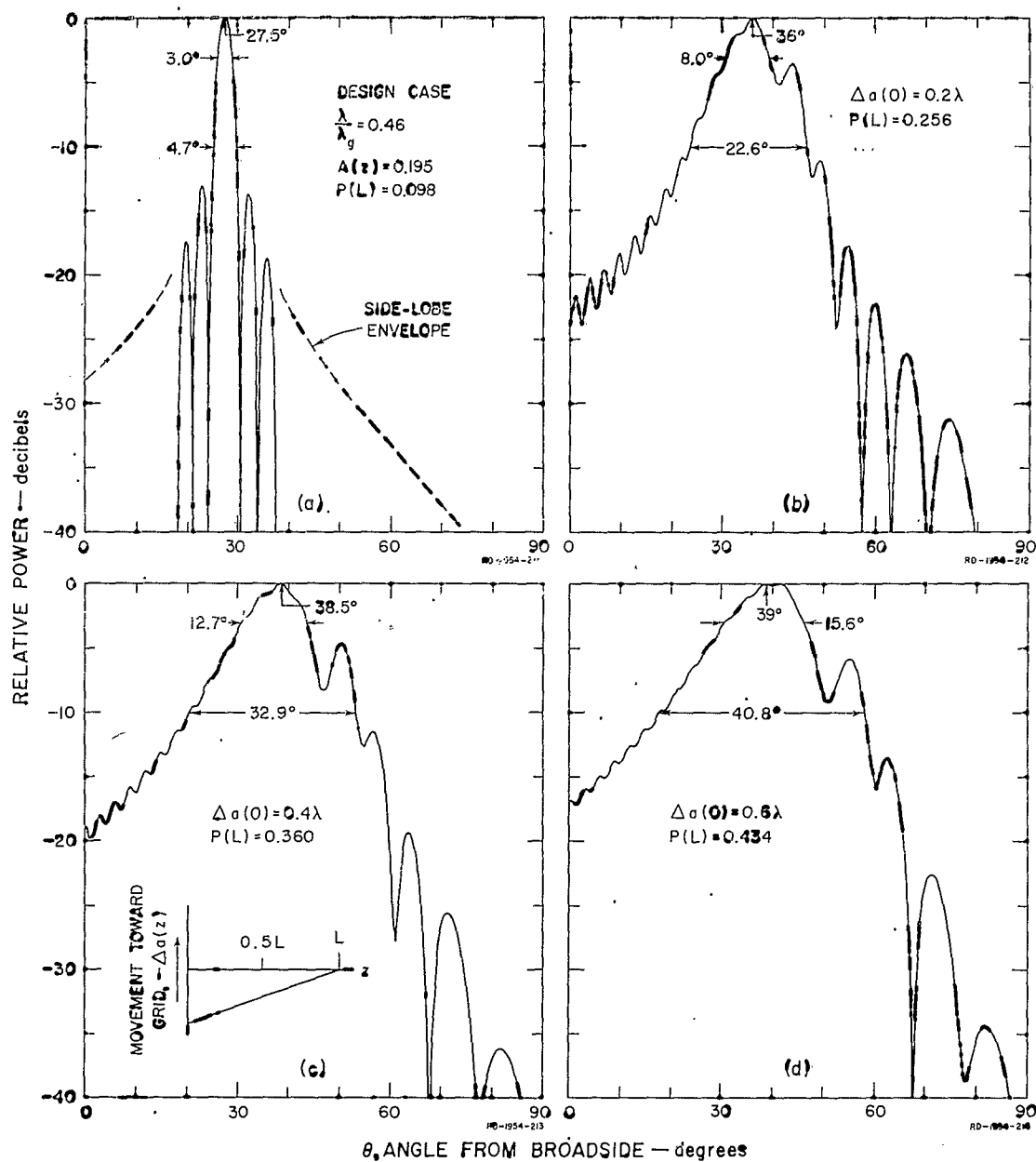


FIG. IV-16

RADIATION PATTERNS OF ANTENNA D WITH THE SOLID WALL MOVED AWAY FROM THE GRID AT THE INPUT END



### 3. ANTENNA D

The second antenna that was designed with constant aperture amplitude, Antenna D, was designed with constant phase velocity as given by  $\lambda/\lambda_g = 0.45$ . This corresponds to the highest phase velocity for which complete design curves are available in Ref. 1. The other design parameters, and the dimensions of Antenna D, are shown in Fig. IV-6, along with those of Antenna C.

The radiation pattern of Antenna D as designed with constant phase velocity is shown in Fig. IV-16(a). The remaining parts of Fig. IV-16 apply for the case where the grid-to-solid-wall spacing is increased at the input end of the antenna, and is fixed at the load end. Equation (IV-1) applies to this case, where  $K$  would now be a negative constant. Comparing Figs. IV-16(a) and IV-16(d), it is seen that the indicated motion of the solid metal wall increases the 3-db beamwidth by a factor of 5.2, and the 10-db beamwidth by a factor of 8.7. The aperture amplitude and phase error corresponding to each pattern of Fig. IV-16 are shown in Fig. IV-17.

Figure IV-18 shows the patterns resulting when the grid-to-solid-wall spacing is increased at the load end as given by Eq. (IV-3) with  $K$  negative. Comparing Figs. IV-16(a) and IV-18(d) it is seen that the indicated motion of the solid metal wall increases the 3-db beamwidth by a factor of 5.0, and the 10-db beamwidth by a factor of 9.0. The corresponding aperture amplitude and phase errors are shown in Fig. IV-19.

The beam broadening resulting from the two types of wall movement tried with Antenna D are summarized in Fig. IV-20.\* Here again, the solid curves apply to beamwidth measured between the closest crossings of the -3-db and -10-db levels, and the dashed curves apply to beamwidth measured between the most widely spaced crossings of the respective reference level. Comparing the solid curves of parts (a) and (b) of Fig. IV-20, it is seen that both types of wall movement produce about the same increase in beamwidth. Comparing the solid curve of  $\Theta_{3db}$  in Fig. IV-20(a) with the dashed curve of  $\Theta_{3db}$  in Fig. IV-20(b) indicates that moving the solid wall away from the grid at the load end is to be preferred over similar movement at the input end for applications where the 6-db dip in the main beam of Fig. IV-18(d) can be tolerated. Either movement of the solid wall of Antenna D away from its grid produced greater changes in beamwidth than was obtained by moving the solid wall of Antenna C toward

---

\* Movement of the solid wall of Antenna D was considered only in the direction away from the grid, since the antenna was designed fairly close to cut-off. An additional movement that might produce good results is to move the solid wall toward the grid at the load end. Calculations were not made for this case, however.

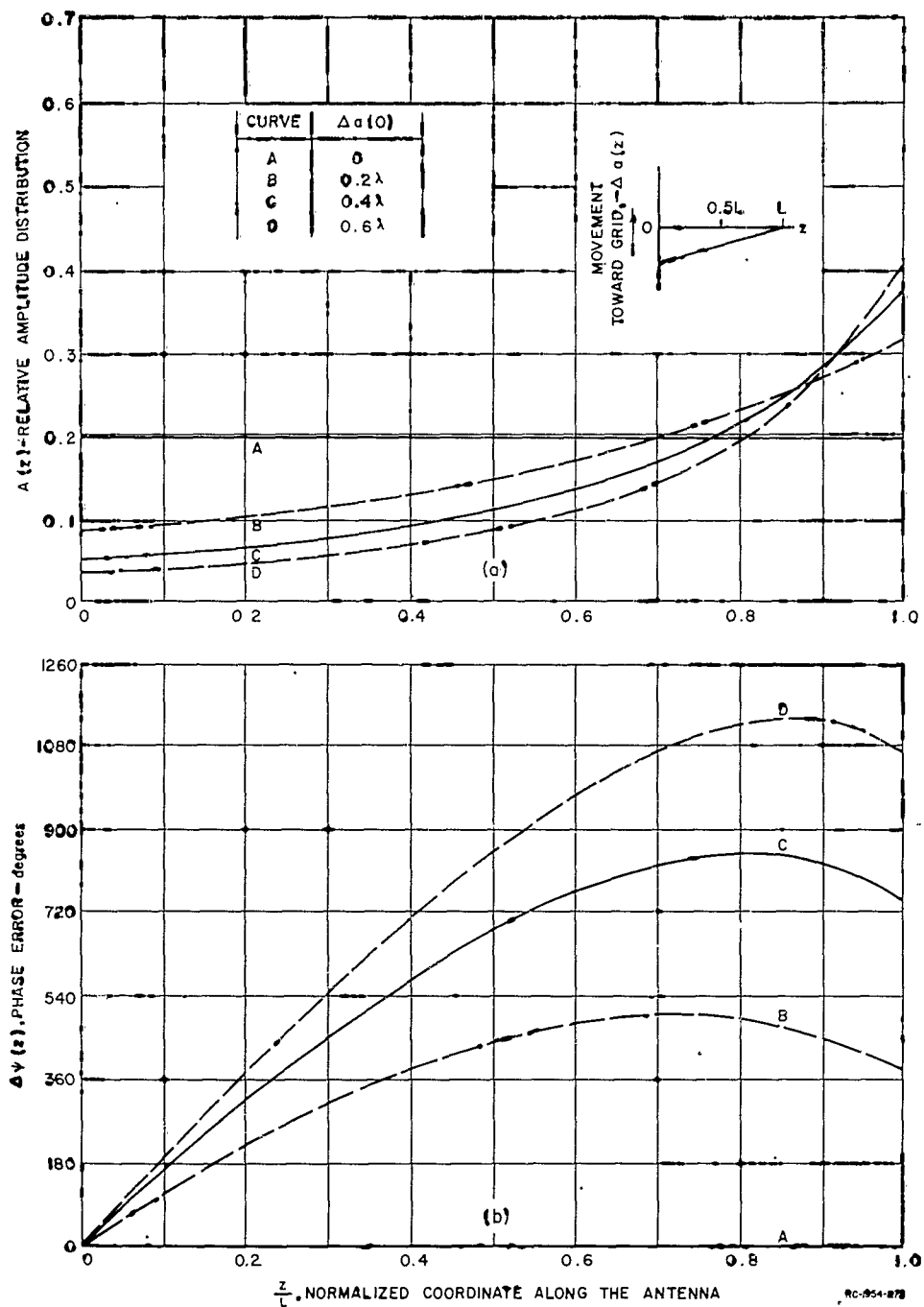


FIG. IV-17

APERTURE DISTRIBUTIONS OF ANTENNA D WITH THE SOLID WALL  
MOVED AWAY FROM THE GRID AT THE INPUT END

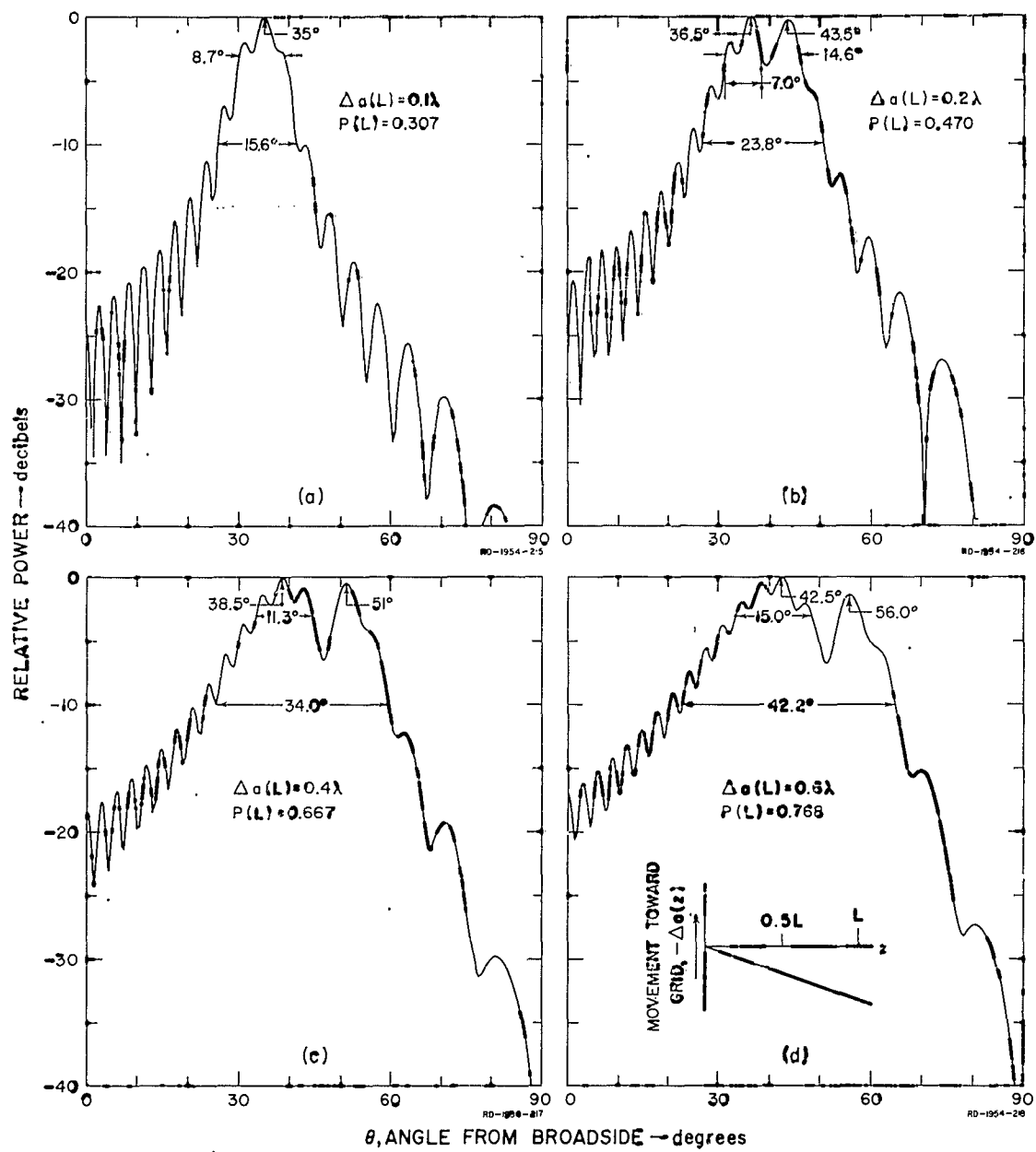


FIG. IV-18  
RADIATION PATTERNS OF ANTENNA D WITH THE SOLID WALL  
MOVED AWAY FROM THE GRID AT THE LOAD END

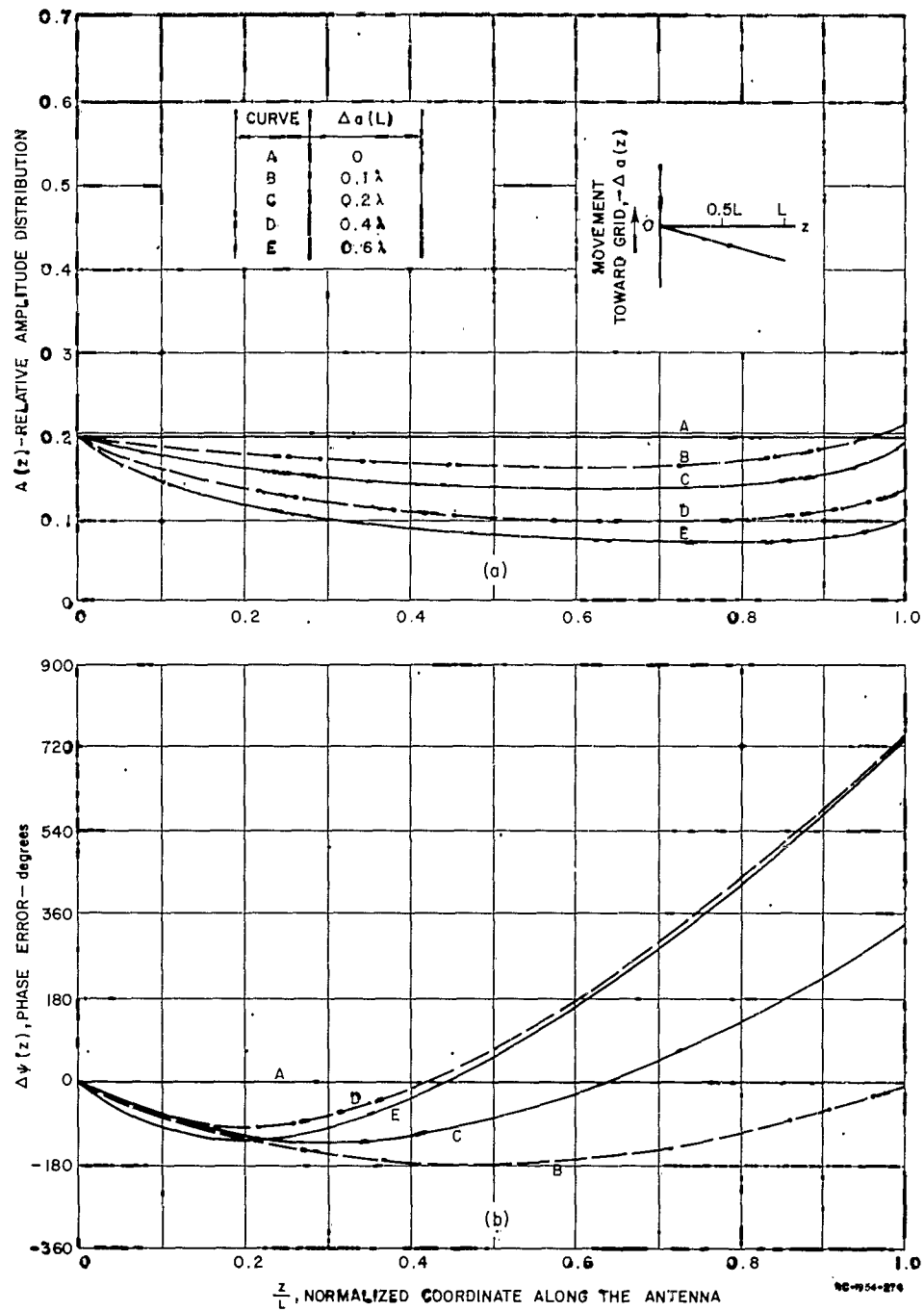


FIG. IV-19  
APERTURE DISTRIBUTIONS OF ANTENNA D WITH THE SOLID WALL  
MOVED AWAY FROM THE GRID AT THE LOAD END

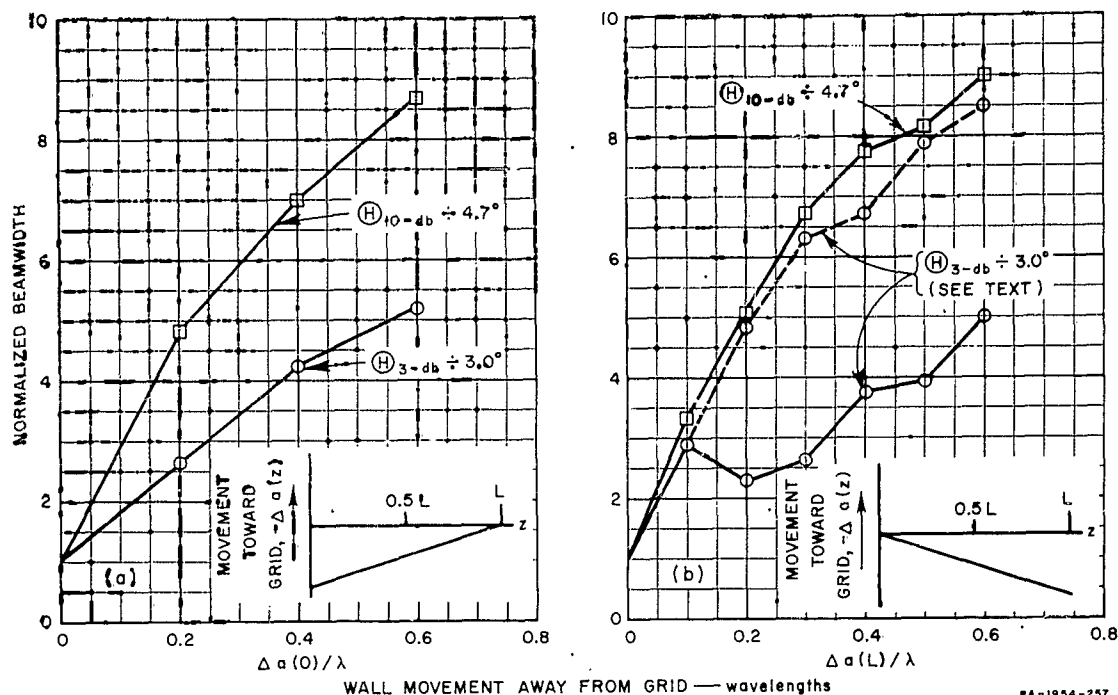


FIG. IV-20

#### BEAM BROADENING RESULTING FROM MOVEMENT OF THE SOLID WALL OF ANTENNA D AWAY FROM ITS GRID

its grid, as is seen by comparing Figs. IV-15 and IV-20. Note that even larger wall motions away from the grid than were considered for Antenna D are possible, but there are definite physical limitations to the amount that the wall of Antenna C can be moved toward its grid. These limitations were discussed in Sec. IV-B-2-f.

Considering only the changes in the beamwidth of the radiation patterns, movement of the solid wall of a leaky-wave antenna away from its wire grid appears better than movement of the wall toward the grid. Movement of the wall away from the grid produces an undesirable effect, however, in that it reduces the amount of the input power that is radiated. From the notations on Figs. IV-16(a) and IV-18(d), it is seen that the indicated wall movement increased the power dissipated in the load from 9.8 to 76.8 percent of the input power. It might be possible to retain the benefits of wall movement away from the grid and still keep the power dissipated in the load within reasonable limits by moving one end of the wall toward the grid as the other end is moved away from the grid. This combination was not investigated, however, for Antennas A, B, C, or D.

## C. DESIGNS BEGINNING WITH BROAD-BEAM ANTENNAS

### 1. ANTENNA E

The approach to the broadening of the radiation pattern that was considered in Sec. IV-B was to start with narrow-beam antennas and to introduce phase errors by simple motions of the solid wall of each antenna. The narrow-beam antennas were designed with constant phase velocities, and with two well-known aperture-amplitude distributions, namely, sinusoidal and uniform distributions. The largest increase in 3-db beamwidth obtained by this approach was a factor of 5.2 for an antenna 20 wavelengths long, as shown by the solid curves in Fig. IV-20. A second approach that will now be considered is to start with an antenna designed to give a broad-beam pattern, and then move the solid wall to produce patterns with narrow and intermediate-width beams. To further increase the range over which the beamwidth can be varied, an antenna length of  $50\lambda$  as well as  $20\lambda$  will be considered.

The shape of the broad-beam pattern to be synthesized was arbitrarily chosen to be a power pattern having the same form as the maximally flat transfer function familiar in filter theory:

$$P(\theta) = \left[ 1 + \left( \frac{\theta - \theta_0}{0.5 \Theta_{3db}} \right)^{2n} \right]^{-1} \quad (IV-8)$$

where

$\theta_0$  = angle about which the pattern is symmetrical

$\Theta_{3db}$  = half-power beamwidth

$n$  = a constant related to the shape of the pattern,  
where  $(2n - 1)$  derivatives of  $P(\theta)$  with respect  
to  $\theta$  are zero at  $\theta_0$ .

In Ref. 2, a functional relationship is derived between the required aperture distributions and the shape of the radiation pattern that it is desired to synthesize. This relationship is found by a stationary phase evaluation of the radiation integral, which is equivalent to using geometric optics approximations. Since the wire grid of the type of leaky-wave antenna being discussed has a  $\cos \theta$  element factor, the desired

radiation pattern  $f(\theta)$  in Eq. (10) of Ref. 2 must be replaced by  $f(\theta)/\cos \theta$  for our application. Making this substitution, and using the present notation,

$$A(z) = \frac{\sec^{1/2} \left[ \theta_l + (\theta_u - \theta_l) \frac{z}{L} \right]}{\sqrt{1 + \left[ \frac{\theta_l - \theta_0 + (\theta_u - \theta_l) \frac{z}{L}}{0.5 \Theta_{3\text{db}}} \right]^{2n}}} \quad (\text{IV-9})$$

where

$A(z)$  = the aperture amplitude distribution required to approximately synthesize the maximally flat power pattern of Eq. (IV-8)

$\theta_l$  = the lower limit of the range on  $\theta$  over which the pattern is to be synthesized

$\theta_u$  = the upper limit of the range on  $\theta$  over which the pattern is to be synthesized.

The phase distribution used in Ref. 2 is obtained with a leaky-wave antenna when the radiation angle  $\sin^{-1} (\lambda/\lambda_g)$  for an incremental length of the antenna varies linearly as a function of  $z$ , from  $\theta_l$  at the input end to  $\theta_u$  at the load end. That is,

$$\frac{\lambda}{\lambda_g} = \sin \left[ \theta_l + (\theta_u - \theta_l) \frac{z}{L} \right] \quad (\text{IV-10})$$

The actual radiation patterns of  $50\lambda$ -long antennas having the aperture amplitude and phase distributions defined by Eqs. (IV-9) and (IV-10) were calculated for  $\theta_0 = 40$  degrees,  $\Theta_{3\text{db}} = 45$  degrees, and  $n = 4, 6$ , and  $10$ . The angular limits  $\theta_l$  and  $\theta_u$  were arbitrarily taken to be the  $-20$ -db points on the desired pattern of Eq. (IV-8), except that  $\theta_l = 5.0$  degrees was used for  $n = 4$ , since the  $-20$ -db point fell at the broadside direction. Radiation in the broadside direction implies that  $\sin^{-1} (\lambda/\lambda_g) = 0$ , i.e., that the antenna be at cut-off. Good agreement between the actual radiation pattern and the maximally flat pattern was obtained for all three values of  $n$ , but the best agreement was obtained for  $n = 6$ .

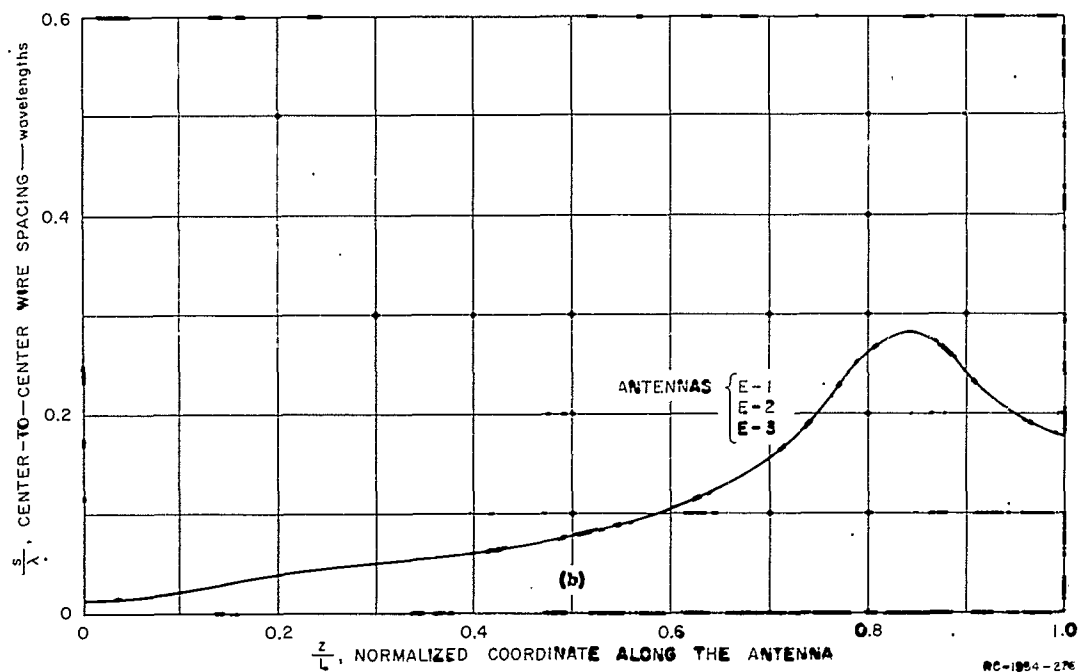
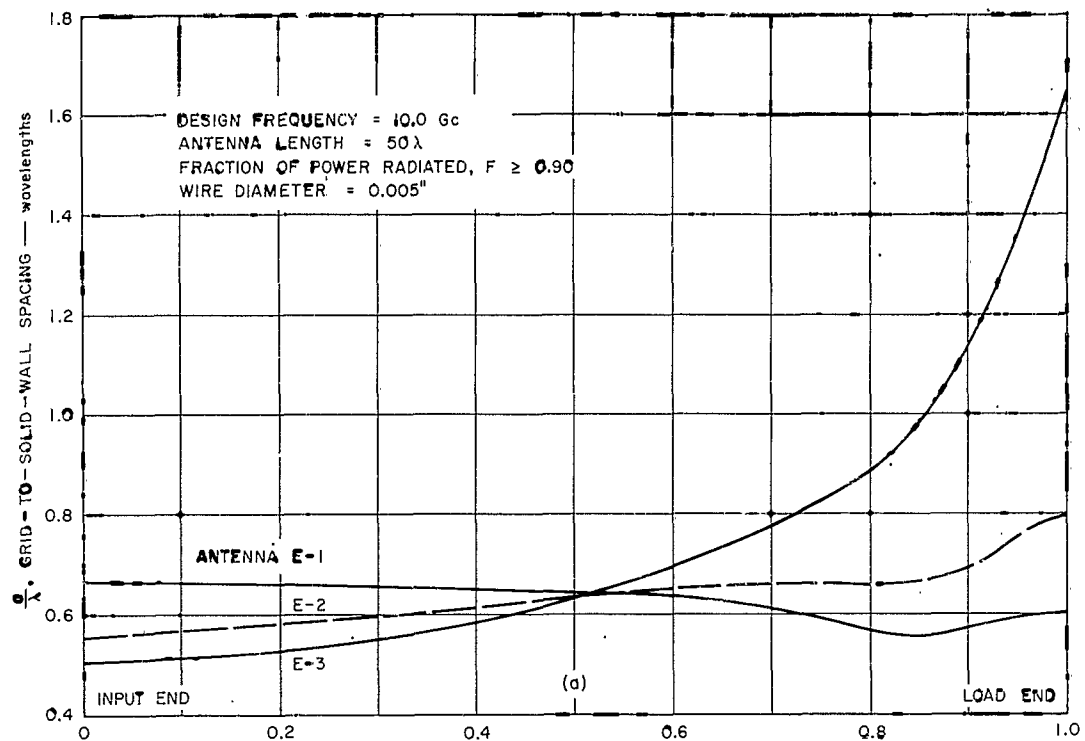


FIG. IV-21  
 DIMENSIONS OF ANTENNA E



The digital computer was then used to solve the transcendental equations describing this type of leaky-wave antenna<sup>1</sup> in order to find the dimensions that would satisfy Eqs. (IV-9) and (IV-10). The constants used are  $n = 6$ ,  $\theta_0 = 40$  degrees,  $\theta_{3\text{db}} = 45$  degrees,  $\theta_i = 6.9$  degrees, and  $\theta_u = 73.1$  degrees. In carrying out these calculations, the computer determined a constant of proportionality required in Eq. (IV-9) in order that 90 percent of the input power be radiated. The resulting antenna dimensions are shown in Fig. IV-21 by the curves labeled Antenna E-3. In order to obtain a narrow-beam radiation pattern from the same antenna, the grid-to-solid-wall spacing was next determined such that the phase velocity was constant along the antenna, given the center-to-center wire spacing taken from the design of the broad-beam antenna. The design curves of Ref. 1 were used in designing the narrow-beam antenna. The design curves for  $\lambda/\lambda_g = 0.66$  were used, since this places the peak of the narrow beam at 41.3 degrees, which is near the center of the broad beam. The resultant dimensions are shown by the curves labeled Antenna E-1 in Fig. IV-21. One final change in the antenna will be described before discussing the radiation patterns. In order to obtain a quick, even if far from optimum, design to give a beam of intermediate width, the grid-to-solid-wall spacing was determined such that the radiation angle  $\sin^{-1}(\lambda/\lambda_g)$  varied linearly over the length of the antenna from  $\theta_i = 25.3$  degrees to  $\theta_u = 54.7$  degrees. These angles are the -20-db points on a maximally flat power pattern with  $n = 6$ ,  $\theta_0 = 40$  degrees, and  $\theta_{3\text{db}} = 20$  degrees. The dimensions of the intermediate-beamwidth antenna are shown by the curves labeled Antenna E-2 in Fig. IV-21. Since  $\alpha(z)$  for Antenna E covers a fairly large range, Fig. IV-21 cannot be read to great accuracy. Thus, the dimensions of Antenna E are tabulated in Table IV-1.

The radiation patterns calculated for the three wall positions for Antenna E discussed above are shown in Fig. IV-22, and the aperture amplitude and phase error are shown in Fig. IV-23. The narrow-beam pattern of Fig. IV-22(a) has a 3-db width of 2.1 degrees and, rather fortuitously, the tapered aperture amplitude distribution produces no side lobes above the -40 db level. The beamwidth is not, of course, the narrowest that could be obtained with an aperture of this size. For a  $50\lambda$ -long aperture radiating at 41.3 degrees from the broadside direction, the 3-db beamwidth would be 1.35 degrees for uniform amplitude distribution, and would be 1.8 degrees for a sinusoidal aperture amplitude distribution.

TABLE IV-1  
DIMENSIONS OF ANTENNA E

DISTANCE ALONG THE ANTENNA, $z/L$	CENTER-TO-CENTER WIRE SPACING, $s/\lambda$	GRID-TO-SOLID-WALL SPACING, $a/\lambda$		
		Antenna E-1	Antenna E-2	Antenna E-3
0	0.0137	0.6656	0.5530	0.5036
0.05	0.0165	0.6643	0.5598	0.5072
0.10	0.0220	0.6630	0.5668	0.5123
0.15	0.0306	0.6616	0.5738	0.5181
0.20	0.0394	0.6601	0.5810	0.5257
0.25	0.0450	0.6584	0.5883	0.5362
0.30	0.0495	0.6564	0.5957	0.5496
0.35	0.0546	0.6541	0.6034	0.5655
0.40	0.0605	0.6515	0.6119	0.5842
0.45	0.0667	0.6480	0.6210	0.6061
0.50	0.0767	0.6444	0.6328	0.6315
0.55	0.0882	0.6394	0.6410	0.6609
0.60	0.1034	0.6329	0.6510	0.6948
0.65	0.1242	0.6234	0.6578	0.7337
0.70	0.1544	0.6094	0.6596	0.7776
0.75	0.2000	0.5903	0.6605	0.8264
0.80	0.2596	0.5643	0.6544	0.8846
0.85	0.2816	0.5556	0.6649	0.9830
0.90	0.2419	0.5718	0.6905	1.1463
0.95	0.1990	0.5895	0.7541	1.3629
1.00	0.1753	0.6002	0.7949	1.6480

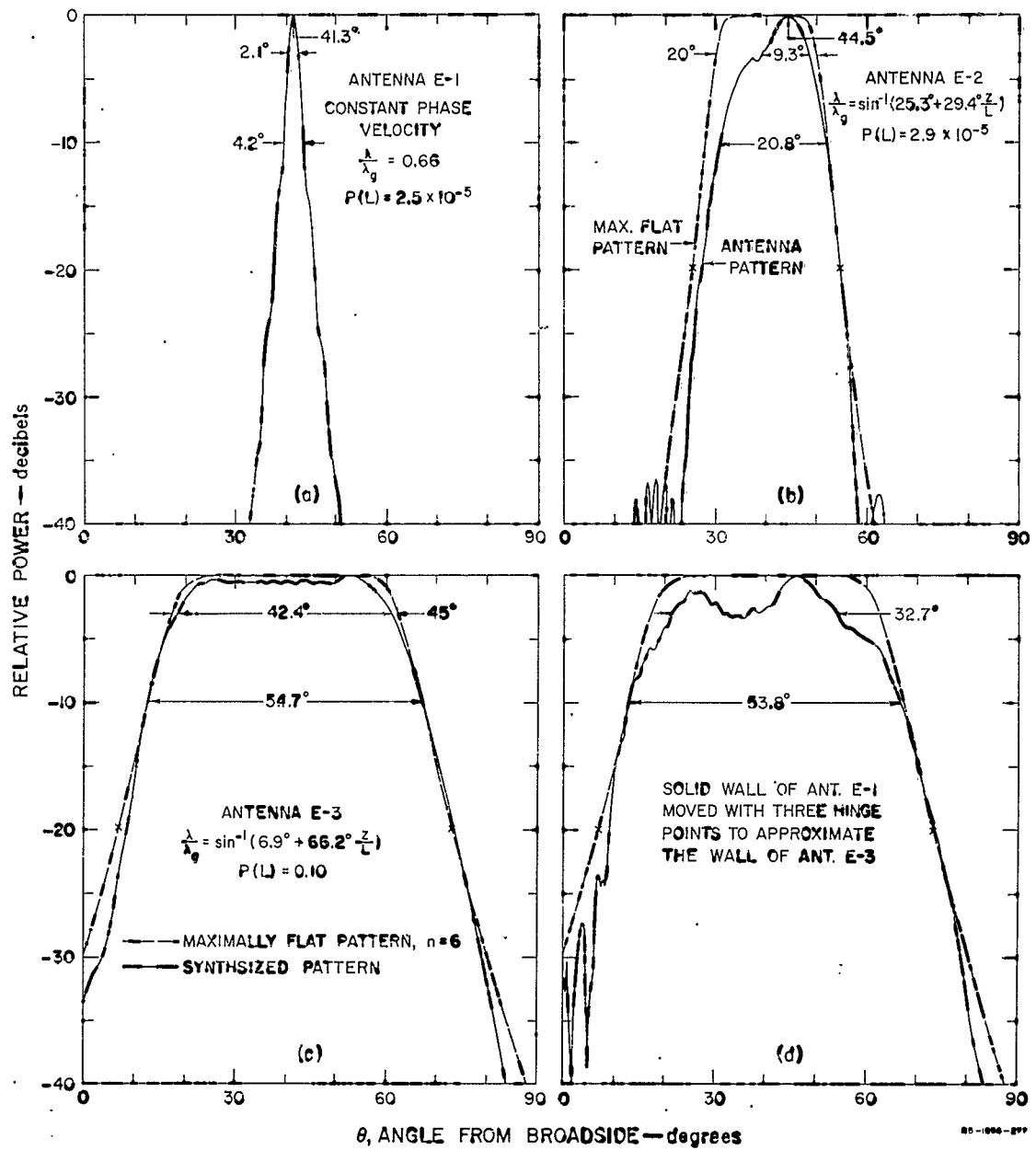


FIG. IV-22  
RADIATION PATTERNS OF ANTENNA E

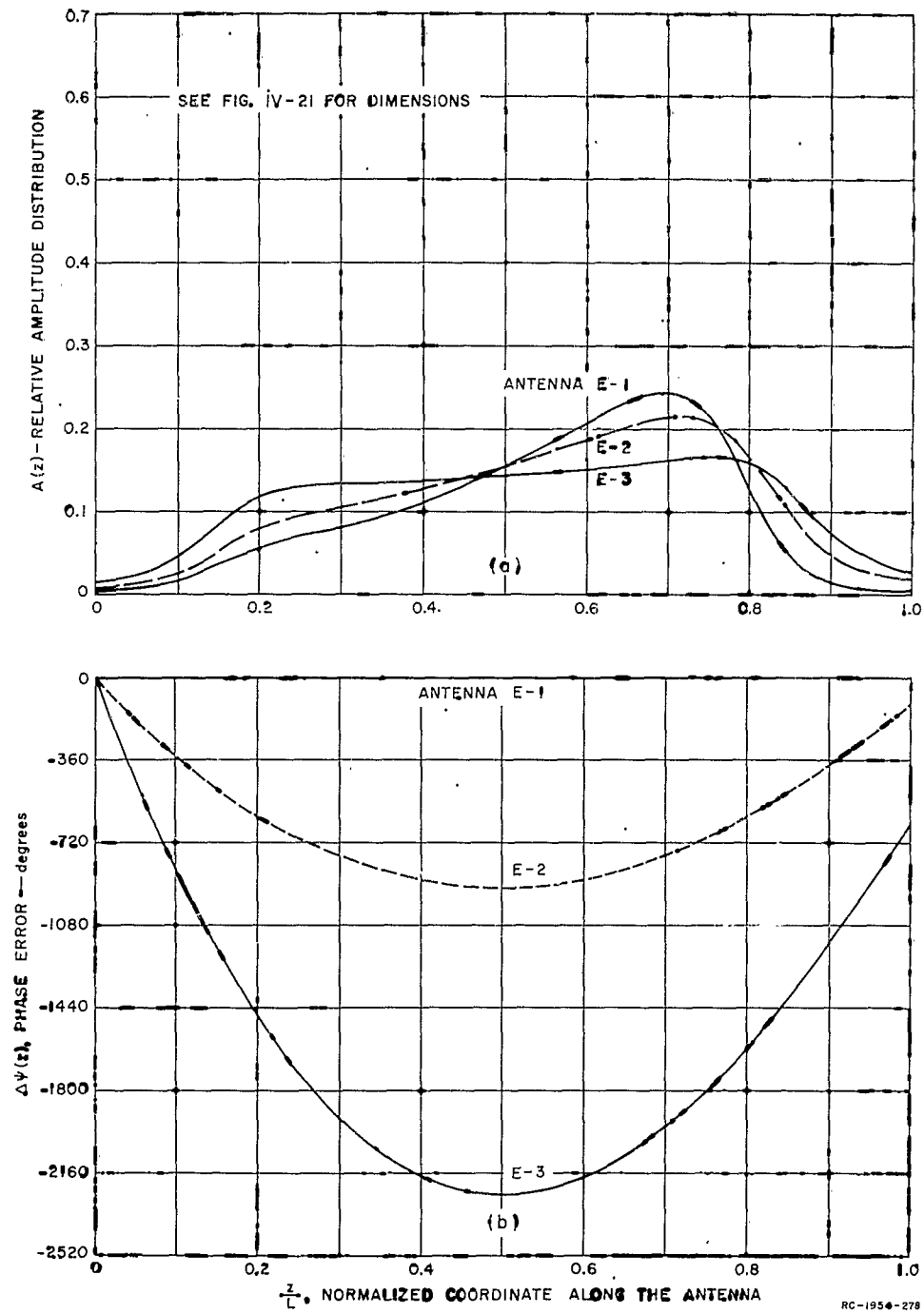


FIG. IV-23  
APERTURE DISTRIBUTIONS OF ANTENNA E

The intermediate-beamwidth pattern of Fig. IV-22(b) has a 3-db beamwidth of 9.3 degrees, an increase by a factor of 4.4 over the narrow-beam pattern. Although the phase velocity of Antenna E-2 was correct for synthesizing a maximally flat beam with  $\Theta_{3\text{dB}} = 20$  degrees, the amplitude distribution was not correct, since the wire center-to-center spacing was the same as calculated for the broad-beam antenna. Thus, it is not surprising that the actual radiation pattern does not more closely approximate the maximally flat pattern indicated by the dashed line in Fig. IV-22(b). The broad-beam pattern of Fig. IV-22(c) has a 3-db beamwidth of 42.4 degrees, an increase by a factor of 20 over the narrow-beam pattern. The actual radiation pattern of Antenna E-3 very closely approximates the desired maximally flat pattern between the angles  $\theta_1$  and  $\theta_n$ , which are indicated by crosses on the maximally flat pattern.

The increase in beamwidths at the -3-db and -10-db levels in changing the solid wall from that of Antenna E-1 to that of Antenna E-2, and to that of Antenna E-3, is plotted in Fig. IV-24. The abscissa in this figure is the magnitude of the change in  $a(z)$  at the input end plus the magnitude of the change in  $a(z)$  at the load end. The points for  $\Theta_{3\text{dB}}$  fall on a curve with slight curvature, and the points for  $\Theta_{10\text{dB}}$  fall on a straight line. It would be desirable to have several more points on these curves in order to establish the smooth variation in beam widths with wall movement.

The wall movements for changing from Antenna E-1 to the other two antennas are not simple movements such as were considered in Sec. IV-B. Given a suitably flexible solid metal wall, however, and a sufficient number of mechanical cams and linkages, it would be possible to change the solid wall of Antenna E-1 to be the shape of Antenna E-2, or Antenna E-3. For example, if the solid wall of Antenna E-1 is hinged at only the three points  $z/L = 0.15, 0.35$ , and  $0.70$ , and is moved without bending other than at the hinge points in order to approximate the phase distribution of Antenna E-3 within plus 23 degrees, minus 19 degrees error, then the radiation pattern of Fig. IV-22(d) results. Although there is a 3-db ripple in the beam peak, and  $\Theta_{3\text{dB}}$  is smaller than for the pattern of Fig. IV-22(c),  $\Theta_{10\text{dB}}$  is nearly the same as for the pattern of Fig. IV-22(c). With more than three hinge points in the wall of Antenna E-1, or with a continuously flexible solid wall, the approximation to the pattern of Antenna E-3 could be made arbitrarily close.

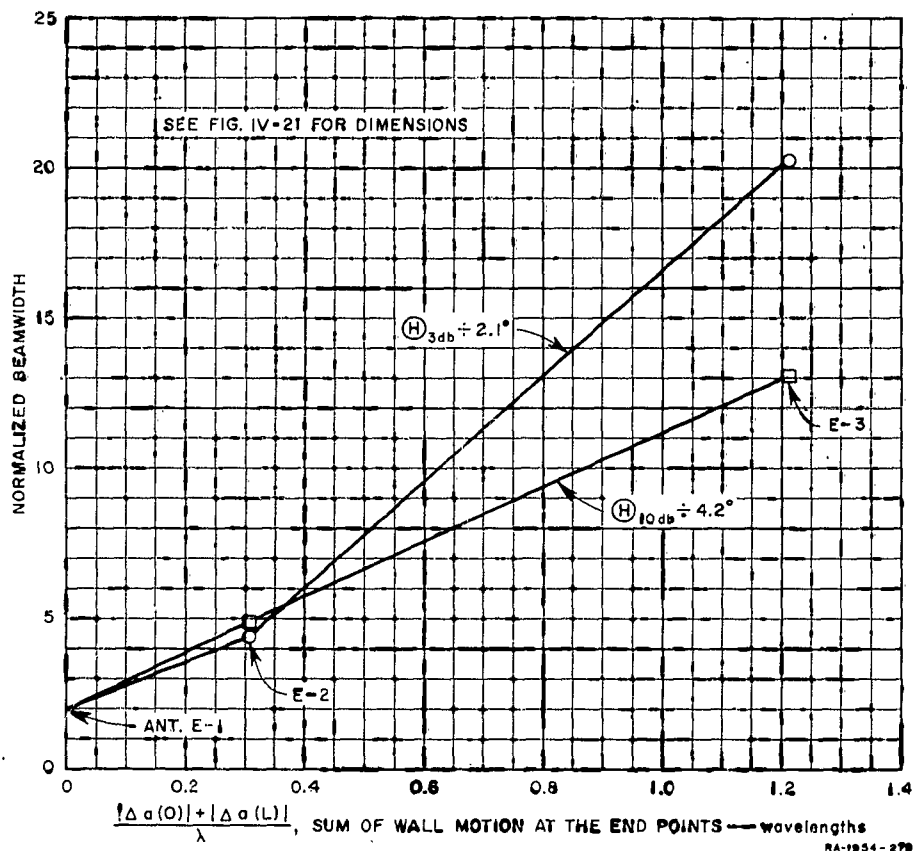


FIG. IV-24  
BEAM BROADENING RESULTING FROM MOVEMENT OF THE SOLID WALL  
OF ANTENNA E

In changing from Antenna E-1 to Antenna E-3, the solid wall is moved away from the grid at the load end, and the solid wall is moved toward the grid at the input end. The amount of power dissipated in the load changes by more than three orders of magnitude, but by designing for only 10 percent power dissipation in the load for the broad-beam case, the power radiated remains reasonably high as the solid wall is moved.

## 2. ANTENNA F

In order to be able to make more direct comparison between the beam broadening obtained by beginning with a broad-beam antenna, and that discussed in Sec. IV-B, a broad-beam antenna designated Antenna F was designed having a length of  $20\lambda$ . (Most of the narrow-beam antennas discussed in

Sec. IV-B were also  $20\lambda$  in length.) The dimensions required to approximately synthesize a maximally flat power pattern with  $n = 6$ ,  $\theta_0 = 40$  degrees,  $\theta_{3db} = 45$  degrees,  $\theta_1 = 6.9$  degrees, and  $\theta_u = 73.1$  degrees are labeled Antenna F-2 in Fig. IV-25 and in Table IV-2. As before, the grid-to-solid-wall spacing was also determined such that the phase velocity was constant with  $\lambda/\lambda_g = 0.66$  to produce a narrow-beam pattern. The dimensions for this condition are labeled Antenna F-1 in Fig. IV-25 and Table IV-2.

The radiation patterns of these two antennas are shown in Fig. IV-26, and the corresponding aperture amplitude and phase error are shown in Fig. IV-27. The 3-db beamwidths of the two patterns differ by a factor of 7.4, and the 10-db beamwidths differ by a factor of 5.7. This pattern change was obtained with a total wall motion

$$|\Delta a(0)| + |\Delta a(L)| = 1.20\lambda$$

Comparing these factors with those shown in Fig. IV-15, it is seen that the beam broadening obtained with Antenna F is significantly greater than that obtained by moving the wall of Antenna C toward its wire grid. Comparing the above factors with the solid curves in Fig. IV-20, it is found that the increase in  $\theta_{3db}$  of

Antenna F is only slightly greater than that obtained by moving the wall of Antenna D away from its grid. The increase of  $\theta_{10db}$  of Antenna F is less than that of Antenna D. It is probably more important in most applications to have a large increase in  $\theta_{3db}$  rather than in  $\theta_{10db}$ . As was pointed out previously, the modifications made on Antenna D were undesirable from the standpoint of keeping the amount of radiated power high.

As is to be expected, the broad-beam pattern of Antenna F-2 does not come as close to synthesizing the given maximally flat pattern as does

TABLE IV-2  
DIMENSIONS OF ANTENNA F

DISTANCE ALONG THE ANTENNA, $z/L$	CENTER-TO- CENTER WIRE SPACING, $s/\lambda$	GRID-TO-SOLID-WALL SPACING, $a/\lambda$	
		Antenna F-1	Antenna F-2
0	0.0151	0.6656	0.5036
0.05	0.0192	0.6631	0.5067
0.10	0.0267	0.6606	0.5111
0.15	0.0387	0.6581	0.5157
0.20	0.0509	0.6553	0.5216
0.25	0.0588	0.6527	0.5311
0.30	0.0653	0.6498	0.5435
0.35	0.0725	0.6468	0.5584
0.40	0.0810	0.6431	0.5758
0.45	0.0914	0.6386	0.5960
0.50	0.1045	0.6329	0.6192
0.55	0.1214	0.6250	0.6458
0.60	0.1441	0.6146	0.6759
0.65	0.1757	0.6002	0.7093
0.70	0.2227	0.5801	0.7452
0.75	0.2960	0.5510	0.7817
0.80	0.3902	0.5113	0.8238
0.85	0.4177	0.5000	0.9150
0.90	0.3525	0.5263	1.0873
0.95	0.2833	0.5550	1.3152
1.00	0.2462	0.5698	1.6068

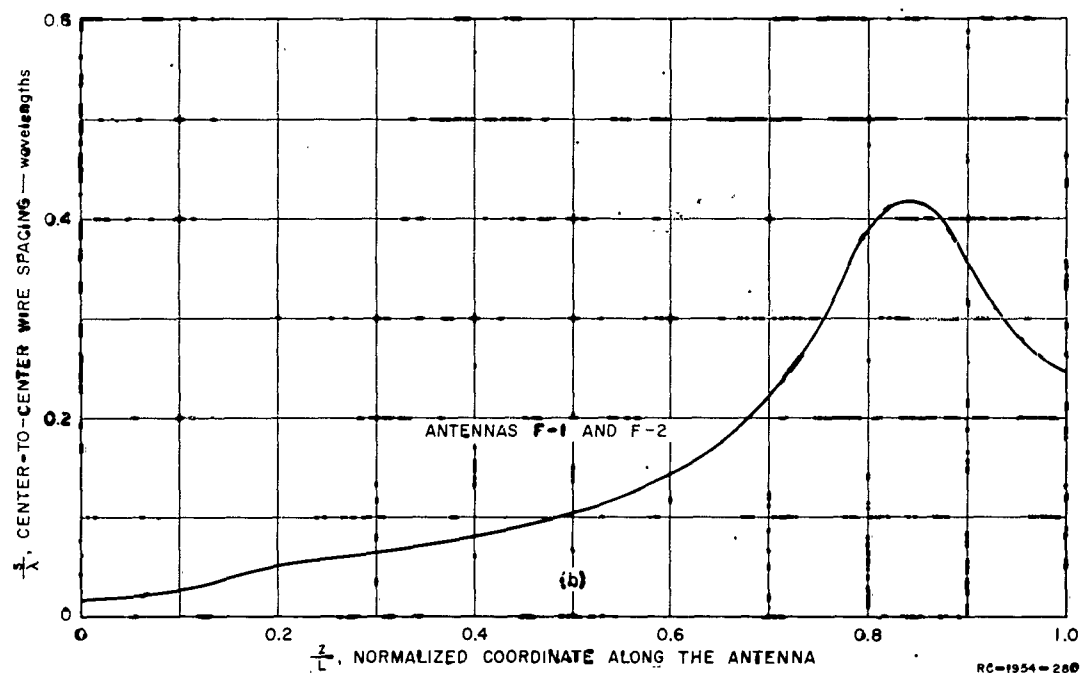
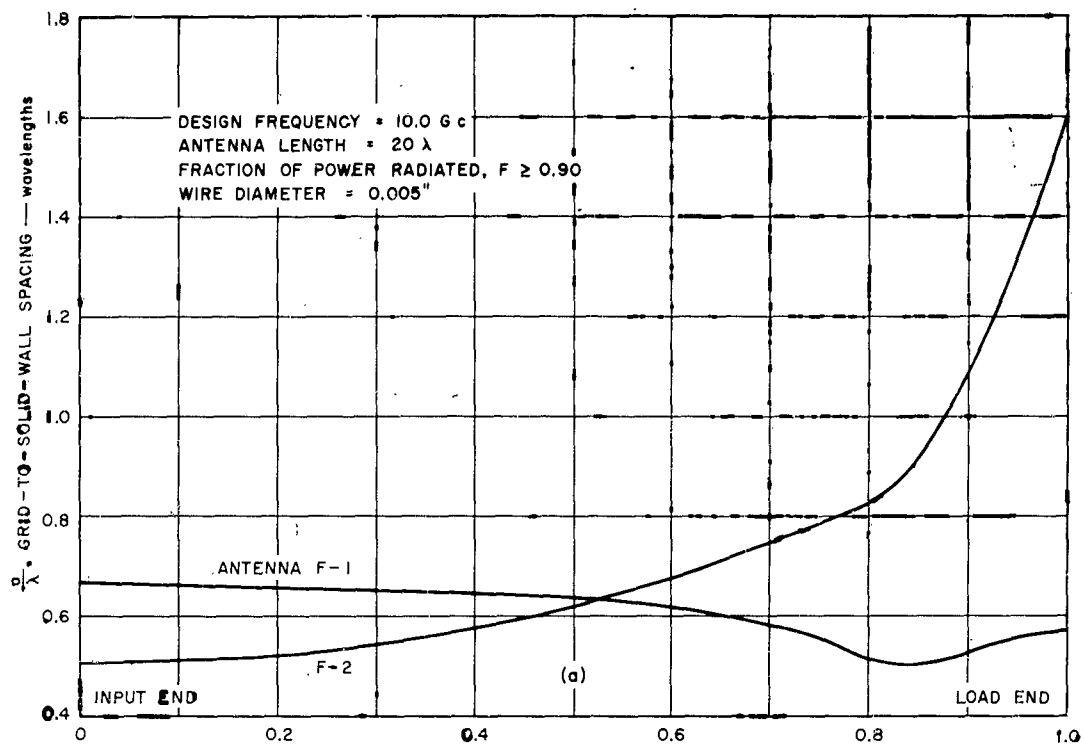


FIG. IV-25  
 DIMENSIONS OF ANTENNA F



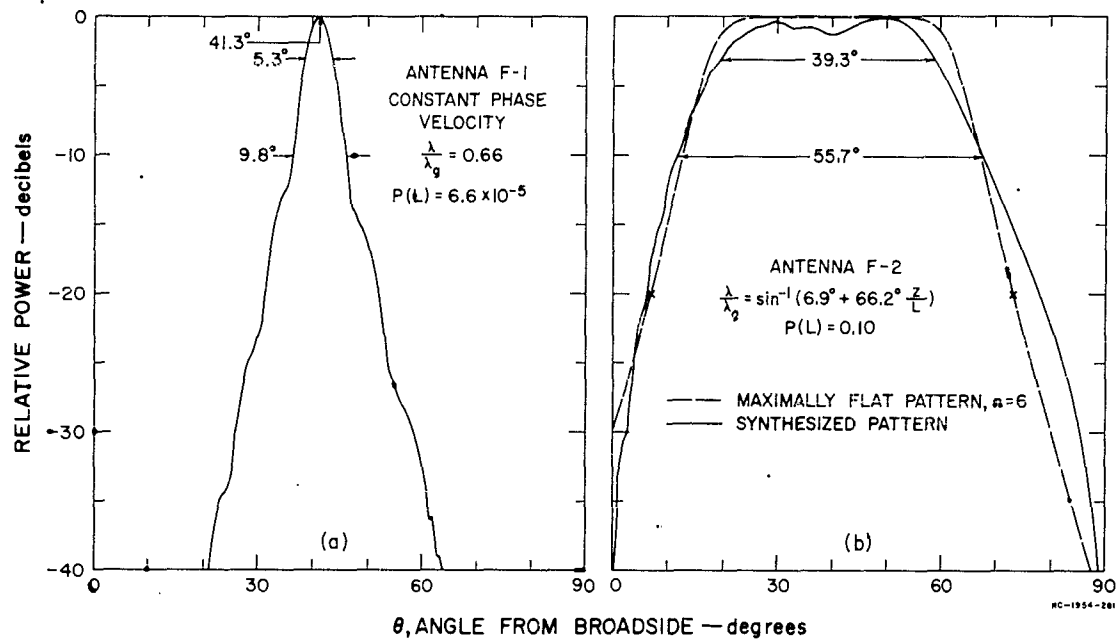


FIG. IV-26  
RADIATION PATTERNS OF ANTENNA F

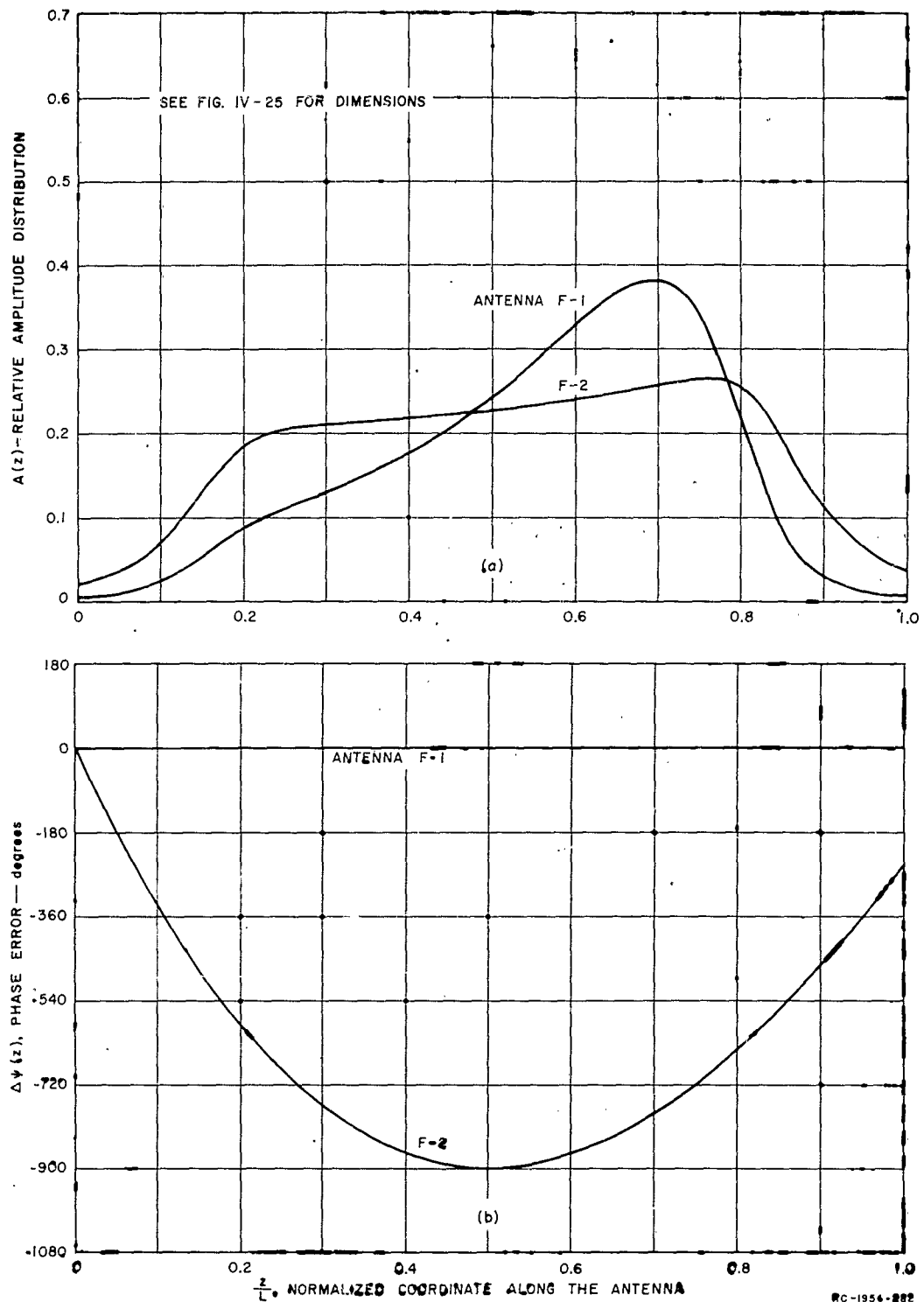


FIG. IV-27  
APERTURE DISTRIBUTIONS OF ANTENNA F

that of Antenna E-3, since Antenna F is smaller in terms of wavelength than is Antenna E. Even at that, the pattern of Antenna F-2 is a reasonably good approximation to the maximally flat pattern. Another consequence of the difference in the length of the two antennas is that the beamwidth of Antenna F is not adjustable over as wide a range as that of Antenna E, even though their broad-beam patterns are nearly the same shape.

#### D. CONCLUSIONS

Several of the modifications considered for leaky-wave antennas produce significant broadening of the main beam of the  $H$ -plane radiation pattern, without causing the pattern to break up into high side lobes. Even simple linear movements of the solid metal wall of the antenna with respect to its wire-grid aperture can produce significant beam broadening. Greater beam broadening can be obtained, however, by using more complex wall movements that require bending of the solid metal wall. For most of the wall movements considered, the beamwidth increased in an approximately linear manner as a function of wall displacement; however, the beamwidth did not change significantly for the first  $0.2\lambda$  of wall displacement in some cases, where  $\lambda$  is free-space wavelength. Moving the solid wall away from the wire grid reduces the rate at which power leaks through the wire grid. Thus, if a portion of the solid wall is moved away from the grid greatly, other portions of the solid wall should be moved toward the grid in order to maintain a reasonably high percent of power radiated.

Half-power beamwidth increases by a factor of at least 5.2 can be obtained by simple motions of the solid wall of  $20\lambda$ -wavelength-long antennas. This increase was obtained by pivoting the solid wall of Antenna D at the load end, and displacing its input end away from the grid by  $0.6\lambda$ . This modification reduced the amount of radiated power, however, from 90 percent to 56.6 percent of the input power. The largest beamwidth increase for a  $20\lambda$  antenna obtained by a simple wall movement that did not result in a reduction of radiated power, was a factor of 3.8. This increase was obtained by pivoting the solid wall of Antenna C at the input end, and moving the load end toward the grid until it touched the grid. Allowing more complex movements of the solid wall, beamwidth increases up to 7.4:1 can be obtained with  $20\lambda$  antennas. This factor resulted from taking the solid

wall of Antenna F designed to radiate a broad, maximally flat beam, and bending it in such a manner as to produce a narrow beam by requiring that the phase velocity be constant along the length of the antenna. Similar calculations for a  $50\lambda$  antenna, Antenna E, produced beam broadening by a factor of 20:1. The results obtained during the study described here indicate that the ultimate in beam-broadening capabilities of leaky-wave antennas was not reached, thus further pursuit of this study would be worthwhile.

#### E. RECOMMENDATIONS

An investigation of the beam-broadening properties of leaky-wave antennas could explore many avenues. Of necessity, most of these were left unexplored and even those topics that were investigated could benefit from further study. Of the designs starting with narrow-beam antennas, it is recommended that the following modifications be investigated: For Antenna C, larger movement of the solid wall toward the grid at its center, with the two ends being kept fixed, might produce significant additional beam broadening. For Antenna D, movement of the solid wall toward the grid at the load end might give usable patterns. This antenna is designed fairly near cut-off, and thus small movement of the solid wall toward the grid should produce significant changes in the aperture amplitude and phase distributions of this antenna. Experience with a leaky-wave antenna with a curved aperture<sup>3</sup> suggests that the beam-broadening properties of this type of antenna should also be investigated. Portions near the load end of that antenna were operated just above cut-off, thus relatively small motions of the solid metal wall would place these portions below cut-off. This would reduce the size of the radiating aperture as well as introducing phase errors, and thus broaden the beam. Alternatively, the solid metal wall could be fixed, and the antenna operated at two frequencies such that part of the antenna was below cut-off at the lower frequency.

It is also recommended that further study be devoted to the concept of initially designing the antenna for prescribed broad-beam radiation patterns. For the designs presented in this report, more intermediate-beamwidth patterns should be calculated. Designs should also be worked out for even wider broad-beam patterns. Considering the good agreement obtained between the actual radiation pattern and the desired maximally

flat beams with 3-db beamwidth equal to 45 degrees, it is to be expected that significantly greater beamwidths could be obtained.

The frequency bandwidth of all the designs presented in this report remains as a topic of investigation. It would also be desirable to construct a model antenna to provide experimental demonstration of the concept of beam broadening by movement of the solid wall of the antenna. It should be pointed out in this connection, however, that there is already sufficient experimental verification of the equations given in Ref. 1 that describe the propagation along, and leakage from, the type of antenna illustrated in Fig. IV-1.<sup>1,3,4</sup> Thus, a high degree of confidence can be placed in the calculated radiation patterns shown in the present report.

## REFERENCES

1. R. C. Honey, "Flush-Mounted Leaky-Wave Antenna with Predictable Patterns," IRE Trans. PGAP-7, 4, pp. 320-329 (October 1959).
2. H. E. Shanks, "A Geometrical Optics Method of Pattern Synthesis for Linear Arrays," IRE Trans. PGAP-8, 5, pp. 485-490 (September 1960).
3. R. C. Honey and J. K. Shimizu, "A Leaky-Wave Antenna with a Curved Aperture," Scientific Report 5, Contract AF 19(604)-3502, SRI Project 2605, Stanford Research Institute, Menlo Park, California (February 1960).
4. J. Aasted and R. C. Honey, "A Dielectric-Loaded Leaky-Wave Antenna," Scientific Report 8, Contract AF 19(604)-3502, SRI Project 2605, Stanford Research Institute, Menlo Park, California (March 1961).

## V BROADBAND ROLLED PILLBOX

### A. GENERAL

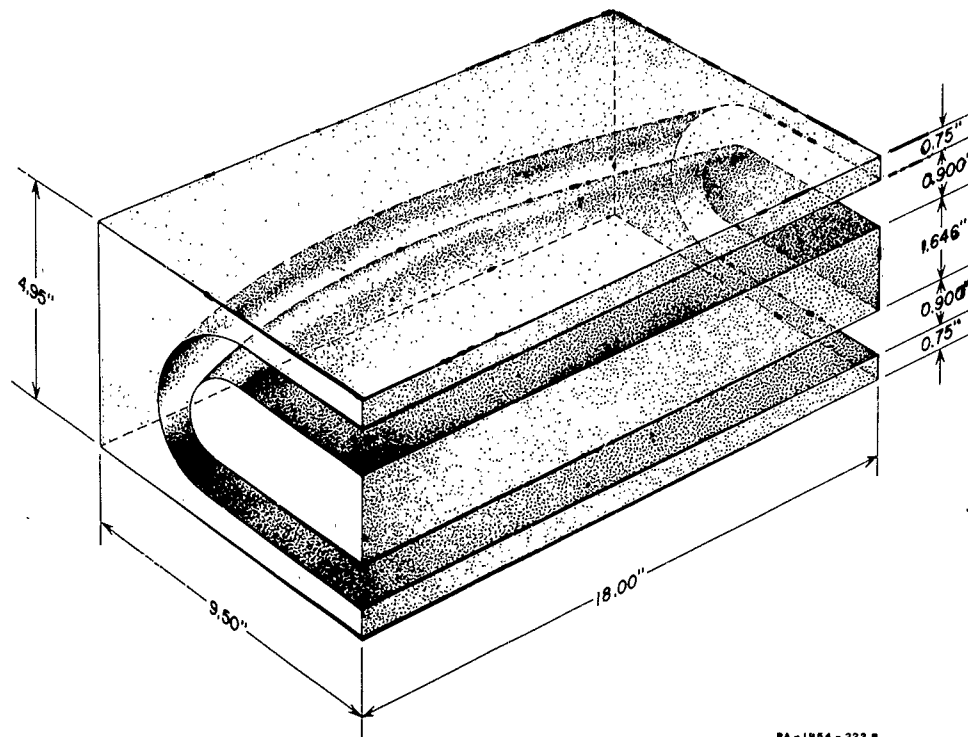
This section describes a rolled pillbox which has several advantages when compared with a regular parabolic pillbox. The lack of sharp corners along the wave path permits a better impedance match over a wide frequency band, and the separation of the input and output apertures eliminates shadows from the primary feed horn. This line source is designed for X-band frequencies and is polarized along the length of the aperture.

The structure can be considered as a flared rectangular waveguide bent into U-form. Figure V-1 shows a sketch of the pillbox. The design is based on an analysis in which the ray path in the bend is approximated with a section of a toroid.<sup>1\*</sup>

If the pillbox is cut along the symmetry line perpendicular to the aperture, the cross section will look as shown in Fig. V-2. The bend in the ray path causes a mismatch at the entrance and at the exit of the curved section. This mismatch is small as long as the radius of curvature  $r_0$  of the bend is large in terms of guide wavelengths. However, too large a radius would mean that a major part of the wave-path is contained in the bend. Since the machining tolerances of this section necessarily must be larger than for the parallel plate region, a large radius could result in a large phase error in the aperture, or would require unrealistically small tolerances. Furthermore, the approximate analysis upon which this pillbox is based becomes less accurate as the radius increases. A compromise should therefore be made. The chosen value of the radius is not critical since the VSWR changes slowly with the radius. This is shown in Fig. V-3 in which the VSWR is plotted for different values of  $r_0/a$ . The VSWR is calculated from the expressions given in Ref. 2 for the mismatch between a straight and a curved waveguide bent in the  $H$ -plane. The curves thus show the mismatch at one discontinuity. The total mismatch of the rolled pillbox due to the bend will lie between zero and twice the value plotted, depending on the phase length of the bend.

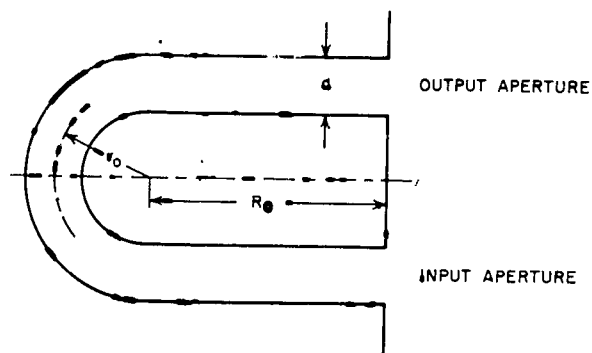
---

\*References are listed at the end of the section.



RA-1954-222 R

FIG. V-1  
SKETCH OF ROLLED PILLBOX



RA-2605-58

FIG. V-2  
CROSS SECTION OF ROLLED PILLBOX

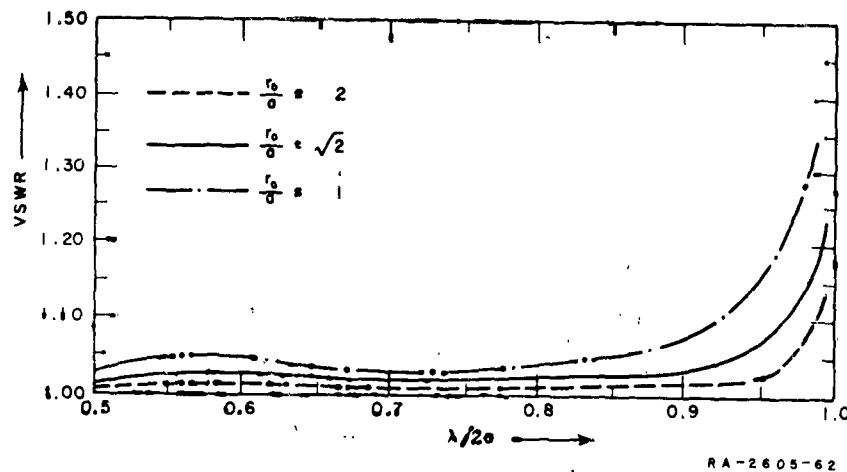


FIG. V-3

VSWR FOR H-PLANE BENDS vs  $\lambda/2a$  FOR DIFFERENT VALUES OF  $r_0/a$

In order to be able to use this rolled pillbox with some existing antennas, an output aperture 18 inches wide by 0.900 inch high was arbitrarily selected. The thickness of the center section of the rolled pillbox is  $2r_0 - a$ . For the values of  $r_0/a$  shown in Fig. V-3 this thickness is 2.7 inches, 1.65 inches and 0.9 inch respectively. With  $r_0/a = \sqrt{2}$  a good compromise between mismatch and aperture separation is reached, and this value was therefore chosen for the present design. Thus

$$r_0 = \sqrt{2} \cdot a = 1.273 \text{ inches}$$

To determine  $R_0$ , assume for a moment that the center section has zero thickness, that is, the rolled pillbox is reduced to an ordinary parabolic pillbox. For this case the relation between focal length,  $f$ , aperture width,  $D$ , and illumination angle  $\theta$  is given by (see Fig. V-4)

$$\tan \frac{\theta}{2} = \frac{8(f/D)}{16(f/D)^2 - 1}$$

Since the rolled feedhorn will be used with different primary feedhorns of varying radiation patterns, an  $f/D$  ratio of 1/2 was arbitrarily selected as a compromise between too large a structure with larger values of  $f/D$  and too wide a primary beamwidth required with smaller values of  $f/D$ .



If the focal length for the rolled pillbox is defined as half the distance from the focal point to the aperture measured along the mean radius in the bend (Fig. V-2), then:

$$f = R_0 + (1/2)\pi r_0$$

Using the same  $f/D$  ratio as for the parabolic pillbox the value of  $R_0$  is found:

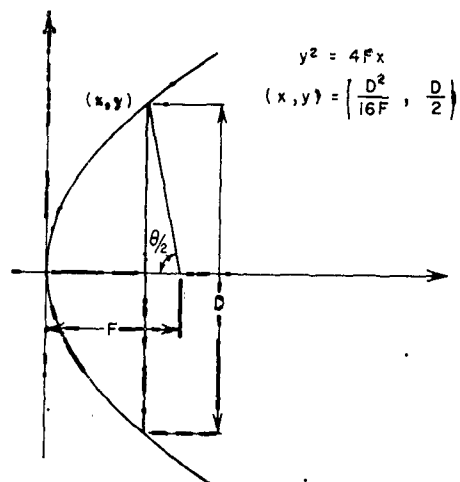
$$f = (1/2)D = 9 \text{ inches}$$

$$R_0 = 9 - (1/2)\pi \cdot r_0 = 7.00 \text{ inches}$$

The geometry is now determined since all waves leaving the primary feed must travel equal distances from the focal point to the aperture independent of  $\phi$  (see Fig. V-5).

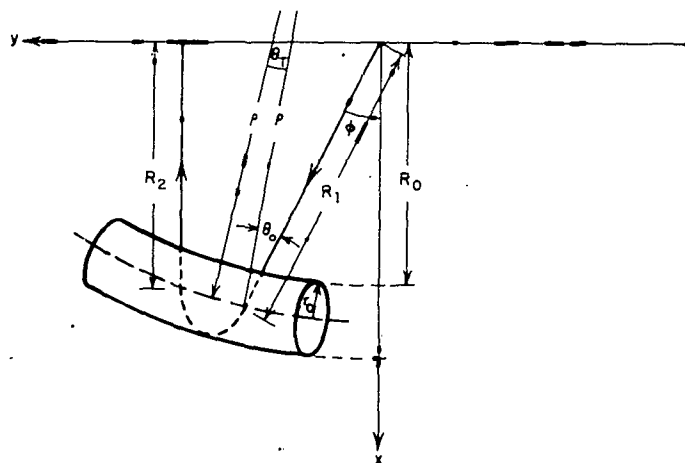
$R_1$  is determined from the following set of equations:<sup>1</sup>

F/D	1/4	1/2	3/4
$\theta$	180°	106°	74°



RA-2605-66

FIG. V-4  
GEOMETRY OF PARABOLA



RA-2605-59

FIG. V-5  
GEOMETRY OF ROLLED PILLBOX WITH TOROIDAL APPROXIMATION

$$\frac{R_1}{R_0} = \frac{1}{1 + \cos \phi} \left[ 2 + \frac{r_0}{R_0} \left( \pi - \frac{2S}{r_0} \right) + \frac{4 \sin \theta_T \sin (\phi/2)}{\cos^3 \theta_0} \right]$$

$$\frac{S}{r_0} = \frac{\pi}{2 \cos \theta_0} - \frac{r_0}{2R_0} \sin^2 \theta_0 - \left( \frac{r_0}{2R_0} \right)^2 \frac{3\pi}{8} \cos \theta_0 \sin^2 \theta_0$$

$$\begin{aligned} \theta_T = & \frac{r_0}{2R_0} \cos^2 \theta_0 \sin \theta_0 \left[ \frac{\pi}{2} - \frac{r_0}{2R_0} \cos \theta_0 (1 + \cos^2 \theta_0) \right. \\ & + \left( \frac{r_0}{2R_0} \right)^2 \frac{\pi}{8} \cos^2 \theta_0 (3 + \cos^2 \theta_0 + 2 \cos^4 \theta_0) \\ & - \left( \frac{r_0}{2R_0} \right)^3 \frac{\cos^3 \theta_0}{3} (5 + \cos^4 \theta_0 + 2 \cos^6 \theta_0) \\ & \left. + \left( \frac{r_0}{2R_0} \right)^4 \frac{3\pi \cos^4 \theta_0}{128} (35 - 10 \cos^2 \theta_0 + 3 \cos^4 \theta_0 \right. \\ & \left. + 4 \cos^6 \theta_0 + 8 \cos^8 \theta_0) \right] \end{aligned}$$

$$\phi = 2(\theta_0 - \theta_T)$$

Corresponding values of  $R_1$  and  $\phi$  can be computed from this set of equations. The rectangular coordinates of the outermost point of the toroid are found by projection on the axes (see Fig. V-6):

$$\begin{aligned} [x, y] = & \{ [R_1 \cos \phi - (d/2) \sin \phi/2 + r_0 \cos \phi/2] \cdot \\ & - [R_1 \sin \phi + (d/2) \cos \phi/2 + r_0 \sin \phi/2] \} \end{aligned}$$

In this expression  $d$  is the distance in the  $x$ - $y$  projection between the points where the ray enters the curved section to where it leaves. This distance equals  $2\rho\theta_T$ , where  $\rho$  is the large radius of the toroid. Reference 1 gives expressions for  $\rho$  and  $\theta_T$ . From these  $d$  is given by

$$\begin{aligned}
d = & 2r_0 \tan \theta_0 \left[ \frac{\pi}{2} - \frac{r_0}{2R_0} \cos \theta_0 (1 + \cos^2 \theta_0) \right. \\
& + \left( \frac{r_0}{2R_0} \right)^2 \cos^2 \theta_0 \frac{\pi}{8} (3 + \cos^2 \theta_0 + 2 \cos^4 \theta_0) - \left( \frac{r_0}{2R_0} \right)^3 \cos^3 \theta_0 \cdot \frac{1}{3} (5 + \cos^4 \theta_0 + 2 \cos^6 \theta_0) \\
& \left. + \left( \frac{r_0}{2R_0} \right)^4 \cos^4 \theta_0 \cdot \frac{3\pi}{16} \left( \frac{35}{8} - \frac{5}{4} \cos^2 \theta_0 + \frac{3}{8} \cos^4 \theta_0 + \frac{1}{2} \cos^6 \theta_0 + \cos^8 \theta_0 \right) - \dots \right]
\end{aligned}$$

The walls surround the curve described by  $(x,y)$  in such a way that the width measured perpendicular to the curved edge is constant and equal to 0.900 inch (see Fig. V-6):

$$\begin{aligned}
\left\{ \begin{matrix} x_i \\ y_i \end{matrix} \right\} = & \left\{ \left[ R_1 \cos \phi - \frac{d}{2} \sin \phi/2 + \left( r_0 \mp \frac{a}{2} \right) \cos \phi/2 \right] \right. \\
& \left. \left[ R_1 \sin \phi + \frac{d}{2} \cos \phi/2 + \left( r_0 \mp \frac{a}{2} \right) \sin \phi/2 \right] \right\}
\end{aligned}$$

These equations determine the dimensions of the rolled pillbox completely.

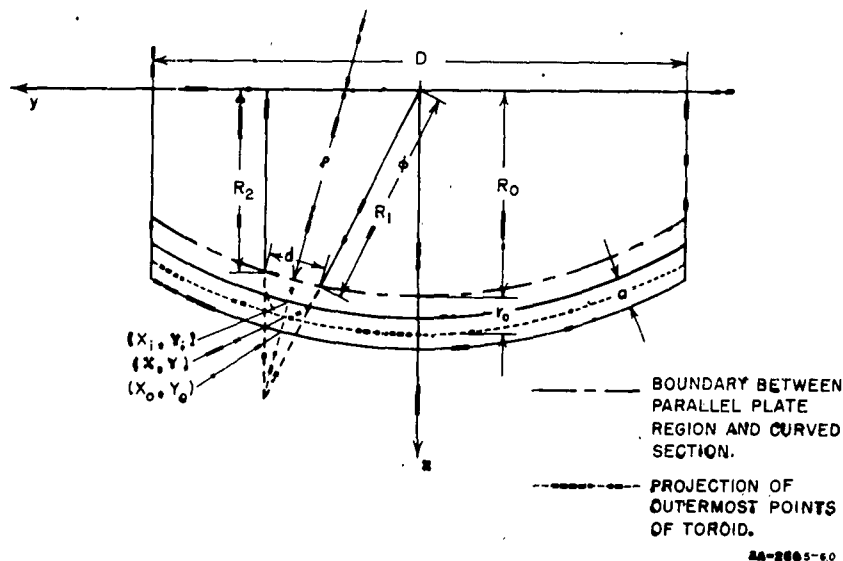


FIG. V-6  
SKETCH OF ROLLED PILLBOX SHOWING APPROXIMATE RAY PATH

## B. ESTIMATE OF PHASE ERROR

The nature of the rolled pillbox makes the distance from the feed to the aperture, as measured along the mean radius in the bend, independent of  $\phi$ . However, the distance each ray travels in the parallel section and in the rolled section varies with the angle.

The spacing in the parallel-plate region can be held to a smaller tolerance than can the spacing in the curved section, and the resultant phase error in the aperture was therefore computed for each section individually. To simplify the calculations it was furthermore assumed that in each section the waves travel a distance that is independent of  $\phi$ . For the parallel plate section this value was chosen as  $2R_0$ , while in the rolled section it was  $\pi r_0 / \cos(26\frac{1}{2}^\circ)$ . This latter value is the length the outermost ray would travel in the bend if the toroid were replaced with a section of a straight circular cylinder. The error resulting from these approximations will cause the calculated error to be on the high side in all cases. In a waveguide the sensitivity in the guide wave length,  $\lambda_g$ , to changes in the width,  $a$ , is given by

$$\frac{d\lambda_g}{\lambda_g} = - \left( \frac{\lambda_g}{2a} \right)^2 \cdot \frac{da}{a}$$

In the parallel plate region the maximum phase error is:

$$A = - \left( \frac{\lambda_g}{2a} \right)^2 \cdot \frac{da_1}{a} \cdot \frac{2R_0}{\lambda_g}$$

while in the rolled section it is:

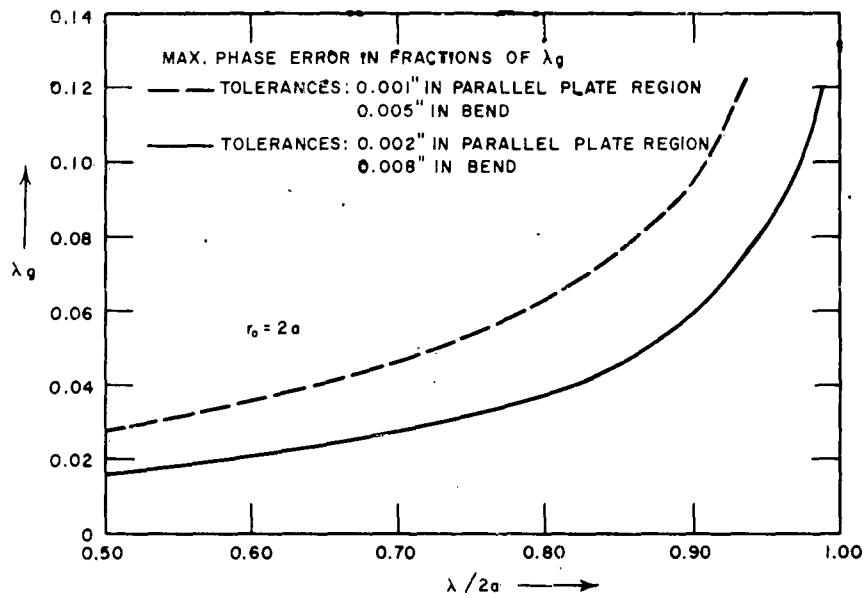
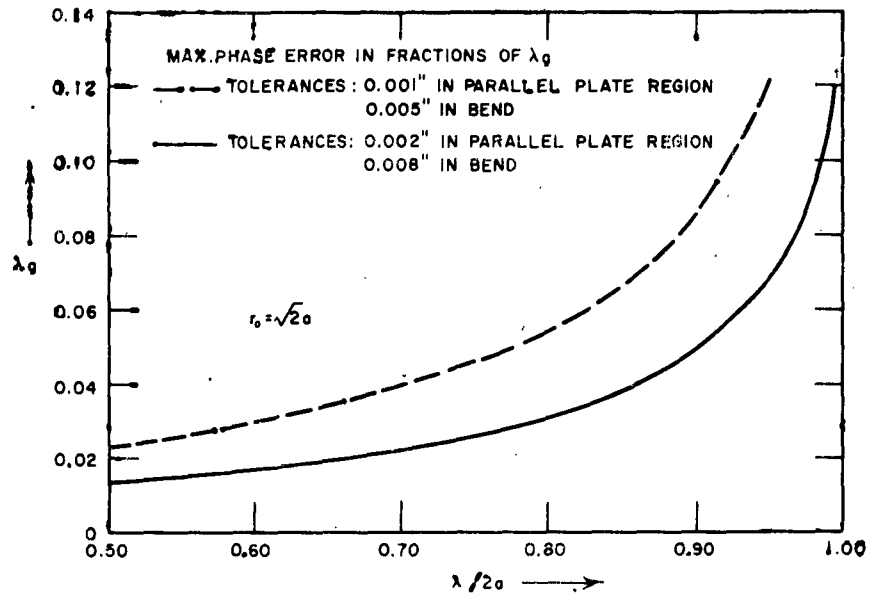
$$B = - \left( \frac{\lambda_g}{2a} \right)^2 \cdot \frac{da_2}{a} \cdot \frac{\pi r_0}{\cos(26\frac{1}{2}^\circ)} \cdot \frac{1}{\lambda_g}$$

The total maximum phase error,  $A + B$ , was calculated for a tolerance of 0.001 inch in the parallel plate region and 0.005 inch in the rolled section. This is plotted in Fig. V-7, which also shows the maximum phase error if the tolerances were 0.002 inch and 0.008 inch respectively.

Figure V-7 furthermore shows the phase error if the value of  $r_0$  were  $2a$  instead of  $\sqrt{2}a$ . As mentioned before this larger radius causes a somewhat higher phase error in the aperture.

# ERRATA

FIG. V-7, interchange solid and dashed curves.



BB-2605-63

FIG. V-7  
MAXIMUM PHASE ERROR IN THE APERTURE VS.  $\lambda/2a$  FOR DIFFERENT TOLERANCES

### C. MECHANICAL DESIGN

A pillbox was built according to the design outlined in the Part B. The construction of the curved surfaces was done with special tools whose cutting surfaces matched the radii of the male and the female parts respectively. The tools were guided by templates, which were shaped after the coordinates  $(x_o, y_o)$  and  $(x_i, y_i)$  as given in Part B. The tools, the male and the female parts, and the partially assembled pillbox are shown in Figs. V-8 through V-11.

### D. MEASUREMENTS

A series of measurements were conducted on the finished pillbox. Three differently flared, rectangular waveguides were used as primary feed horns. Figure V-12 shows the flared rectangular waveguide together with a table of dimensions for the three horns. The dimensions were chosen in such a way that at the lowest frequency, 8.5 Gc, the radiation from Horn A, as measured between the -10 db points, would just illuminate the whole toroidal bend. The other horns were made to radiate slightly narrower beams in order to reduce reflections from the sides of the pillbox. The -10 db beamwidth of a singly flared rectangular waveguide is given by the approximate empirical formula:<sup>3</sup>

$$\theta_{10} = 88 \cdot \frac{\lambda}{B'} \quad (\text{degrees})$$

where

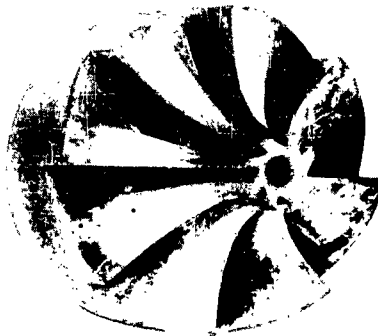
$\lambda$  is the free space wavelength and

$B'$  is the width of the flare as shown in Fig. V.12.

The -10 db beamwidths calculated from this formula are given in the following table for the three horns.

	HORN A	HORN B	HORN C
8.5 Gc	98°	82°	66°
12.4 Gc	67°	56°	45°

The radiation outside the -10 db points was strong enough to interfere with the measurements due to reflections in the pillbox. In order to reduce this, long strips of absorbent material were placed along the metallic side panels.



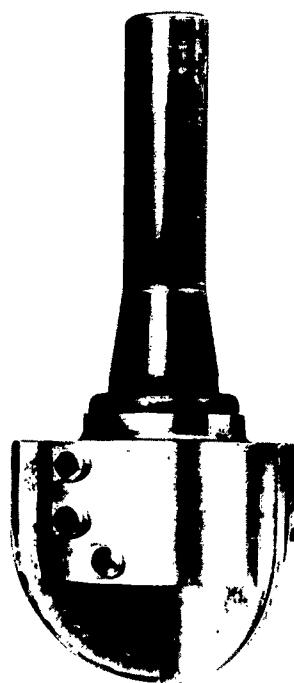
(b) TOOL FOR INNER SURFACE



(d) TOOL FOR OUTER SURFACE  
RP-1854-223



(a) TOOL FOR INNER SURFACE



(c) TOOL FOR OUTER SURFACE

FIG. V-8  
TOOLS FOR CUTTING CURVED SURFACES, ROLLED PILLBOX

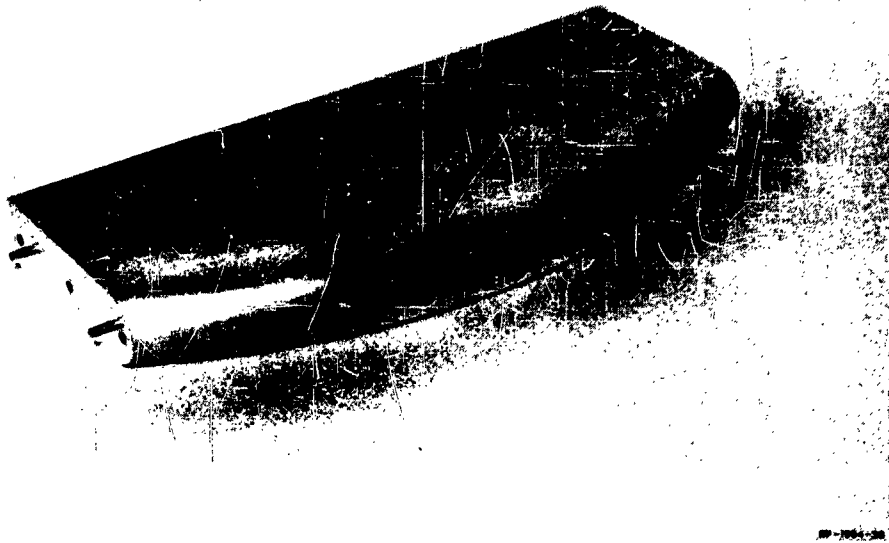


FIG. V-9  
MALE PART, ROLLED PILLBOX

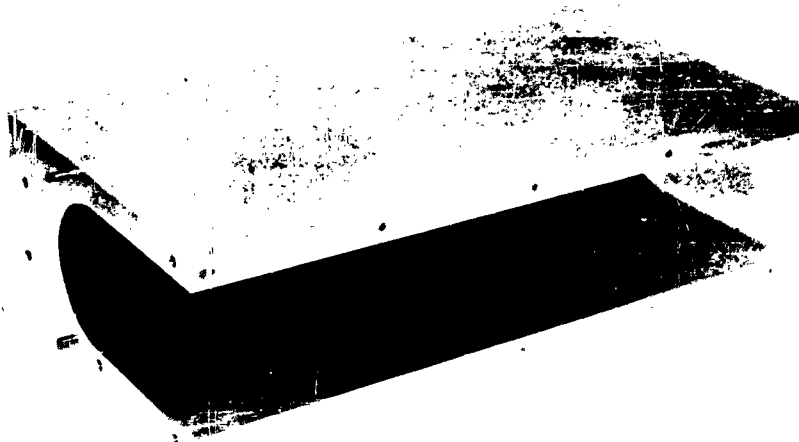


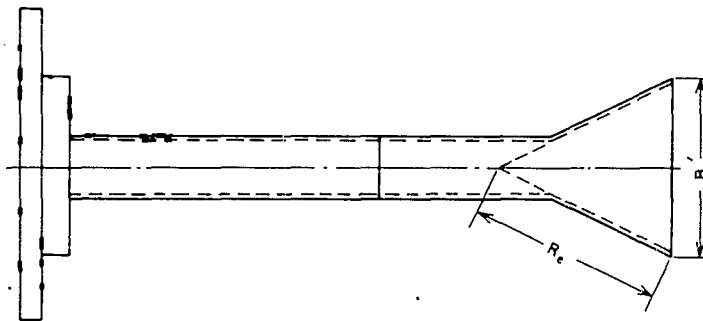
FIG. V-10  
FEMALE PART, ROLLED PILLBOX



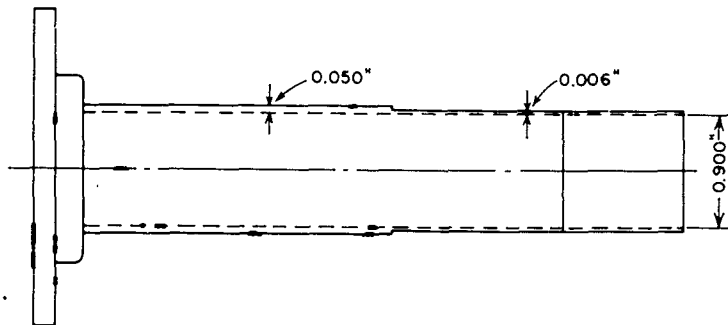


10-1018-40

FIG. V-11  
PARTIALLY ASSEMBLED PILLBOX



	B'	R <sub>e</sub>
A	1.25"	0.81"
B	1.50"	2.18"
C	1.85"	1.75"



A-1954-24B

FIG. V-12  
SKETCH OF PRIMARY FEED HORN

A flared section was attached to the output aperture of the pillbox to provide a better match when no secondary antenna was connected to this aperture. At the input aperture, two parallel plates enclose the feed horn in the *E*-plane. These plates allow the primary feed horn to be moved along the symmetry axis of the pillbox for proper focusing. A cross-sectional sketch of the completed pillbox is shown in Fig. V-13.

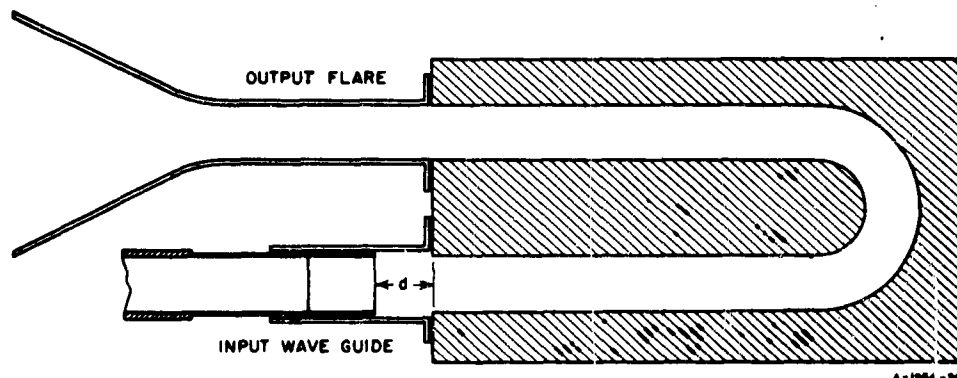


FIG. V-13  
SKETCH OF CROSS SECTION OF THE PILLBOX WITH PRIMARY FEED HORN

The finite thickness of the feed horn walls creates two steps in the *H*-plane along the wave path. The effect of this discontinuity was reduced by removing the 0.050 inch waveguide walls and replacing them with a 0.006-inch copper foil. A piece of Styrofoam, shaped to fit the flare, supported the thin walls.

The best position of the primary feed horn will be the position where the focal points of the pillbox and the horn coincide. However, since the focal point of a flared waveguide moves with frequency, a compromise position must be found for the band of frequencies over which the pillbox is to operate.

In order to do this, *E*-plane radiation patterns were first recorded for four different positions of each feed horn at five frequencies in the range 8.5 Gc to 12.4 Gc. The level of the first side lobe or shoulder below the main lobe was then plotted as a function of the feed position. These plots are shown in Fig. V-14, and the best compromise between low side-lobe level and bandwidth was then made on the basis of these plots. These positions are indicated on the plots. The variable, *d*, indicates the distance from the front plane of the pillbox to the edge of the feed horn as shown on Fig. V-13.

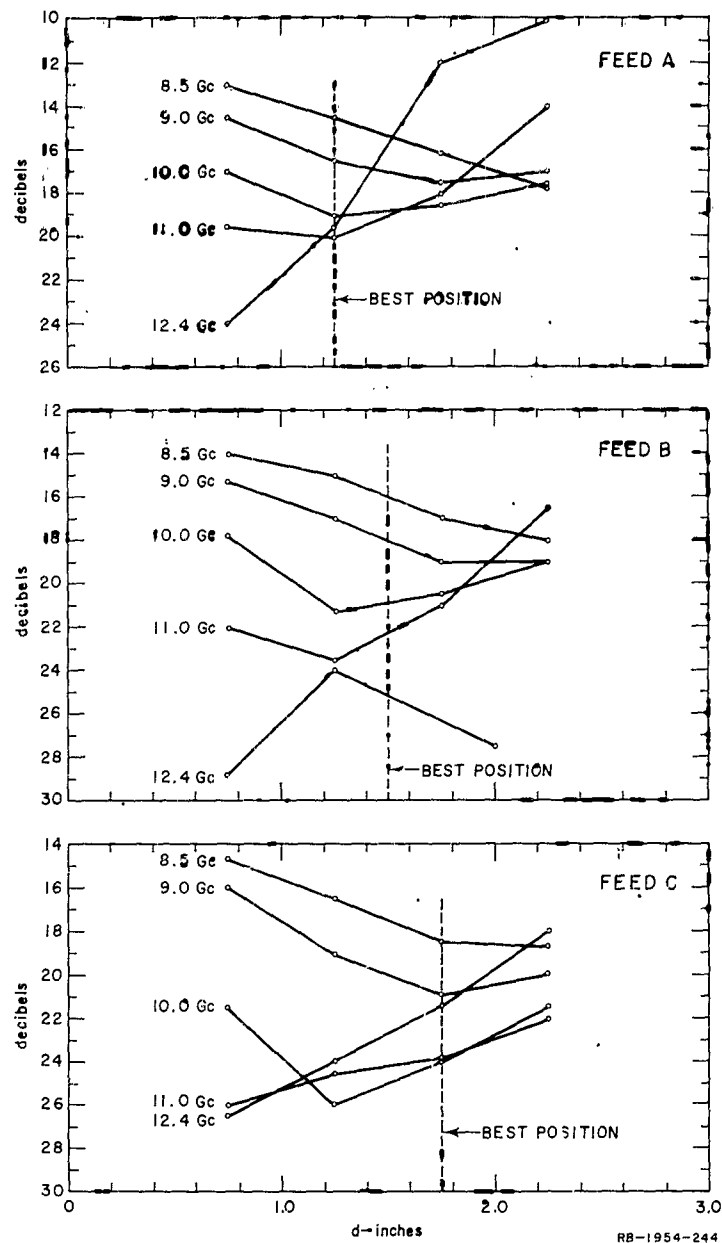


FIG. V-14  
LEVEL OF FIRST SIDELOBES OR HIGHEST SHOULDER  
BELOW MAIN LOBE AS A FUNCTION OF FEED POSITION

Next the radiation patterns in the *E*-plane were recorded over the frequency range with the feed horns mounted in the indicated positions. These patterns are shown in Figs. V-15, V-16, and V-17. At each frequency the 3-db beamwidth and gain were measured and are shown in Fig. V-18 and Fig. V-19, respectively. Finally, Fig. V-20 shows the level of the highest shoulder or side lobe as a function of the frequency for the chosen positions of the three feeds.

The pillbox was then used as a feed for an existing leaky-wave antenna. This antenna required a linearly polarized line source as a feed.<sup>4</sup> The pillbox mounted on the leaky-wave antenna is shown in Fig. V-21.

Radiation patterns for this combination at 11.4 Gc were taken both in the *H*-plane and in the *E*-plane using feed horn C as the primary feed for the rolled pillbox. These radiation patterns are shown in Fig. V-22. They should be compared with the radiation patterns of the leaky-wave antenna taken when fed by the original line source, an asymmetrically fed pillbox with nearly uniform aperture illumination.<sup>4</sup> These patterns are shown in Fig. V-23, and indicate how the pillbox has improved the *E*-plane pattern without significant changes in the *H*-plane pattern. Due to the tapered aperture distribution in the *E*-plane the gain of the complete antenna dropped from 33.0 db to 29.9 db.

The step along the wave path created by the walls of the feed horn tends to defocus the radiation from the primary feed. The reason for this is that the change in dimensions of the path in the *H*-plane will cause a change in the phase velocity, setting up refractions at the boundaries. This refraction will produce an apparent additional movement of the phase center of the feed horn as well as an additional taper of the amplitude distribution. These effects are illustrated in Fig. V-24, which is a radiation pattern taken at 12.4 Gc with a feed of the same flare dimensions as Feed B, but with the full wall thickness preserved out to the aperture. The step in the wave path was then increased from 0.012 inch to 0.100 inch. The asymmetry in the radiation pattern at the -35 db level is probably caused by a slight misalignment of the primary feed, a trait which also shows up in some of the other radiation patterns. Although the side-lobe level was extremely low in this position of the feed horn, the discontinuity in the wave path caused severe defocusing at the lower frequencies, raising the side-lobe level above those shown in Fig. V-20 for Feed B.

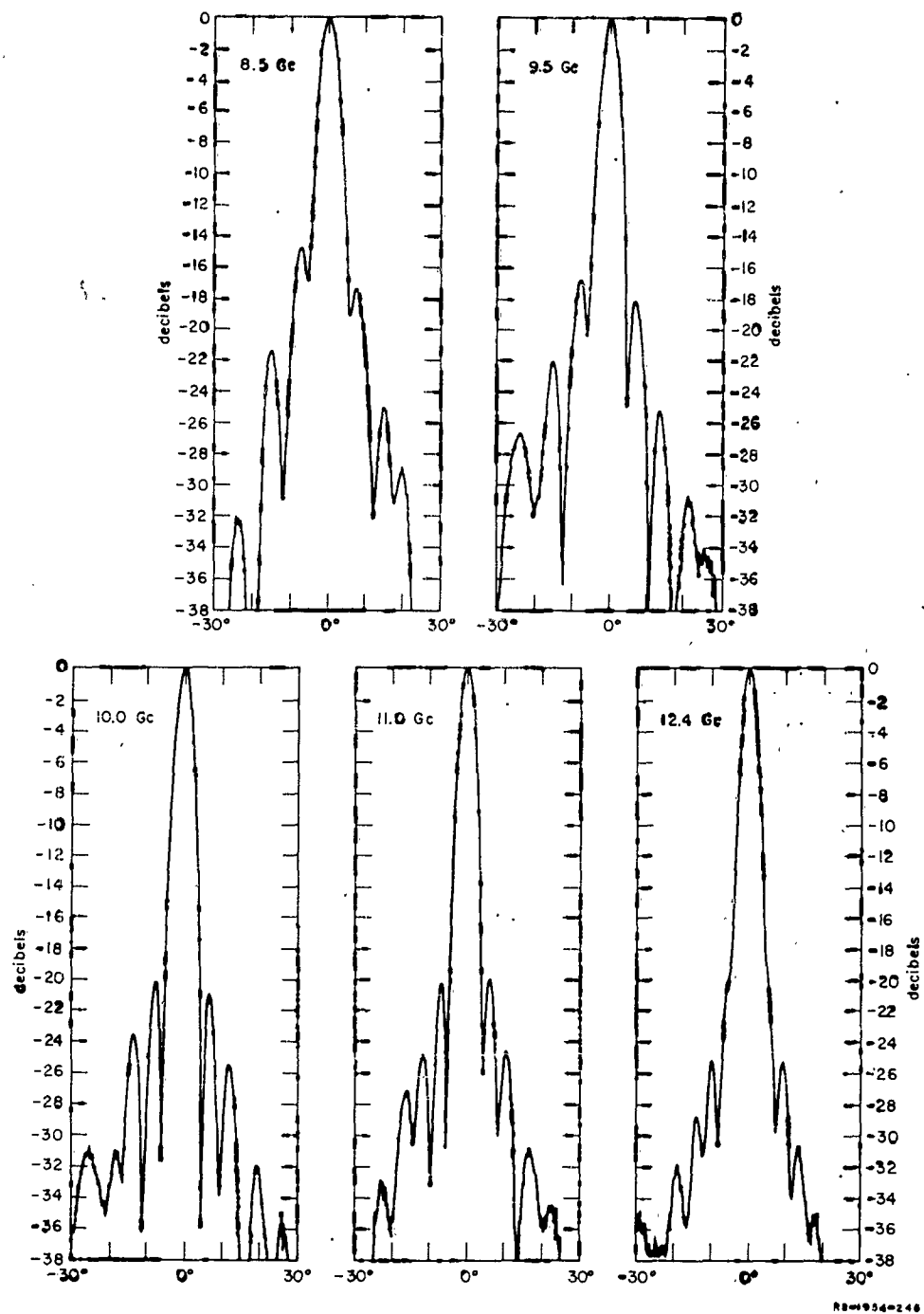


FIG. V-15  
E-PLANE RADIATION PATTERNS, PILLBOX WITH FEED A,  $d = 1\frac{1}{4}''$

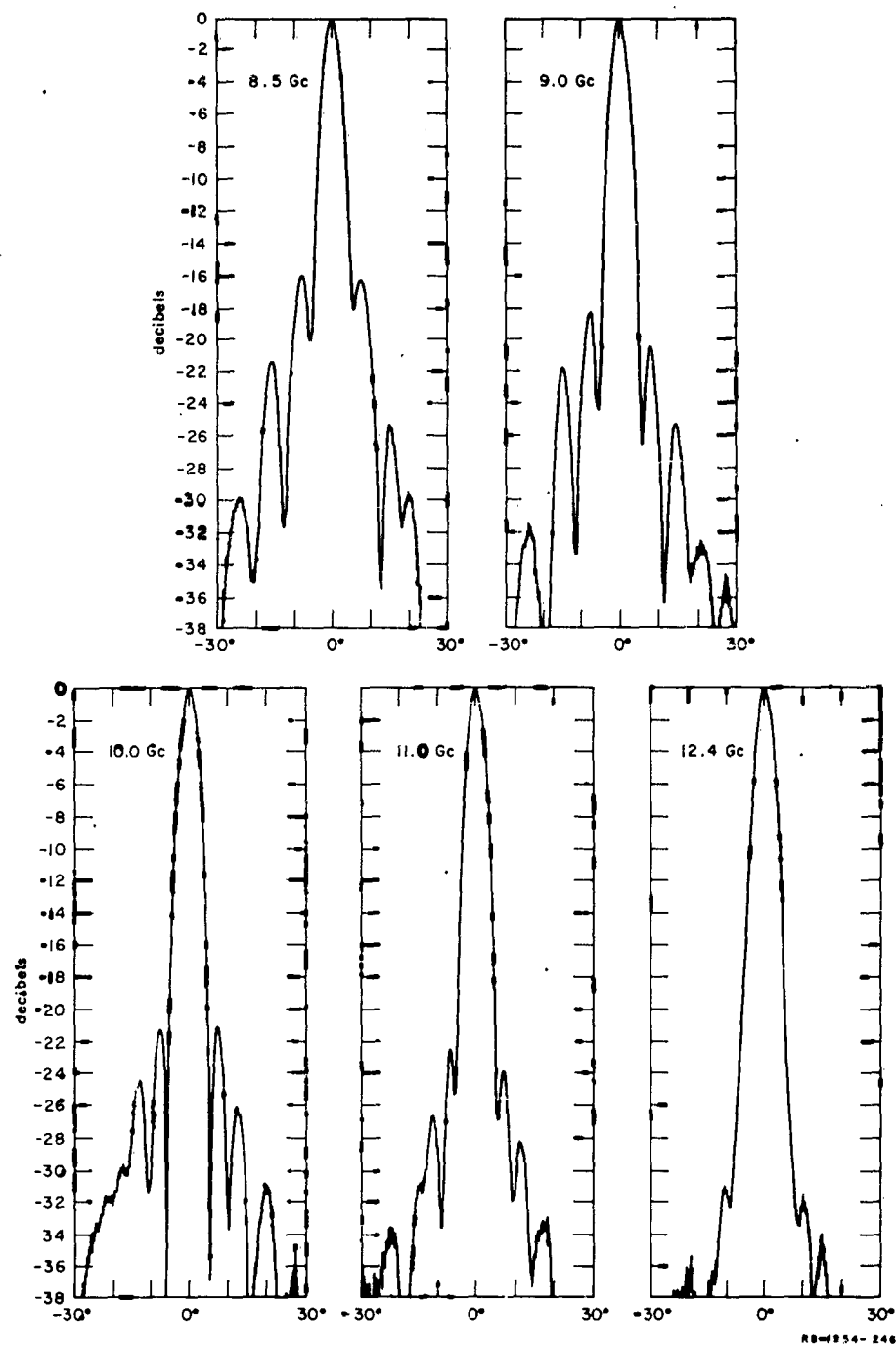


FIG. V-16  
E-PLANE RADIATION PATTERNS, PILLBOX WITH FEED B,  $d = 1\frac{1}{2}''$

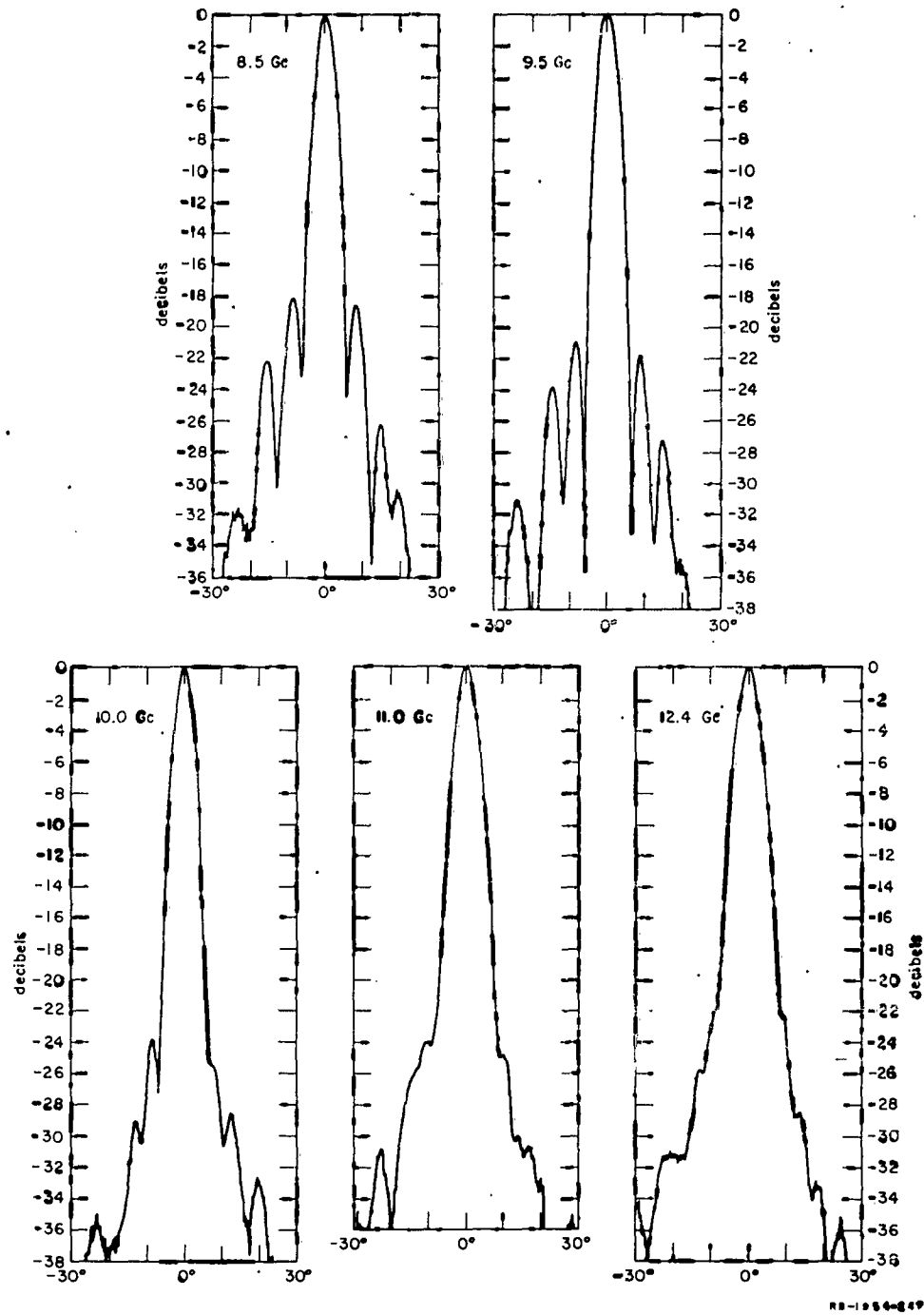


FIG. V-17  
E-PLANE RADIATION PATTERNS, PILLBOX WITH FEED C,  $d = 1\frac{3}{4}$ "

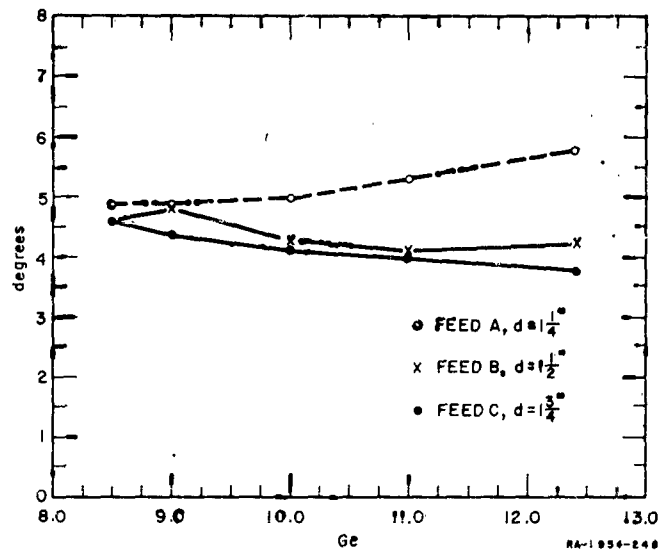


FIG. V-18  
HALF-POWER BEAMWIDTH OF PILLBOX VS FREQUENCY

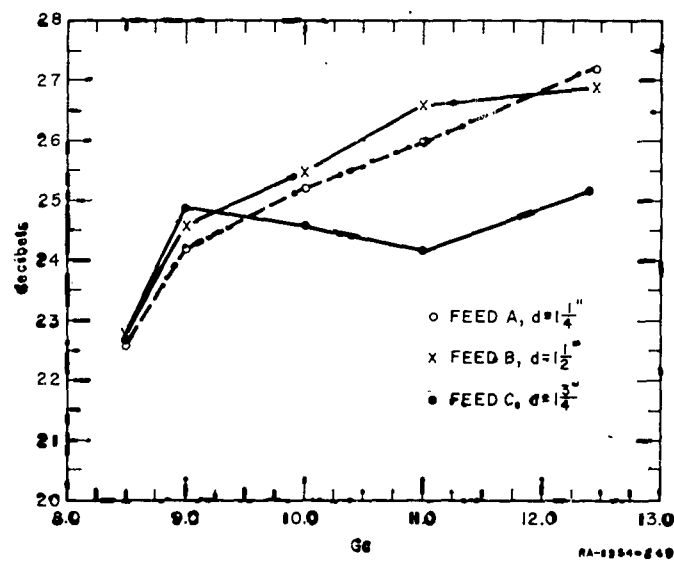


FIG. V-19  
GAIN OF ROLLED PILLBOX VS FREQUENCY



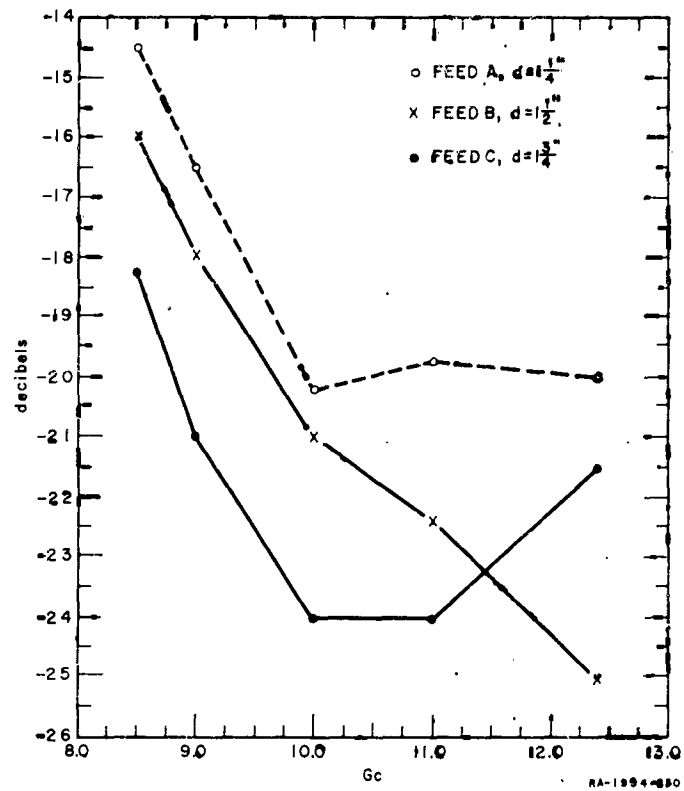


FIG. V-20  
SIDE-LOBE LEVEL VS FREQUENCY FOR THREE DIFFERENT  
FEED HORNS

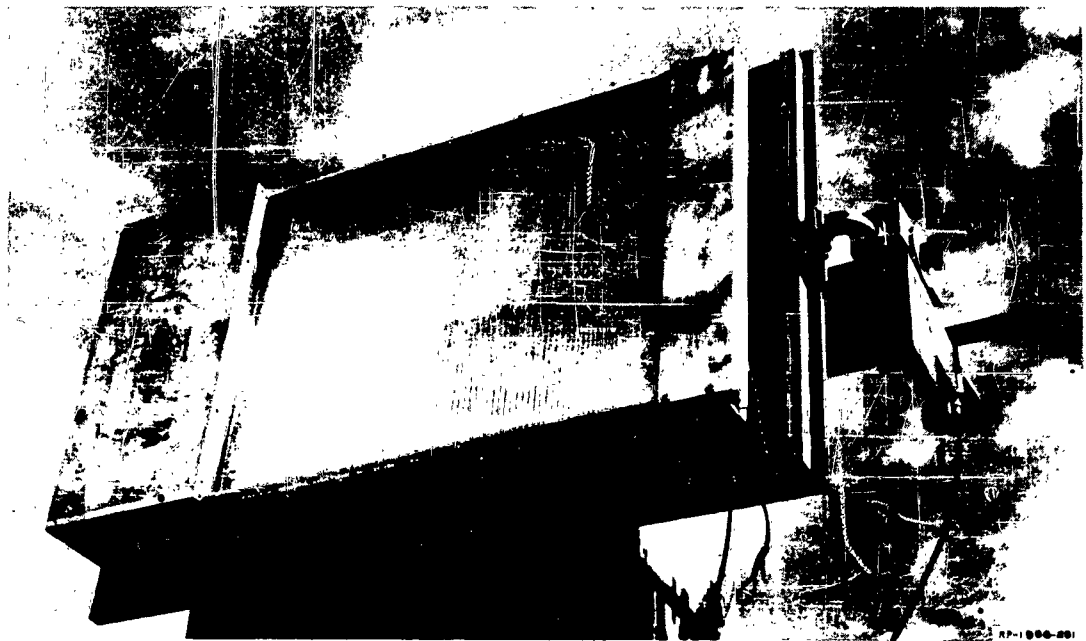


FIG. V-21  
ROLLED PILLBOX FEEDING LEAKY-WAVE ANTENNA

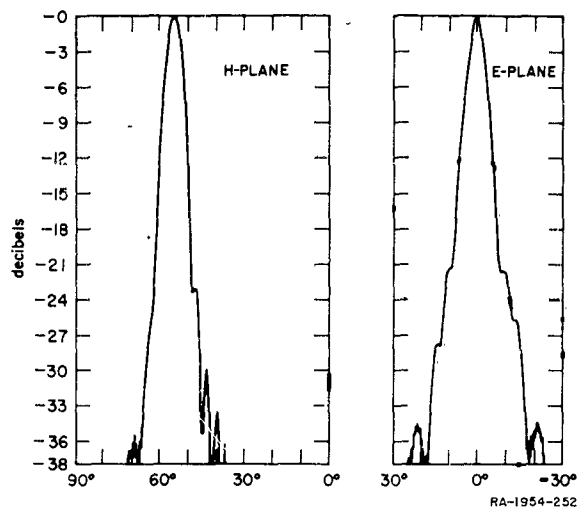


FIG. V-22  
RADIATION PATTERNS OF LEAKY-WAVE ANTENNA  
FED WITH ROLLED PILLBOX

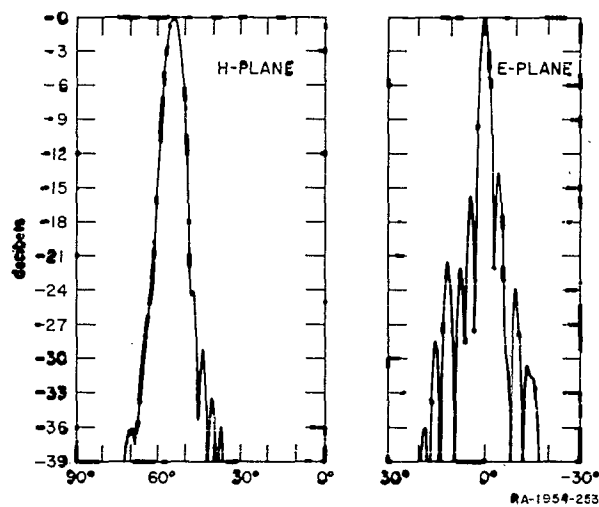


FIG. V-23  
RADIATION PATTERNS OF LEAKY-WAVE ANTENNA  
FED WITH HOG HORN

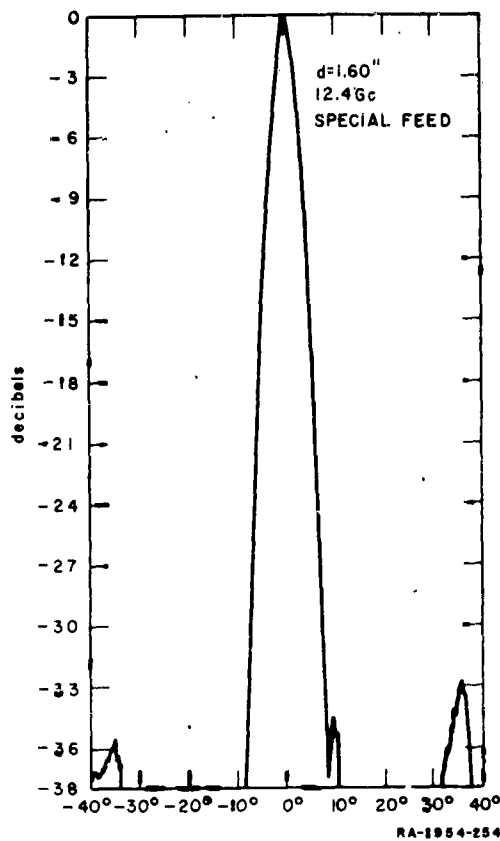


FIG. V-24  
RADIATION PATTERN OF ROLLED PILLBOX  
WITH SPECIAL FEED HORN

#### REFERENCES

1. E. M. T. Jones, R. C. Honey and R. A. Folsom, "Millimeter Wavelength Antenna Studies," Contract DA 36-039 SC-5503, SRI Project 430, Stanford Research Institute, Menlo Park, California (30 July 1953).
2. N. Marcuvitz, "Waveguide Handbook," pp. 334, Rad. Lab. Series, Vol. 10 (McGraw-Hill Book Company, Inc., New York, N.Y., 1951).
3. S. Silver, "Microwave Antenna Theory and Design," p. 365, Rad. Lab. Series, Vol. 12 (McGraw-Hill Book Company, Inc., New York, N.Y., 1949).
4. R. C. Honey, "A flush Mounted Leaky-Wave Antenna with Predictable Patterns," Contract AF 19(604)-1571, Stanford Research Institute, Menlo Park, California (January 1956).

## VI INSTANTANEOUS DIRECTION-FINDING ANTENNAS

### A. GENERAL

This section of the report summarizes the important properties of three instantaneous direction-finding antennas that have been studied both theoretically and experimentally on Signal Corps Contracts DA 36-039 SC-63236 and DA 36-039 SC-73106. Each of these antennas together with appropriate display circuitry is capable of instantaneously determining the direction of arrival of an electromagnetic wave, whether it be a continuous (CW) signal or a single short pulse. They can do this for signals arriving from any azimuth direction without any sort of scanning, either mechanical or electronic, with typical bearing errors of the order of a few degrees. In addition, they can perform this function over quite wide frequency bandwidths, varying from 1.5:1 for the narrowest to 3:1 for the widest. Some of the systems can be wide open to all signals in the band simultaneously, and some can be tuned over the band electronically by varying a local oscillator frequency.

Each antenna utilizes a biconical horn that is perfectly symmetrical about its vertical axis. The size of this horn, both in diameter and height, depends only on the coverage or antenna gain that is required in the elevation plane. These can be varied over very wide limits without affecting in any way the direction-finding properties of the circuitry connected to the antenna.

The biconical antenna and its associated coaxial line are proportioned so that only the vertically polarized component of an incoming signal is received. If, however, polarization-rotating devices were placed around the aperture of the biconical horn, it could then receive other polarizations as well.

The biconical antenna is connected, by means of a low-reflection tapered section, into a coaxial line which is large enough to propagate the  $TE_{11}$  coaxial-line mode in addition to the fundamental TEM transmission-line mode. It is this  $TE_{11}$  coaxial-line mode which is utilized in all of the direction-finding antennas to determine the direction of arrival of the signal. This mode, as well as the TEM mode and many higher-order modes

are excited by a plane wave incident on the biconical antenna, but the coaxial line is cut off to all higher modes. (In the widest-band system, the  $TE_{2,1}$  mode can also propagate in the coaxial line over part of the band, but later portions of the circuitry reflect all of this mode, as well as the TEM mode, back out of the antenna.) It is this filtering action of the coaxial line that results in the very low bearing errors that can be realized in these antenna systems.

The coaxial line is then divided into four symmetrical waveguide channels by a device that is functionally a very-wide-band seven-port turnstile junction. The seven ports are composed of the four single-mode waveguide ports (ridged waveguide in the wide-band versions) and three ports for the orthogonal modes in the coaxial line, the TEM mode and two orthogonal  $TE_{1,1}$  modes. This turnstile junction has been designed to be extremely well matched to the three coaxial-line modes over bandwidths in excess of 3:1, hence it does not limit the operating bandwidths of any of the antenna systems described here.

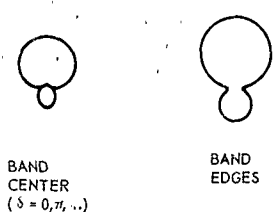
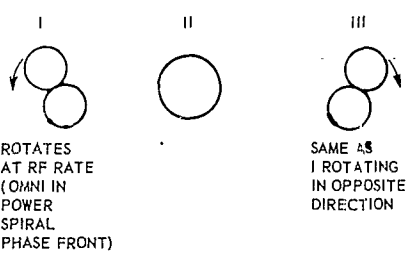
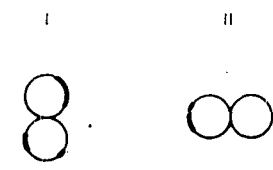
The three different types of instantaneous, omniazimuth direction-finding antennas to be compared here differ only in the manner in which the energy from these four waveguide ports is handled. The accompanying fold-out chart (Fig. VI-1) indicates these differences and compares the important characteristics of the three different antennas. All three antennas and the associated waveguide and coaxial components have been built and tested at SRI for the Signal Corps. The first two were developed on Contract DA 36-039 SC-63236, and are described in detail in the Final Report on that contract<sup>1</sup> and in the *Proceedings of the IRE*.<sup>2</sup> The third type was developed on the present contract, Contract DA 36-039 SC-73106, and is described in detail in the Second and Third Annual Reports.

With the RF preamplifiers shown by the dashed lines for the first direction-finding antenna, the sensitivities of all three systems to low-level signals become comparable, and depend more upon the noise figures of the amplifiers and the detectors than upon the antenna characteristics. The third antenna system may be slightly less sensitive, other things being equal, since it does not utilize any information from the TEM mode which is excited in the antenna by an incoming signal.

The 180-degree ambiguity associated with the third type of direction finder is inherent in that system as long as it remains perfectly

TYPE	BLOCK DIAGRAM	RF OUTPUT SIGNALS	DETECTORS	POST-DETECTION SIGNALS	BEARING AMBIGUITIES	BEARING ERROR (Large ?)
FOUR-PORT ANTENNA FOR SQUARE-LAW DETECTORS		I. $\sin \omega t + 2 \sin \phi \sin(\omega t - \delta)$ II. $\sin \omega t + 2 \cos \phi \sin(\omega t - \delta)$ III. $\sin \omega t - 2 \sin \phi \sin(\omega t - \delta)$ IV. $\sin \omega t - 2 \cos \phi \sin(\omega t - \delta)$	FOUR MATCHED SQUARE-LAW (SUCH AS CRYSTAL DIODES OR BOLOMETERS)	DIFF. CHANNEL I-III: $4 \cos \phi \cos \delta$ DIFF. CHANNEL II-IV: $4 \sin \phi \cos \delta$	NONE	INTER-MEDIATE
THREE-PORT ANTENNA FOR LINEAR DETECTORS		I. $2 \sin(\omega t - \delta - \phi)$ II. $2 \sin \omega t$ III. $-2 \sin(\omega t - \delta + \phi)$	TWO OR THREE MATCHED LINEAR (SUCH AS MIXERS)	SAME AS RF SIGNAL, TRANSLATED TO i-f OR d-c (MUST MEASURE RELATIVE PHASE BETWEEN PORTS I OR III AND II TO DETERMINE DIRECTION)	NONE	MOST SUSCEPT
TWO-PORT ANTENNA FOR LINEAR DETECTORS		I. $2\sqrt{2} \sin \phi \sin(\omega t - \delta)$ II. $2\sqrt{2} \cos \phi \sin(\omega t - \delta)$	TWO MATCHED LINEAR (SUCH AS MIXERS)	I. $2\sqrt{2} \sin \phi$ II. $2\sqrt{2} \cos \phi$	180° (SEE TEXT)	LEAST SUSCEPT (PROBABLY ERROR C IN FIRST MODEL)

FIG. VI-1  
COMPARISON OF INSTANTANEOUS, OMNIAZIMUTH, DI

ION S	BEARING AMBIGUITIES	BEARING ERRORS (Large Signal)	BANDWIDTH	TYPICAL RADIATION PATTERNS	MECHANICAL COMPLEXITY	NOTES
I-III: 8 II-IV: 3	NONE	INTER- MEDIATE	APPROX. 1.5:1 FOR 2 db DROP IN SENSI- TIVITY AT EDGES OF BAND	<p>FROM ONE DETECTOR:</p> 	LEAST COMPLEX	<p>1. THE FOUR LINEAR RF PREAMPLIFIERS SHOWN BY DASHED LINES MAY BE USED TO INCREASE THE SENSITIVITY OF THE SYSTEM. THEY SHOULD HAVE IDENTICAL AMPLITUDE VS. FREQUENCY CHARACTERISTICS, BUT NEED NOT PRESERVE PHASE INFORMATION.</p> <p>2. THE SQUARE-LAW DETECTORS MAY BE FOLLOWED BY FOUR VIDEO AMPLIFIERS OR TWO DIFFERENTIAL VIDEO AMPLIFIERS (WITH DC RESPONSE FOR CW SIGNALS).</p>
L, IVE ID	NONE	MOST SUSCEPTIBLE	1.5:1 WITH AVAILABLE COMPONENTS (LIMITED BY BANDWIDTHS OF DIRECTIONAL COUPLERS AND MAGIC-T's)  ALMOST 2:1 MAXIMUM	 <p>ROTATES AT RF RATE (OMNI IN POWER SPIRAL PHASE FRONT)</p> <p>SAME AS I ROTATING IN OPPOSITE DIRECTION</p>	MOST COMPLEX	<p>1. THE DETECTORS AND IF AMPLIFIERS SHOULD HAVE IDENTICAL PHASE AND AMPLITUDE CHARACTERISTICS.</p> <p>2. THE DETECTION SCHEME SHOWN IS ONE OF SEVERAL POSSIBLE ALTERNATIVES. ANOTHER IS DESCRIBED IN REF. 1.</p>
	180° (SEE TEXT)	LEAST SUSCEPTIBLE (PROBABLE ERROR OF 1.7° IN FIRST MODEL)	ALMOST 3:1 (IN THEORY AND PRACTICE)		INTER- MEDIATE	<p>1. THE DETECTORS AND IF AMPLIFIERS SHOULD HAVE IDENTICAL PHASE AND AMPLITUDE CHARACTERISTICS.</p>

RD-4959-490

FIG. VI-1

IEOUS, OMNIAZIMUTH, DIRECTION-FINDING ANTENNAS



symmetrical, since this information is simply not contained in the  $TE_{11}$  modes which reach the detectors. If, however, some asymmetry is introduced into the antenna or coaxial-line portions of the RF circuitry, some of the TEM and  $TE_{21}$  modes will, in effect, be coupled to the  $TE_{11}$  modes, and hence, in general the bearing indication will shift both in angle and in amplitude. From the nature of this shift, the ambiguity can be resolved. To make this sort of technique as insensitive to frequency as possible, the asymmetry should be placed near the transition region from the biconical antenna to the coaxial line. It may be possible to introduce this asymmetry very rapidly by using, for instance, a symmetrical configuration of crystal-diode switches in this region, and switching them on and off in any desired sequence.

## B. RECOMMENDATIONS

Although the antennas and the associated waveguide circuitry for these direction-finding systems have been thoroughly investigated and are now well understood, a number of practical problems remain before a complete instantaneous direction-finding system can be tested in the field. For instance, it will probably be necessary in any of these systems to increase the dynamic range of the data presentation schemes diagrammed in Fig. VI-1. This might be done with instantaneous AGC circuits coupling the amplifiers in the various branches together, or by still other, more sophisticated means which can also increase the information storage capacity of the systems.<sup>5</sup> Another problem associated with any of the three systems, the requirement for well-matched, identical detectors (whether they be square-law detectors or linear mixers), may require some development effort, depending on the particular frequency bands selected.

It should become apparent from a study of the chart (Fig. VI-1) that the first and the third direction-finding antenna systems offer the most attractive possibilities for further development, the choice between the two depending on the particular application. The first system offers the advantage of no bearing ambiguity; the third system offers greater bandwidth and smaller bearing errors. Other things being equal, it is felt that the third system has fewer unsolved problems associated with the development of a complete direction-finding system.

## REFERENCES

1. R. C. Honey, E. M. T. Jones, L. A. Robinson, P. M. Sherk, David Carter, S. B. Cohn, and Tetsu Morita, "Investigation of Wide-Band Antennas Above 2000 Mc," Final Report, SRI Project 1115, Contract DA 36-039 SC-63236, Stanford Research Institute, Menlo Park, California (October 1956).
2. R. C. Honey and E. M. T. Jones, "A Versatile Multiport Biconical Antenna," Proc. IRE 45, 10, pp. 1374-1383 (October 1957).
3. R. C. Honey, L. A. Robinson, J. K. Shimizu, and W. J. Getsinger, "Antenna Design Parameters," Second Annual Report, Contract DA 36-039 SC-73106, SRI Project 1954, Stanford Research Institute, Menlo Park, California (January 1959).
4. R. C. Honey, L. A. Robinson and J. K. Shimizu, "Antenna Design Parameters," Third Annual Report, Contract DA 36-039 SC-73106, SRI Project 1954, Stanford Research Institute, Menlo Park, California (January 1960).
5. W. B. Bachelor, "An Instantaneous Microwave Direction-Finding Display System," NRL Report 5424 (CONFIDENTIAL), Naval Research Laboratory, Washington, D.C. (December 18, 1959). AD-314620

## VII CONCLUSIONS

The modified form of the Purcell array has been shown to be feasible. The simple and rugged mechanical form of the array makes it possible to scale such arrays to millimeter wavelengths and to maintain constant phase velocity on a very long array. It may be possible to obtain design data of sufficient accuracy for very long arrays from a promising new analytical technique.

Linear arrays with variable interelement spacings can be designed using computer techniques with many fewer elements than Dolph-Tchebyscheff arrays with the same beamwidths and side-lobe levels. The lower limit on the side-lobe levels attainable in widely spaced arrays of this type is primarily a function of the total number of elements in the array. The radiation patterns of such arrays can be steered over wider angles and wider frequency bands than those of comparable equispaced arrays.

The optimum spacings required in a linear array of isotropic, uniformly spaced elements have been placed on a mathematically rigorous foundation for both odd and even numbers of elements.

The technique of beam shaping and beam broadening by distorting the conducting sheet beneath an inductive-grid leaky-wave antenna shows great promise.

The tests of the rolled pillbox have demonstrated the wideband, low-side-lobe characteristics of this type of line source, and verified the design calculations.

Of the three broadband, instantaneous direction-finding antennas developed, the four-port antenna with square-law detectors and the two-port antenna with linear detectors show the most promise for eventual systems application.

## VIII RECOMMENDATIONS

In this report, detailed recommendations are contained in many of the separate sections; however, all recommendations will be summarized here for convenient reference.

Further work on the modified Purcell array should proceed along two separate lines: (1) refine the measurements of the coupling coefficients from uniform arrays of slots, particularly very small slots, and (2) continue the analysis of the Purcell array junction and compute design data with sufficient accuracy for very long arrays.

The investigations of linear arrays should also proceed along two parallel paths: (1) refine the computer techniques for finding optimum solutions for variably spaced arrays, investigate promising initial array solutions, and compute optimum arrays for large numbers of elements (100 or over), and (2) apply the most advanced analytical techniques and talent to the variably spaced array problem in an attempt to find the true optimum solution.

The relatively simple technique of beam broadening and beam shaping by distorting leaky wave antennas should be studied in more detail, investigating the many promising avenues that have been exposed in this initial investigation, and attempting to find the simplest or most nearly optimum solutions to given problems.

One or both of the most promising broadband, instantaneous direction-finding antennas should be built into a complete direction-finding system for testing and evaluation.

## IDENTIFICATION OF KEY TECHNICAL PERSONNEL

### A. PERSONNEL FOR PRESENT YEAR

Mr. John Aasted <i>Research Engineer</i>	PART TIME
Dr. Clarence M. Ablow* <i>Head, Applied Mathematics Group</i>	PART TIME
Dr. Mogens G. Andreassen <i>Senior Research Engineer</i>	PART TIME
Dr. Joel L. Brenner* <i>Senior Mathematician</i>	PART TIME
Dr. Richard C. Honey (Project Leader) <i>Technical Program Coordinator, Electromagnetics Laboratory</i>	PART TIME
Mr. Lloyd A. Robinson <i>Research Engineer</i>	PART TIME
Mr. Eugene D. Sharp* <i>Research Engineer</i>	PART TIME

### B. PERSONNEL FOR PREVIOUS YEARS

David Carter	PART TIME
F. S. Coale	PART TIME
S. B. Cohn	PART TIME
W. J. Getsinger	PART TIME
J. S. Honda	PART TIME
P. M. Sherk	PART TIME
J. K. Shimizu	PART TIME

---

\* Since biographies of these personnel have not been included in any previous report, they are given here.

Ablow, Clarence M.—*Senior Research Mathematician, Mathematical Sciences Department*

Dr. Ablow received a B.A. degree in Mathematics and Physics in 1940 and an M.A. in Mathematics in 1942, both from the University of California at Los Angeles. In 1951 he received a Ph.D. degree in Applied Mathematics from Brown University. From 1942 to 1946 he was an Aerological Officer in the U.S. Naval Reserve. He was an Instructor in Mathematics at the University of Miami in 1946-49 and a Research Assistant and Teaching Fellow at Brown University in 1949-51. In 1951 Dr. Ablow became a Research Specialist at the Boeing Airplane Company, engaged in applied mathematics, and remained there until he joined the staff of Stanford Research Institute in 1955. At the Institute he has been concerned with problems in hydrodynamics, heat transfer, and chemical kinetics. This work has led to several publications in technical journals.

He is a member of Phi Beta Kappa, Sigma Xi, the American Mathematical Society, the Mathematical Association of America, the Society of Industrial and Applied Mathematics, and the American Rocket Society.

Brenner, Joel L.—*Senior Mathematician, Physics Department*

Dr. Brenner has an A.B. degree in chemistry and a Ph.D. degree in mathematics, both from Harvard University. He has served on the staffs of New York University, University of Minnesota, Princeton University, University of California, and State College of Washington. He has done mathematical work for insurance companies and industrial organizations in the field of demography. He is a reviewer for the international journals *Mathematical Reviews*, *Zentralblatt für Mathematik*, and *Applied Mechanics Reviews*.

Dr. Brenner has published some forty articles in mathematics and applied mathematics. He translated and revised Gantmaher's *Applications of the Theory of Matrices*, and N. N. Krasovskii's book *Some Problems in the Stability of Motion*.

Dr. Brenner is a member of Phi Beta Kappa, Sigma Xi, American Mathematical Society, Mathematical Association of America, American Rocket Society, and the Society for Industrial and Applied Mathematics.

Sharp, Eugene D. --*Research Engineer, Microwave Group, Electromagnetics Laboratory*

Mr. Sharp received a B.S. degree in 1954 and an M.S. degree in 1956, both in Electrical Engineering from Stanford University. In 1954-55 he was employed by the Air Research Organization, Inc., in Tullahoma, Tennessee. During 1955-56 he was a Teaching Assistant at Stanford University, in the Electronic Measurements Laboratory. From 1956 to 1958 he was a Project Officer of the U.S. Air Force at the Rome Air Development Center, Griffiss Air Force Base, New York, working in the Antenna Development Section.

In April 1958 Mr. Sharp joined the staff of Stanford Research Institute, where he has been working on a study of electronic scanning antennas, ECM antennas, and high-power waveguide filters. He is studying for the Ph.D. degree in Electrical Engineering at Stanford University, on a part-time basis under the Honors Cooperative Program.

Mr. Sharp is a member of Tau Beta Pi, the Institute of Radio Engineers, and the IRE Professional Groups on Antennas and Propagation, on Microwave Theory and Techniques, and on Radio Frequency Interference.

*APPENDIX A*

**PROOFS OF THEOREMS**



## APPENDIX A

### PROOFS OF THEOREMS

The Tchebyscheff polynomial

$$T_n(x) = 2^{1-n} \cos(n \arccos x) = 2^{-n} [(x + \sqrt{x^2 - 1})^n + (x - \sqrt{x^2 - 1})^n] = x^n + \dots$$

has degree  $n$ , leading coefficient 1, and its deviation from 0 on the interval  $-1 \leq x \leq 1$  is less than that of any other polynomial of degree  $n$  with leading coefficient 1. The proof of this fact is given in standard texts.<sup>1,2\*</sup>

Another important property of the Tchebyscheff polynomial  $T_n(x)$  is Corollary 2 of the theorem in this appendix. This property is used in the discussion.

*Theorem:* Suppose  $Q(x)$  is a polynomial of degree  $\leq n$  such that

$$\max_{-1 \leq x \leq 1} |Q(x)| = M/2^{n-1},$$

and suppose  $x_0 > 1$ . Then

$$|Q(x_0)| \leq MT_n(x_0);$$

furthermore, if  $Q(x)$  is not equal to  $MT_n(x)$ , then  $Q(x_0) < MT_n(x_0)$ .

*Proof:* Set  $P(x) = Q(x)/M$ . Then

$$\max_{-1 \leq x \leq 1} |P(x)| = \max_{-1 \leq x \leq 1} |T_n(x)| = 1/2^{n-1};$$

it has to be proved that  $|P(x_0)| \leq T_n(x_0)$ .

---

\*References are listed at the end of the Appendix

The graph of  $T_n(x)$  is illustrated in Fig. A-1 for the case  $n = 5$ . There are  $n + 1$  values  $r_i$  of  $x$ :

$$-1 = r_0 < r_1 < \dots < r_{n-1} < r_n = 1$$

including  $-1$  and  $1$  at which  $T_n(x)$  is alternately plus and minus  $1/2^{n-1}$ .

In Fig. A-1,  $n$  is odd and  $T_n(-1) = -1/2^{n-1}$ .

It is given that for  $x \in [-1, 1]$ , the graph of  $P(x)$  lies between  $y = \pm 1/2^{n-1}$ .

To make the argument definite, suppose  $n$  is odd. (The reasoning for the case where  $n$  is even is entirely similar.) Next, note that if two polynomials agree over an interval, however small, they are identical. If two polynomials of degree  $\leq n$  in  $x$  have the same value for  $n + 1$  distinct

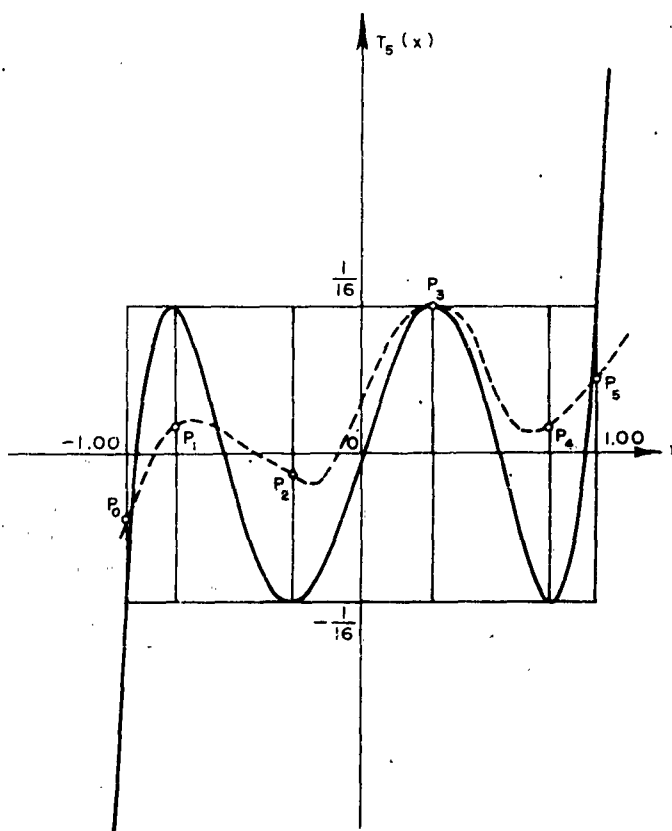


FIG. A-1  
RELATION BETWEEN GRAPHS OF  $T_n(x)$  AND  $P(x)$ , WHERE  $n = 5$

values of  $x$ , they are identical. (If the graphs of the two polynomials are tangent for a value of  $x$ , this value of  $x$  counts as two distinct values for the purposes of this statement.)

Let us mark the  $n + 1$  points,  $P_i$ , at which the graph of  $P(x)$  crosses the lines  $x = r_i$  ( $i = 0, 1, \dots, n$ ). Since each point  $P_i$  lies in the rectangle, the graph of  $P(x)$  must cross the graph of  $T_n(x)$  at least once in each of the  $n$  closed arcs  $(P_{i-1}, P_i)$  into which the  $n + 1$  points  $P_i$  separate the graph of  $P(x)$ ,  $0 \leq x \leq 1$ . In making this statement it is understood that a closed arc includes its end-points. Thus a tangency at  $P_i$  is correctly counted as a double crossing, with one crossing point being allotted to each of the arcs that end at  $P_i$ .

There are two cases. First, if the graph of  $P(x)$  is above the graph of  $T_n(x)$  in an open interval  $(-a, -1)$  just to the left of  $x = -1$ , and if there are precisely  $n$  crossings, then at the  $n$ th crossing ( $x = r'_n$ ) the sign of  $P(x) - T_n(x)$  becomes negative.

If  $P(x)$  is not identical with  $T_n(x)$ , there can be no more crossings, so that  $P(x) < T_n(x)$  for  $x > r'_n$ ; in particular,  $P(x_0) < T_n(x_0)$ . In the second case,  $P(x) - T_n(x)$  is negative on an open interval  $(-a, -1)$  just to the left of  $x = -1$ . Hence the graphs of  $P(x)$ ,  $T_n(x)$  are either tangent at  $(-1, -1/2^{n-1})$  or else the graph of  $P(x)$  crosses the graph of  $T_n(x)$  as shown in Fig. A-2. In either case there are  $n + 1$  crossing points and  $P(x) \equiv T_n(x)$ ,  $P(x_0) = T_n(x_0)$ .

To prove that  $-P(x_0) \leq T_n(x_0)$ , the same reasoning is applied to the graph of  $-P(x)$ . The theorem is proved.

*Corollary 1:* Let  $R(x)$  be a polynomial of  $\deg \leq n$ ,  $x_0 > 1$ , and suppose  $R(x_0) = 1$ . Either  $R(x) = T_n(x)/T_n(x_0)$ , or else

$$\max_{-1 \leq x \leq 1} |R(x)| > \max_{-1 \leq x \leq 1} \left| \frac{T_n(x)}{T_n(x_0)} \right| = \frac{1}{2^{n-1} T_n(x_0)}$$

*Proof:* Define  $M$  by

$$\max_{-1 \leq x \leq 1} |R(x)| = \frac{M}{2^{n-1} T_n(x_0)}$$

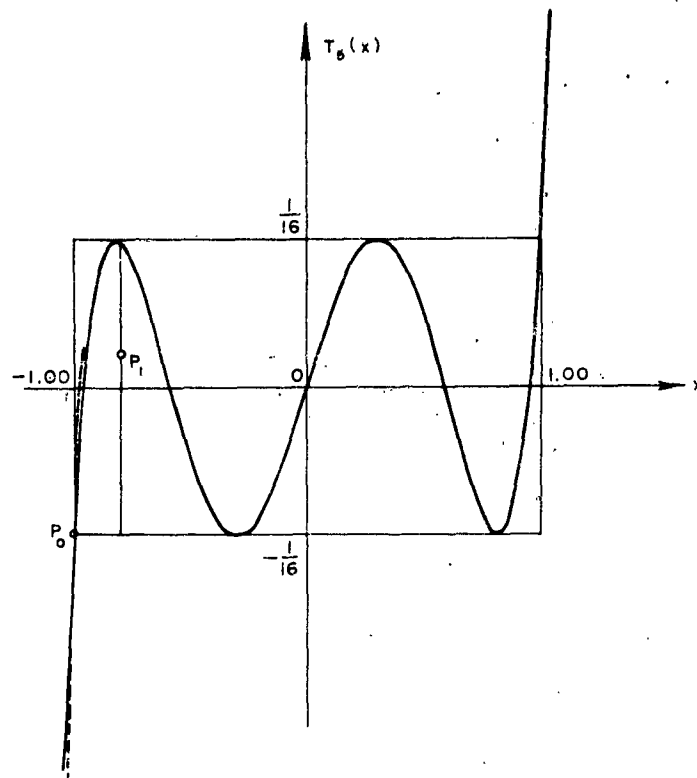


FIG. A-2  
SPECIAL CASE OF FIG. A-1

and set  $Q(x) = T_n(x_0)R(x)$ . Then

$$\max_{-1 \leq x \leq 1} |Q(x)| = \frac{M}{2^{n-1}},$$

and if  $Q(x) \neq T_n(x)$  it would follow from the theorem that

$$Q(x_0) < MT_n(x_0).$$

But  $Q(x_0) = T_n(x_0)$ , so that  $M > 1$  unless  $R(x) = T_n(x)/T_n(x_0)$ . This is the assertion of the corollary.

**Corollary 2:** Let  $x_0 > 1$ . The unique polynomial of degree  $\leq n$  which has the value 1 at  $x_0$  and which deviates least from 0 on  $(-1, 1)$  is  $T_n(x)/T_n(x_0)$ , where  $T_n(x)$  is the Tchebyscheff polynomial

$$T_n(x) = \frac{1}{2^{n-1}} \cos(n \arccos x) = 2^{-n}[(x + \sqrt{x^2 - 1})^n + (x - \sqrt{x^2 - 1})^n]$$

This is a restatement of Corollary 1.

**Lemma:** It is required to show that  $x_0$  increases as  $kd_1$  increases on the range  $0 < kd_1 < \pi$ . That positive  $x_0$  increases is equivalent to  $X$  decreasing where

$$\begin{aligned} X &= \frac{2}{x_0 + 1} - 1 \\ &= \frac{\cos(kd_1 \sin \epsilon) - \cos kd_1}{1 - \cos kd_1} - 1 \\ &= \frac{\cos(kd_1 \sin \epsilon) - 1}{1 - \cos kd_1} \end{aligned}$$

But, as  $kd_1$  increases on  $0 < kd_1 < \pi$ , the numerator of this last fraction decreases and the denominator increases without changing sign. Thus  $X$  decreases and  $x_0$  increases as was to be shown.

## REFERENCES

1. I. P. Natanson, *Konstruktive Funktionentheorie* (Akademie Verlag, Berlin, 1955, translated from the Russian).
2. N. Achieser, *Theory of Approximation* (F. Ungar, New York City, 1956).

<p>AD STANFORD RESEARCH INSTITUTE, Menlo Park, California</p> <p>Accession No.</p> <p>ANTENNA DESIGN PARAMETERS—R. C. Honey, E. D. Sharp, M. G. Andreasen, C. M. Ablow, J. L. Brenner, L. A. Robinson, J. Aasted</p> <p>Final Report, May 1961, 180 pp., 87 Figs., 11 Tables</p> <p>UNCLASSIFIED</p> <p>SRI Project 1954, Contract DA 36-039 SC-73106, Department of the Army Project 3-99-00-100, Signal Corps Task 3-99-06-106</p> <p>This report describes the results obtained during the last year of a four-year study program on antenna design parameters. Thus, the complete results of this program are contained in the three previous annual reports and in this final report. A summary of the project discusses the various investigations carried out during the course of the project.</p> <p>A modified Purcell linear array was designed and built for the 35-Gc band. A novel analytical technique has been developed that promises to yield design data sufficiently precise for even very long arrays.</p>	<p>UNCLASSIFIED</p> <ol style="list-style-type: none"> <li>1. Microwave antennas, design data, summary</li> <li>2. Purcell array modified</li> <li>3. Linear arrays, computer techniques for</li> <li>4. Dolph-Tchebyscheff array</li> <li>5. Isotropic elements, spacing of an antenna</li> <li>6. Leaky-wave antennas, design data</li> <li>7. Pillbox antenna</li> <li>8. Direction-finding antenna</li> </ol>	<p>AD STANFORD RESEARCH INSTITUTE, Menlo Park, California</p> <p>Accession No.</p> <p>ANTENNA DESIGN PARAMETERS—R. C. Honey, E. D. Sharp, M. G. Andreasen, C. M. Ablow, J. L. Brenner, L. A. Robinson, J. Aasted</p> <p>Final Report, May 1961, 180 pp., 87 Figs., 11 Tables</p> <p>UNCLASSIFIED</p> <p>SRI Project 1954, Contract DA 36-039 SC-73106, Department of the Army Project 3-99-00-100, Signal Corps Task 3-00-06-106</p> <p>This report describes the results obtained during the last year of a four-year study program on antenna design parameters. Thus, the complete results of this program are contained in the three previous annual reports and in this final report. A summary of the project discusses the various investigations carried out during the course of the project.</p> <p>A modified Purcell linear array was designed and built for the 35-Gc band. A novel analytical technique has been developed that promises to yield design data sufficiently precise for even very long arrays.</p>	<p>UNCLASSIFIED</p> <ol style="list-style-type: none"> <li>1. Microwave antennas, design data, summary</li> <li>2. Purcell array modified</li> <li>3. Linear arrays, computer techniques for</li> <li>4. Dolph-Tchebyscheff array</li> <li>5. Isotropic elements, spacing of an antenna</li> <li>6. Leaky-wave antennas, design data</li> <li>7. Pillbox antenna</li> <li>8. Direction-finding antenna</li> </ol>	<p>AD STANFORD RESEARCH INSTITUTE, Menlo Park, California</p> <p>Accession No.</p> <p>ANTENNA DESIGN PARAMETERS—R. C. Honey, E. D. Sharp, M. G. Andreasen, C. M. Ablow, J. L. Brenner, L. A. Robinson, J. Aasted</p> <p>Final Report, May 1961, 180 pp., 87 Figs., 11 Tables</p> <p>UNCLASSIFIED</p> <p>SRI Project 1954, Contract DA 36-039 SC-73106, Department of the Army Project 3-99-00-100, Signal Corps Task 3-99-06-106</p> <p>This report describes the results obtained during the last year of a four-year study program on antenna design parameters. Thus, the complete results of this program are contained in the three previous annual reports and in this final report. A summary of the project discusses the various investigations carried out during the course of the project.</p> <p>A modified Purcell linear array was designed and built for the 35-Gc band. A novel analytical technique has been developed that promises to yield design data sufficiently precise for even very long arrays.</p>	<p>UNCLASSIFIED</p> <ol style="list-style-type: none"> <li>1. Microwave antennas, design data, summary</li> <li>2. Purcell array modified</li> <li>3. Linear arrays, computer techniques for</li> <li>4. Dolph-Tchebyscheff array</li> <li>5. Isotropic elements, spacing of an antenna</li> <li>6. Leaky-wave antennas, design data</li> <li>7. Pillbox antenna</li> <li>8. Direction-finding antenna</li> </ol>
---	---	---	---	---	---

<p>Computer techniques have been developed for designing linear arrays with widely and variably spaced elements. The problem of finding the optimum spacing for the elements in an array of isotropic elements has been set up precisely, and solutions found for two cases.</p> <p>Beam-broadening modifications have been studied for six leaky-wave antennas. For wall displacements that did not reduce the radiated power, the largest change was an increase of 20 in the beamwidth of 50λ-long antennas. Even larger changes may be possible.</p> <p>A doubled-layered pillbox antenna was designed and built that has wide-band operation, no aperture blocking, and low-side-lobe patterns.</p> <p>Three types of wide-band omniazimuthal direction-finding antennas have been built and tested.</p>	<p>UNCLASSIFIED</p>	<p>Computer techniques have been developed for designing linear arrays with widely and variably spaced elements. The problem of finding the optimum spacing for the elements in an array of isotropic elements has been set up precisely, and solutions found for two cases.</p> <p>Beam-broadening modifications have been studied for six leaky-wave antennas. For wall displacements that did not reduce the radiated power, the largest change was an increase of 20 in the beamwidth of 50λ-long antennas. Even larger changes may be possible.</p> <p>A doubled-layered pillbox antenna was designed and built that has wide-band operation, no aperture blocking, and low-side-lobe patterns.</p> <p>Three types of wide-band omniazimuthal direction-finding antennas have been built.</p>	<p>UNCLASSIFIED</p>
<p>Computer techniques have been developed for designing linear arrays with widely and variably spaced elements. The problem of finding the optimum spacing for the elements in an array of isotropic elements has been set up precisely, and solutions found for two cases.</p> <p>Beam-broadening modifications have been studied for six leaky-wave antennas. For wall displacements that did not reduce the radiated power, the largest change was an increase of 20 in the beamwidth of 50λ-long antennas. Even larger changes may be possible.</p> <p>A doubled-layered pillbox antenna was designed and built that has wide-band operation, no aperture blocking, and low-side-lobe patterns.</p> <p>Three types of wide-band omniazimuthal direction-finding antennas have been built and tested.</p>	<p>UNCLASSIFIED</p>	<p>Computer techniques have been developed for designing linear arrays with widely and variably spaced elements. The problem of finding the optimum spacing for the elements in an array of isotropic elements has been set up precisely, and solutions found for two cases.</p> <p>Beam-broadening modifications have been studied for six leaky-wave antennas. For wall displacements that did not reduce the radiated power, the largest change was an increase of 20 in the beamwidth of 50λ-long antennas. Even larger changes may be possible.</p> <p>A doubled-layered pillbox antenna was designed and built that has wide-band operation, no aperture blocking, and low-side-lobe patterns.</p> <p>Three types of wide-band omniazimuthal direction-finding antennas have been built and tested.</p>	<p>UNCLASSIFIED</p>